TABLE DES MATIÈRES

Page

COMPORTEMENT VISCOÉLASTIQUE À GRANDE DÉFORMATION DES COMPOSITES ÉLASTOMÈRES-TEXTILES UTILISÉS DANS LES ÉQUIPEMENTS DE PROTECTION

Lotfi HARRABI

RÉSUMÉ

Le but de cette thèse consiste à étudier le comportement mécanique des matériaux de protection. Nous nous sommes intéressés particulièrement au comportement viscoélastique de ces matériaux à des grandes déformations lors d'un cycle charge-décharge. Les modèles développés ici sont basés sur l'utilisation du modèle rhéologique de Zener pour pouvoir prédire ce comportement à différentes vitesses dans le cas des matériaux élastomères et des matériaux textiles. Les résultats qui ont été trouvés montrent une bonne corrélation entre la modélisation et l'expérimentation. L'utilisation des modèles proposés dans cette étude permet de prédire l'effort nécessaire ainsi que l'énergie à dissiper pour accomplir une certaine tache à une vitesse donnée. Par ailleurs, deux nouvelles méthodes mécaniques sont proposées dans ce travail pour l'évaluation de la souplesse des gants de protection.

Mots clés : composite, élastomère, textile, grande déformation, viscoélastique, souplesse, gants de protection.

LISTE DES TABLEAUX

LISTE DES FIGURES

LISTE DES SYMBOLES ET UNITÉS DE MESURE

C_1, C_2	Mooney-Rivlin coefficients
E	Tensile modulus (MPa)
F	Applied force (N)
F_A	Applied force in the spherical probe zone (zone A)
F_B	Applied force in the conical probe zone (zone B)
λ	Extension ratio
σ	Engineering stress (MPa)
σ_{True}	True stress (MPa)
T_1	Resulting stress per unit edge length along the radial direction
T_2	Resulting stress per unit edge length along the circumferential direction
ε	True strain (%)
W	Strain energy density (J/m^3)
$\lambda_1, \lambda_2, \lambda_3$	Principal extension ratios
I_1, I_2, I_3	Strain invariants
$\overline{\lambda}$	Average extension ratio
p	Hydrostatic pressure
μ	Shear modulus
h	Thickness of the membrane
$\tau_{1/2}$	Half cycle time
H	Heaviside function
η	Damper viscosity
ζ	Cyclic strain rate test
$\lambda_{chain}^{R_1}, \lambda_{chain}^{R_2}$	Molecular chain extension of both springs R_1 and R_2
λ_{lim}	Limit network stretch
L	Langevin function

n	Number of chains contained in unit volume of the network
K_B	Boltzmann's constant
T	Absolute temperature (°K)
$C^{(R_1)}, N^{(R_1)}$	Elastomer spring R_1 parameters
$C^{(R_2)}, N^{(R_2)}$	Elastomer spring R_2 parameters
A, B	Elastomer damper constants
$E^{(R_1)}, E^{(R_2)}$	Modulus of springs R_1 and R_2
A_1, B_1, A_2, B_2	Textile springs parameters
$\hat{m}, \hat{C}_1, \hat{C}_2$	Textile damper viscosity parameters
ASTM	American Society for Testing and Materials
IRSST	Institut de Recherche en Santé et en Sécurité du Travail du Québec

CHAPITRE 1

INTRODUCTION

1.1 Problématique

Les blessures aux mains, aux doigts et aux poignets comptent pour environ 18% de l'ensemble des lésions indemnisées par la CSST avec des déboursés de 138 millions de dollars pour les années 1998-2000 [1]. Dans certains secteurs industriels tels que l'industrie des produits en métal, des produits métal-électriques, des produits métalliques d'ornement, des services à l'extraction minière et des industries du bois, elles peuvent atteindre jusqu'à 29%. Les heurts, coincements, écrasements, coupures et piqûres avec des objets, machines ou déchets-rebuts-débris sont les principales blessures et les agents causaux prépondérants.

Le port de gants de protection permet de diminuer le nombre et la gravité des lésions aux mains. Toutefois, en pratique plusieurs facteurs rendent difficile leur utilisation dont leur manque de souplesse découlant du type de matériau utilisé en fabrication. En effet, la rigidité et l'épaisseur des matériaux peuvent exiger un plus gros effort pour effectuer une activité de préhension. De plus, il n'existe pas de matériaux de gants résistant aux agresseurs mécaniques multiples, coupure et piqûre simultanées. Pour se protéger, les travailleurs doivent ainsi souvent enfiler deux gants un par-dessus l'autre, l'un résistant à la coupure et l'autre résistant à la piqûre. Ce type de situation peut mener à une forte résistance, de la part des travailleurs, au port de gants de protection, ce qui a pour conséquence l'augmentation des blessures directes.

L'analyse de la littérature a montré qu'il n'existe pas de moyen actuellement permettant l'évaluation de la souplesse des gants de protection, pour ce fait on se propose d'en développer une et de la faire valider par des tests biomécaniques et des tests psychophysiques de perception.

Une deuxième méthode est également mise au point pour l'évaluation de la souplesse des gants portés serrés. D'autre part, on se propose d'étudier l'effet de la vitesse sur le comportement mécanique des matériaux de protection tels que les élastomères et les textiles. L'idée consiste à prédire l'évolution de la contrainte de sollicitation en fonction de la déformation lors d'un cycle charge-décharge à plusieurs vitesses et à des grandes déformations.

Dans ce chapitre, nous présentons une étude bibliographique concernant la souplesse des gants de protection, les matériaux utilisés dans la fabrication des gants de protection ainsi que l'état de l'art sur leurs lois de comportement. Nous soulignons également l'importance de ce projet, son originalité scientifique en se basant sur l'étude de la littérature, la méthodologie adoptée et les objectifs à atteindre.

1.2 Étude de la souplesse des gants de protection

L'étude de la souplesse des gants de protection composés de plusieurs matériaux différents est, à notre connaissance, un sujet peu exploré. La norme ISO 17235 [2] présente une méthode d'essai pour caractériser la souplesse du cuir. Pour sa part, la norme ISO 5979 [3] traite des textiles revêtus de caoutchouc ou de plastique. Dans ce dernier cas, la souplesse est caractérisée par la technique de la boucle plate. Il s'agit ici de former une boucle avec le matériau à tester pour ensuite le soumettre à une pression. L'hypothèse fondamentale de cette méthode est une relation inversement proportionnelle entre la souplesse et la hauteur de la boucle formée précédemment suite à l'application de ladite pression. Finalement, la méthode la plus utilisée dans l'industrie textile est celle développée par Kawabata en 1980 [4]. Dans ce cas, on caractérise la souplesse des tissus par des mesures de la rigidité en flexion uniaxiale du matériau.

Cependant, les sollicitations subies par les gants lorsqu'ils sont utilisés sont de type multidirectionnel et le comportement en souplesse dans ce cas peut ne pas être caractérisé de manière satisfaisante par des tests uniaxiaux. La norme ASTM D 4032 qui caractérise la

rigidité des tissus utilise une sonde cylindrique à tête plate pour forcer un carré d'étoffe dans un trou, ce qui correspond à des déformations equi-biaxiales [5]. Cette méthode a été modifiée afin de caractériser la souplesse des gants de protection et est décrite dans les articles 1-2 de cette thèse sous la dénomination « méthode multidirectionnelle » : elle devrait permettre de caractériser la souplesse des gants d'une manière qui corresponde mieux aux types de sollicitations subies lors de leur usage. Les résultats obtenus avec la méthode multidirectionnelle seront comparés aux données issues de mesures utilisant la méthode Kawabata ainsi qu'aux résultats des tests de perception et biomécanique.

De toutes les méthodes permettant d'évaluer la souplesse des matériaux textiles, aucune ne considère la complexité des effets produits par l'interface main-gant. Nelson et al. [6] ont comparé l'effet de la variation de l'épaisseur des gants sur la sensibilité tactile des individus. Bien qu'ils aient négligé la fatigue et ses effets sur la performance au travail à long terme, les auteurs ont conclu, lors de cette étude, que l'épaisseur des gants n'influence pas la capacité d'un individu à identifier la taille des objets qu'il touche ni à accomplir sa tâche dans les délais requis.

La plupart des études considérant les aspects biomécaniques ont évalué l'effet du port de gants sur le déploiement de la force maximale de préhension [7]. Selon Mital et al., le port d'un gant diminue de 7 à 30% la force maximale de préhension. Une étude récente confirme cette plage de valeurs (5-23%) pour différents types de gants [8]. Cependant, ce type d'évaluation requiert la production de plusieurs contractions maximales, supposant le concours de sujets sains (sans douleur) et motivés, ainsi qu'un nombre limité de contractions musculaires dans une même session de mesure afin de ne pas introduire l'effet confondant de la fatigue musculaire. De plus, une telle procédure d'évaluation des gants ne permet pas de contrôler les différences interindividuelles au niveau de la force maximale. Ceci rend la comparaison des résultats d'études difficile, voire impossible. Pour contourner ces difficultés, une méthode d'évaluation basée sur des mesures d'électromyographie (EMG) de surface a été proposée [9]. Elle consiste à mesurer le niveau d'activité musculaire (muscles fléchisseurs et extenseurs des doigts et du poignet) correspondant à une contraction sous-

maximale dont l'intensité (en proportion de la force maximale) est mesurée par un dynamomètre. On parvient ainsi à limiter le nombre de contractions maximales et à contrôler les différences interindividuelles au niveau de la force maximale. Les résultats obtenus par le biais de cette méthode ont été combiné à ceux obtenus par le test psychophysique de perception afin de valider les résultats de notre méthode mécanique [9].

1.3 Revue de la littérature sur les matériaux de protection

Dans cette section, on se propose de présenter une étude bibliographique concernant les matériaux utilisés dans la fabrication des gants de protection tels que les élastomères, les textiles et les composites. Nous proposons également un aperçu sur leurs lois de comportement mécanique tels que rapportées dans la littérature.

1.3.1 Matériaux élastomères

Cette partie introduit les matériaux type caoutchouc. Les applications des élastomères sont en effet multiples dans le milieu de travail tant pour ses propriétés élastiques que pour sa capacité à résister aux agressions multiples (mécaniques ou chimiques). Nous proposons ici un aperçu sur les différents types de ces matériaux. Nous présentons également une revue de la littérature sur leurs lois de comportement mécanique.

1.3.1.1. Qu'est ce que le caoutchouc?

Le caoutchouc naturel et ses homologues synthétiques, les élastomères, sont fortement répandus dans le domaine de l'industrie. La multiplicité des utilisations des élastomères provient surtout de leur capacité à subir des grandes déformations et leur résistance aux agressions multiples (coupure et/ou piqûre) présentes dans les postes de travail.
La terminologie ''élastomère'' regroupe des matériaux ayant des compositions chimiques différentes, mais une structure moléculaire et de propriétés mécaniques similaires. Le préfixe

''élasto'' rappelle les grandes déformations élastiques possible, tandis que le suffixe ''mère'' évoque leur nature de polymères, et donc leur constitution macromoléculaire [10, 11].

La matière première d'un élastomère peut être aussi bien naturelle que synthétique : le caoutchouc naturel est le produit de la coagulation du suc de différentes espèces végétales, principalement de l'hévéa. La fabrication des caoutchoucs synthétiques se fait par polymérisation. Les monomères de départ sont des molécules renfermant au moins une double liaison, ce qui permet un réarrangement des liaisons conduisant à la formation d'une longue chaîne macromoléculaire [10, 11].

Cependant, à l'état brut, le caoutchouc n'a pas de possibilité d'emploi pratique. Pour obtenir un produit présentant de meilleures propriétés, le caoutchouc brut doit subir un traitement chimique. Ce traitement, appelé vulcanisation, fut découvert accidentellement par Good Year en 1839 et est encore à la base de l'industrie de fabrication du caoutchouc. Au cours de la vulcanisation, les longues molécules en chaîne du caoutchouc se trouvent chimiquement unies à chaînes adjacentes par formation de liaisons pontales. Cette réticulation (pontage entre les chaînes) est nécessaire car sans elle le comportement serait de type fluide avec un écoulement libre des molécules les unes par rapport aux autres. Après polymérisation, en présence d'un système réticulant, les macromolécules forment un réseau tridimensionnel sans direction privilégiée. La capacité du caoutchouc vulcanisé à subir de forts taux de déformation est due essentiellement à la nature repliée de ces chaînes : elles peuvent être étirées et s'orienter elles mêmes dans la direction de l'allongement, les liaisons les poussant à revenir à l'état initial quand la contrainte est relâchée [11].

En pratique, le matériau élastomère est fabriqué en présence de plusieurs additifs. Certains sont nécessaires pour la vulcanisation (soufre, oxyde de zinc ...), d'autres permettent d'en accélérer le processus. Certains d'autres protègent (antioxygène, ...), ramollissent (huiles, graisses, acides gras, ...), ou encore colorent le vulcanisat (oxyde de zinc, lithopone, ...). Pour faciliter le mélange de ces ingrédients au caoutchouc brut, on peut ajouter une huile de mise en œuvre. La majorité des caoutchoucs utilisés pour les applications mécaniques

contiennent des charges pour améliorer l'élasticité du produit final sans augmenter sa résistance (ce sont des produits à base de carbonate de calcium ou de sulfate de baryum) ou améliorer la résistance du produit final (noir de carbone, oxyde de zinc, carbonate de magnésium ou différentes argiles) [11].

1.3.1.2. Exemples d'élastomères utilisés dans les gants de protection

La majorité des gants de protection qu'on retrouve sur le marché sont fabriqués en caoutchouc naturel ou en néoprène ou en nitrile ou en butyle. Pour cette raison, nous allons présenter dans cette partie uniquement ces quatre élastomères.

Polychloroprène

Le polychloroprène est généralement connu sous son nom commercial Néoprène. Il se distingue par une bonne résistance aux huiles. C'est le premier élastomère synthétique, ou caoutchouc qui a eu un succès commercial. Il a été inventé par Arnold Collins, pendant qu'il travaillait avec l'homme qui a inventé le nylon, Wallace Carrothers. Il se caractérise par une densité aux alentours de 1240 kg/m^3 et une température de transition vitreuse Tg avoisinant -50°C. Il est fabriqué à partir du monomère chloroprène (Figure 1.1).

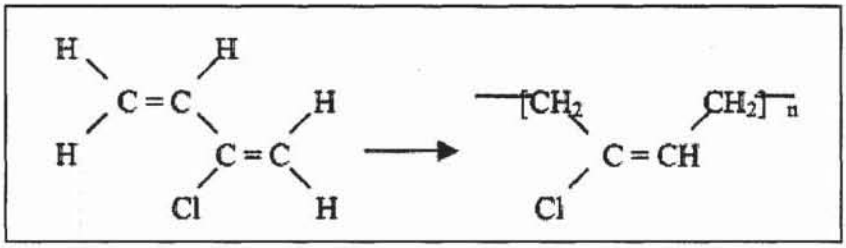

Figure 1.1 Polymérisation du Polychloroprène

Nitrile

Ce caoutchouc est un copolymère de butadiène et d'acrylonitrile (Figure 1.2). Il est remarquablement résistant aux huiles et aux graisses. Sa résistance à la déchirure est plus faible que celle du caoutchouc naturel [12-19].

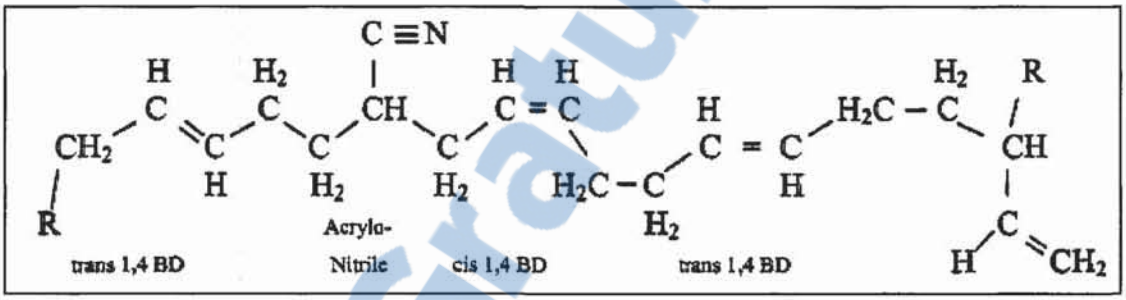

Figure 1.2 Formule du Nitrile

Caoutchouc naturel

Le caoutchouc naturel est le produit de la coagulation du suc de différentes espèces végétales, principalement de l'hévéa. Du point de vue chimique, le caoutchouc naturel est un produit de polymérisation de l'isoprène de formule chimique $(C_5H_8)_n$, n ayant une valeur d'environ 10000, et C_5H_8 étant le monomère isoprène (Figure 1.3). C'est un polymère amorphe dont la température de transition vitreuse Tg est aux alentours de -70°C.

Le caoutchouc naturel se distingue par une grande élasticité ainsi qu'un faible hystérésis dans la zone des petites déformations de la courbe contrainte déformation. Il se caractérise aussi par une bonne résistance à la déchirure et à l'abrasion, mais Il se gonfle sous l'effet du pétrole, du benzène et des huiles lubrifiantes. Il est connu également pour sa faible résistance à l'oxydation et à l'ozone [12-19].

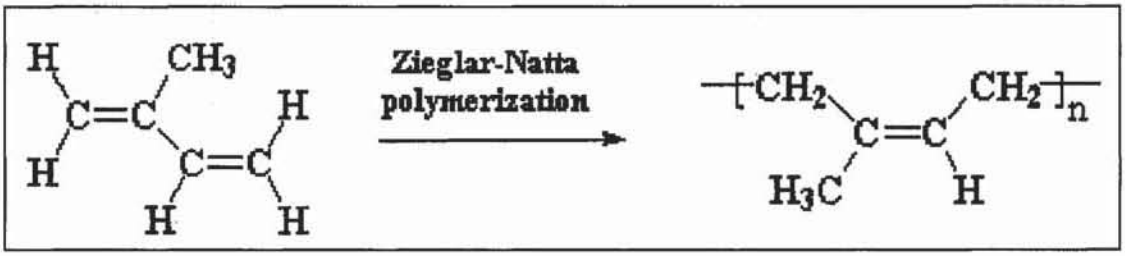

Figure 1.3 Polymérisation du Polyisoprène

Butyle

Le butyle représente un caoutchouc très utilisé dans la fabrication des gants de protection contre les solvants et les agressions de nature chimique. Il a été élaboré à la fin des années 30 par Thomas et Sparks [20]. C'est un copolymère d'iso butylène et d'isoprène (Figure 1.4). Il se caractérise par ses bonnes propriétés mécaniques et physique, il présente une excellente imperméabilité aux gaz et une bonne résistance aux agressions chimiques et à l'oxydation. Cependant, il a une faible résistance aux solvants non polaires. Sa structure chimique est présentée dans la Figure 1.4.

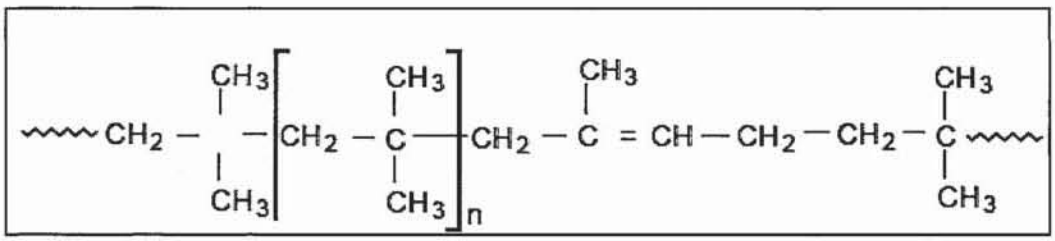

Figure 1.4 Formule du butyle

1.3.1.3 Revue de la littérature sur le comportement mécanique des matériaux élastomères

Les matériaux élastomères sont souvent considérés comme isotropes, incompressibles et hyper élastiques. Leur lois de comportement en terme de contrainte déformation est généralement déduite à partir de l'expression de la fonction d'énergie correspondante de la façon suivante :

$$\begin{cases} \sigma_{ii} = 2\left(\lambda_i^2 \dfrac{\partial W}{\partial I_1} - \dfrac{1}{\lambda_i^2}\dfrac{\partial W}{\partial I_2}\right) + p \\ \sigma_{ij} = 0 \end{cases} \tag{1.1}$$

avec $\lambda_1, \lambda_2, \lambda_3$ sont les extensions dans les trois directions principales du matériau et p désigne la pression hydrostatique. I_1, I_2, I_3 représentent les invariants de déformation, leurs expressions sont données par le système (1.2). Plus de détails concernant l'obtention de cette équation sont présentés dans l'ANNEXE I :

$$\begin{cases} I_1 = \lambda_1^2 + \lambda_2^2 + \lambda_3^2 \\ I_2 = \lambda_1^2\lambda_2^2 + \lambda_2^2\lambda_3^2 + \lambda_1^2\lambda_3^2 \\ I_3 = \lambda_1^2\lambda_2^2\lambda_3^2 \end{cases} \tag{1.2}$$

avec I_3 est souvent égale à 1 du fait de l'incompressibilité des élastomères.

Dans le cas d'un test de traction unidirectionnel, on aura : $\lambda_1 = \lambda, \lambda_2 = \lambda_3 = 1/\lambda^{1/2}$. La contrainte réelle σ, déterminée à partir de l'équation précédente, devient :

$$\sigma = 2\left(\lambda^2 - \frac{1}{\lambda}\right)\left(\frac{\partial W}{\partial I_1} + \frac{1}{\lambda}\frac{\partial W}{\partial I_2}\right) \tag{1.3}$$

Dans ce qui suit, nous présentons un aperçu sur les fonctions d'énergie les plus connues. En effet, de nombreuses formes de l'énergie de déformation ont été proposées dans la littérature. Certaines se basent sur une théorie statistique, d'autres sont purement phénoménologiques.

Le modèle de Rivlin généralisé [21] est donné par le développement en série suivant :

$$W = \sum_{i+j=1}^{N} C_{ij}(I_1 - 3)^i (I_2 - 3)^j \tag{1.4}$$

Ce type de loi est généralement le plus utilisé. Pour $N = 3$, on a généralement une bonne corrélation avec l'expérience.

En pratique, la plupart des lois polynomiales utilisées correspondent à un cas particulier du développement de Rivlin. Par exemple, en ne gardant que le premier terme de développement, on obtient la loi Néo Hookéenne:

$$W = C_{10}(I_1 - 3) \tag{1.5}$$

qui a d'abord été élaborée à partir de la théorie statistique en considérant que le caoutchouc vulcanisé est un réseau tridimensionnel de longues chaînes moléculaires connectées en quelques point. Le modèle Néo Hookéen permet d'avoir une bonne corrélation pour des taux de déformation avoisinant les 50%.

Le second cas particulier du développement de Rivlin correspond au modèle phénoménologique de Mooney Rivlin [22], très utilisé dans l'industrie des élastomères. Dans ce cas, on prend les 2 premiers termes du développement de Rivlin, ce qui permet d'écrire :

$$W = C_{10}(I_1 - 3) + C_{01}(I_2 - 3) \tag{1.6}$$

Avec cette loi, on obtient une bonne corrélation avec l'expérience jusqu'à l'ordre de 150 % de déformation.

De son côté, Yeoh [23, 24] a proposé une fonction d'énergie à 3 coefficients où le second invariant n'apparaît pas. L'énergie proposée s'écrit de la façon suivante :

$$W = C_{10}(I_1 - 3) + C_{20}(I_1 - 3)^2 + C_{30}(I_1 - 3)^3 \tag{1.7}$$

De leurs cotés, Arruda et Boyce [25] ont proposé une fonction d'énergie qui permet d'avoir de bonne corrélation avec l'expérience jusqu'à la rupture. Cette fonction d'énergie est représentée par l'expression suivante :

$$W = \mu\left[\frac{1}{2}(I_1 - 3) + \frac{1}{20n}(I_1^2 - 9) + \frac{11}{1050n^2}(I_1^3 - 27) + \ldots\right] \tag{1.8}$$

avec μ représente le module de cisaillement et n le nombre de segment ayant la même longueur d'une chaîne moléculaire.

D'autres chercheurs ont exprimé l'énergie de déformation en fonction des élongations principales au lieu des invariants. Par exemple, Ogden [26, 27] a proposé la fonction suivante:

$$W = W(\lambda_1, \lambda_2, \lambda_3) = \sum_{n=1}^{N} \frac{\mu_n}{\alpha_n}(\lambda_1^{\alpha_n} + \lambda_2^{\alpha_n} + \lambda_3^{\alpha_n} - 3) \tag{1.9}$$

où N désigne le nombre de termes de l'énergie de déformation, les μ_n désignent les coefficients de cisaillement et les α_n sont des constantes sans dimension. Par linéarisation, on obtient la relation suivante entre le coefficient de cisaillement linéaire μ (pente à l'origine lors de l'essai de cisaillement) et les coefficients de l'énergie de déformation d'Ogden.

$$2\mu = \sum_{n=1}^{N} \mu_n \alpha_n \text{ avec } \mu_n \alpha_n > 0 \text{ et } n=1 \ldots N \tag{1.10}$$

En général, il est possible d'obtenir une très bonne corrélation avec les résultats expérimentaux pour $N=3$.

Un autre exemple d'énergie de déformation développée en fonction des élongations est l'expression proposée par Valanis et Landel [28]. Les auteurs ont postulé que la fonction d'énergie peut être écrite comme une somme de 3 fonctions séparables $W(\lambda_k)$, $k=1...3$:

$$W = w(\lambda_1) + w(\lambda_2) + w(\lambda_3) \tag{1.11}$$

1.3.1.4 Propriétés élastiques des élastomères

Une propriété mécanique particulièrement prisée des matériaux élastomères est leur remarquable élasticité, due à leurs structures moléculaires. Le caoutchouc peut subir des grandes déformations et revenir ensuite à sa configuration initiale. On peut toutefois remarquer que le matériau n'est pas parfaitement élastique. La Figure 1.5 présente à titre d'illustration le résultat d'un essai cyclique, à vitesse de déformation constante, sur différents types d'élastomères. On observe une différence entre la contrainte mesurée au cours de la charge, et la contrainte mesurée lors de la décharge. Pour un chargement cyclique, il y aura donc dissipation d'énergie sous forme de chaleur, la quantité d'énergie dissipée correspond à l'aire entre les courbes. Cette hystérésis, (ie le travail représenté par la surface comprise entre les courbes d'application et de relâchement des contraintes dans un cycle) est présente pour tous les caoutchoucs.

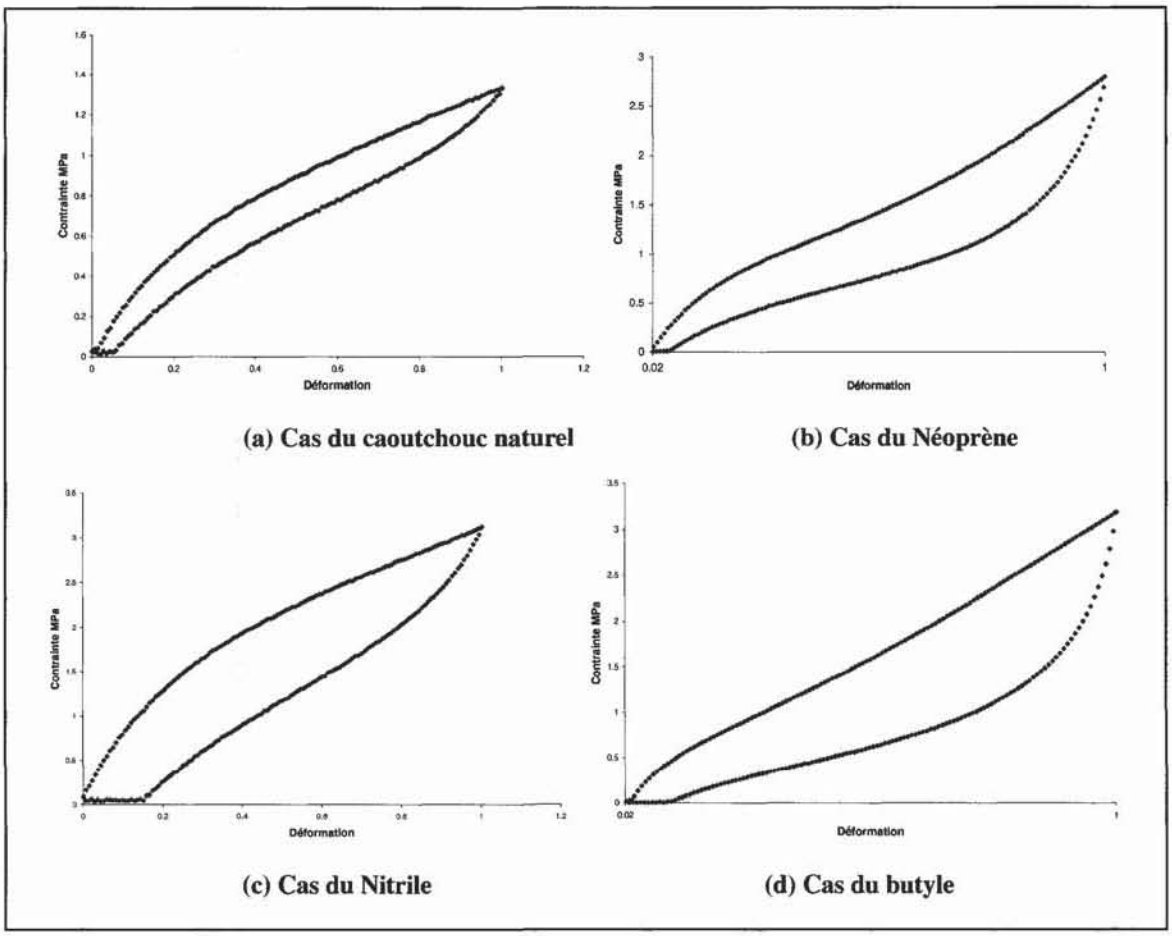

Figure 1.5 Boucle d'hystérésis des élastomères

1.3.2 Matériaux textiles

Nous proposons ici un aperçu sur les différents types de renforts textiles utilisés dans la fabrication des gants de protection. Nous présentons également une étude bibliographique sur les modèles développés dans la littérature pour l'étude du comportement mécanique de ces matériaux.

1.3.2.1. Les tissus

Les tissus sont réalisés sur des métiers à tisser par entrelacement de fils, dans deux directions perpendiculaires. On appelle chaîne le fil placé dans le sens de la longueur du tissu, et trame celui entraîné transversalement par la navette pour former le motif du tissage. Le mode d'entrecroisement de ces fils est appelé armure. On peut distinguer :

- La toile : le fil de trame passe alternativement dessus puis dessous chaque mèche de chaîne. Le produit obtenu est plat et relativement rigide mais peu déformable.
- Le sergé n×m : le fil de trame passe au dessous de m fils de chaîne, chacun passant à son tour sur n fils de trames. Les points de liage successifs forment une diagonale. Cette armure est à la fois souple et dense.
- Le satin de n: chaque fil de trame flotte au dessus de (n-1) fils de chaîne; les points de liage ne sont pas consécutifs. Ces tissus sont très souples, plats et déformables.

1.3.2.2. Les tricots

Les tricots sont formés par bouclage d'un ou de plusieurs fils et offrent de plus grandes possibilités de motifs que le tissage. Leur principale caractéristique est leur très grande déformabilité. Ces tricots sont classés selon deux grandes familles [29-31]: les tricots à mailles cueillies (weft knits) et les tricots à mailles jetées (warp knits) (Figure 1.6). Les géométries des mailles élémentaires ainsi que les propriétés mécaniques des deux types de tricot sont différents. Leong et Ramakrishna [30, 31] ont mis en évidence une description exhaustive des différents procédés de tricotage. Notons qu'il existe deux techniques de fabrication des tricots à mailles cueillies : le tricotage plan et le tricotage circulaire. Nous trouvons également dans [31] une classification des différents tricots existants.

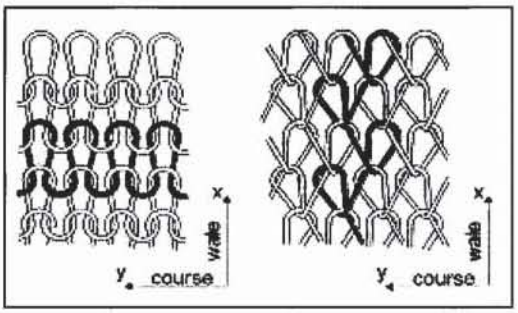

Figure 1.6 Jersey simple de type plain weft (à gauche) et tricot de type warp (à droite) : tirée de [29]

L'élasticité représente une propriété mécanique particulière des tricots, due à la nature de liage des fils. Le tricot peut subir des grandes déformations, mais moins importantes que les élastomères, et revenir ensuite à sa configuration initiale. On peut également remarquer, d'une façon similaire aux élastomères, que le tricot n'est pas parfaitement élastique. La Figure 1.7 présente à titre d'illustration le résultat d'un essai cyclique, à vitesse de déformation constante, sur un exemple de tricot utilisé dans la fabrication des gants de protection. On observe une différence entre la contrainte mesurée au cours de la charge, et la contrainte mesurée lors de la décharge. Pour un chargement cyclique, il y aura donc dissipation d'énergie sous forme de chaleur, la quantité d'énergie dissipée correspond à l'aire entre les courbes.

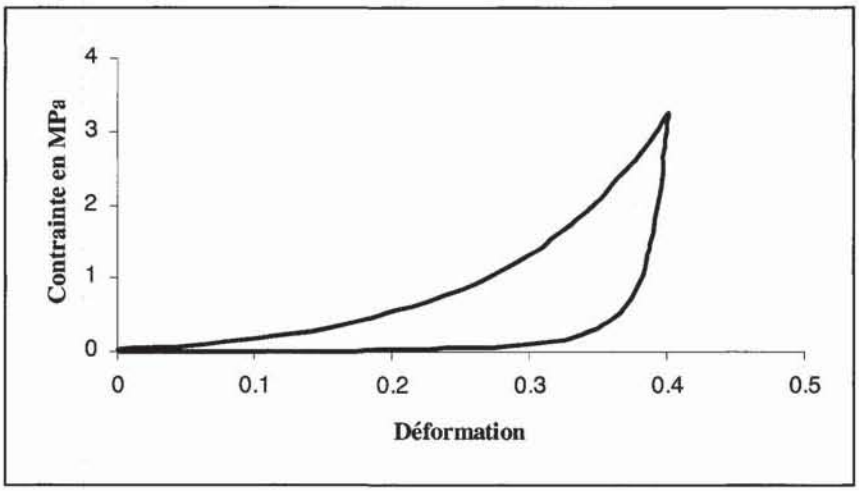

Figure 1.7 Exemple de boucle d'hystérésis de tricot

1.3.2.3 Les fibres textiles dans les gants de protection

Les fibres qui sont très utilisées dans la fabrication des vêtements de protection d'une façon générale et les gants de protection d'une façon particulière sont le Kevlar®, la Spectra® et le cotton.

Fibre de kevlar®

Le Kevlar® est la nomination commerciale du poly-para-phénylène téréphtalamide déposé par la société Dupont en 1965. C'est un polymère hautement cristallin, constitué de noyaux aromatiques séparés par des groupements amide (Figure 1.8). Il appartient au groupe des fibres d'aramides. Il est insoluble dans la majorité des solvants chimiques et thermiquement stables au delà de 545 °F. Sa densité est aux alentours de 1440 kg/m^3. Le poly-para-phénylène téréphtalamide possède un réseau de liaisons hydrogène entre les chaînes polymères qui lui confère une grande rigidité, supérieure à celle de l'acier. Les caractéristiques mécaniques de cette fibre sont sa faible élongation (de 2 à 4 %), son haut module (de 80 à 190 GPa) et sa bonne résistance à la traction (de 2.8 à 3.6 GPa). Toutefois,

cette fibre se caractérise par une faible résistance aux UV à cause de la présence des ponts d'amides [32-34].

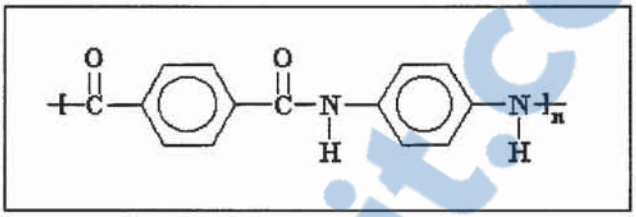

Figure 1.8 Formule du Kevlar®

La fibre de Kevlar® est très utilisée dans la fabrication des vêtements de protection pour ses bonnes propriétés mécaniques et thermiques. Elle est également utilisée dans d'autres domaines comme par exemple les matériaux composites dans des applications aéronautiques.

Fibre Spectra ®

La fibre Spectra® est la nomination commerciale du polyéthylène à haut poids moléculaire, connue sous l'abréviation du UHMWPE (Ultra-High Molecular Weight Polyethylene). La Figure 1.9 montre sa structure chimique. Sa densité volumique est de 970 kg/m^3. Sa déformation à la rupture est de 2.7 à 3 %. Son module varie de 2.6 à 3 GPa. Cette fibre se distingue par ses bonnes propriétés mécanique, toutefois elle est instable thermiquement. Sa température de fusion est de l'ordre de 149 °C [33, 34].

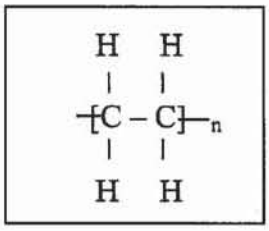

Figure 1.9 Formule du polyéthylène

Cotton

Le coton est une fibre cellulosique, qui est utilisée dans la majorité de nos vêtements, est formé à partir du monomère de glucose. C'est une fibre qui est connu par le fait qu'elle ne fond pas et ne casse pas facilement dans l'eau. La densité de coton est de 1540 kg/m^3, sa température de décomposition est de 255 °C. Son élongation à la rupture est de 3 à 8 %, son module d'Young peut varier de 5.3 jusqu'à 8 GPa [33].

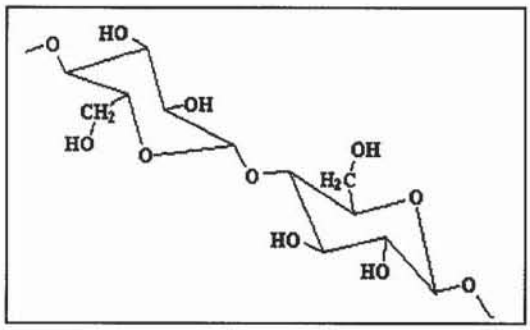

Figure 1.10 Formule de cellulose

1.3.2.4 Revue de la littérature sur la modélisation du comportement mécanique des matériaux textile

Dans la littérature, des modèles ont été développés à l'échelle microscopique pour caractériser le comportement des mèches, d'autres sont plutôt à l'échelle mésoscopique pour caractériser le comportement au niveau de la maille élémentaire constituant le textile. Plus récemment, des modèles rhéologiques ont été développés afin de caractériser le comportement viscoélastique des matériaux textiles.

Modèles microscopiques

À l'échelle microscopique, le but de ces modèles consiste à caractériser le comportement des mèches. Ce comportement est très complexe, ceci étant dû à l'effet de structure des centaines de fibres en contact avec leurs voisines. La difficulté réside au niveau de la prise en compte de tous ces détails. Dans le cas de milieux fibreux secs, l'approche pratiquée est la mise en œuvre des outils numériques, à savoir l'utilisation de modeleurs géométriques couplés à des codes de calcul éléments finis. Malheureusement, cela conduit à l'heure actuelle à des modèles trop lourds dont les temps de calcul sont trop importants. C'est pourquoi cette approche est peu pratiquée. Dans le cadre d'une étude sur les câbles, Duville [35] a formulé des éléments finis spéciaux pour gérer le contact et ainsi modéliser un paquet de fibres avec des temps de calcul extrêmement lents. D'autres éléments, dénommés digitaux, sont construits par Wang et Sun [36] pour modéliser le procédé de tressage. Chaque mèche est alors considérée et mise en contact avec les autres pour former la tresse résultante.

Modèles mésoscopiques

À l'échelle mésoscopique, la mèche est souvent assimilée à un milieu continu et c'est la caractérisation du comportement de la maille élémentaire qui est recherchée. Les deux difficultés résident dans le choix d'un comportement traduisant le caractère fibreux de la mèche et dans la définition de la géométrie de la maille élémentaire. Comme le comportement de la maille élémentaire dépend de l'effet de structure dû à l'évolution de cette géométrie, qui n'est connu qu'à l'instant initial, c'est surtout sur ce dernier aspect que portent les efforts des différents chercheurs. Ainsi, dans la littérature, l'étude du comportement de la maille élémentaire va systématiquement de pair avec les modèles descriptifs de sa géométrie.

Modèles éléments finis

Le principe général de ces modèles se base sur le maillage de géométries complexes et la prise en compte du contact entre les mèches, ce qui rend ce problème complexe. Par exemple, nous devons à Hanklar [37] la construction de plusieurs modèles éléments finis relatifs à des mailles de tissu différentes, les mèches étant assimilées à des milieux continus orthotropes. L'étude est menée en traction biaxiale. Le cisaillement est, lui, étudié, par Peng et Cao [38]. Boissé a étudié les deux comportements biaxial et en cisaillement des textiles tricotés et tissés [39, 40].

Modèles analytiques

Ces modèles sont les plus anciens et proviennent du milieu du textile, mais ils sont toujours d'actualité et continuent d'être développés à l'heure actuelle. Ils consistent à faire des hypothèses sur la géométrie de la maille élémentaire et sur sa cinématique afin d'en dériver des modèles mécaniques. Nous devons à Kawabata [41] et à Postle [42] les modèles analytiques de tissus et de tricots en grande déformation. La géométrie des tricots y est approximée par un ensemble de portions de cercle et de droites.

Modèles rhéologique

Ces modèles sont tous récents, ils consistent à simuler le matériau à un système composé de plusieurs éléments (ressort et amortissement) selon le cas. Par exemple, Matsu [43] a utilisé le modèle à 4 éléments pour analyser la relaxation des contraintes dans le cas des matériaux textile. Le même modèle a aussi été utilisé pour analyser les chargements cycliques sur des structures textiles tricotées. Ces types de modèle sont également utilisés dans l'étude du comportement viscoélastique d'autres types de matériaux comme les élastomères ou encore les matériaux composites.

1.3.3 Composites de protection

Généralement, les fibres comme le Kevlar ou la Spectra se distinguent par leurs très bonnes performances mécaniques dans la direction des fibres en plus d'une très bonne résistance à la coupure. Toutefois ces fibres se caractérisent par une faible élongation à la rupture, en plus ils sont perméables à l'eau et aux huiles. D'autre part, les élastomères ont des performances mécaniques en terme de module, résistance à la coupure et de contrainte à la rupture beaucoup plus faible que le Kevlar et la spectra, cependant ils ont de meilleures performances en terme d'imperméabilité à l'eau et aux huiles et de plus grandes élasticités. La combinaisons des deux permettrait d'avoir le composite et de bénéficier des avantages de chacun des deux dans la nouvelle structure composite. Souvent sur le marché, on trouve le Cotton, le Kevlar ou la Spectra tricoté est combiné avec le poly isoprène, néoprène ou le Nitrile [44, 45]. Ces composites sont obtenus par le principe de trempage (Figure 1.11). Les travaux existants dans la littérature portent en particulier sur les performances en terme de résistance aux agressions mécaniques tels que la coupure et/ou piqûre de ces matériaux[46].

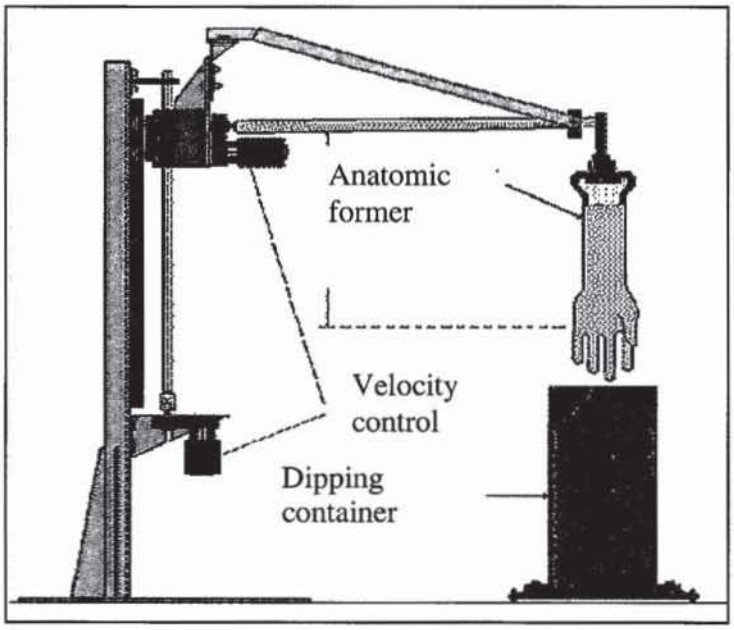

Figure 1.11 Processus de fabrication des composites de protection

1.4 Importance de l'étude et méthodologie adoptée

1.4.1 Importance de l'étude

La majorité des travaux touchant les performances des gants de protection rapportés dans la littérature ont porté sur les performances mécaniques des gants de protection tels que la résistance à la coupure et/ou à la perforation. Les études qui ont porté sur la souplesse des gants jusqu'à date sont de nature biomécanique à notre connaissance. L'objet principal de ce travail est de proposer de nouvelles méthodes mécaniques permettant l'évaluation de la souplesse des gants de protection en plus de la proposition de nouvelles lois de comportement mécanique des matériaux de protection tels que les élastomères et les textiles.

1.4.2 Présentation de l'étude

La première phase de cette thèse consiste à proposer de nouvelles méthodes d'essai pour la caractérisation de la souplesse des gants de protection formés de matériaux différents. La deuxième phase portera sur la modélisation du comportement mécanique des matériaux de protection à des grandes déformations et à différentes vitesses de sollicitation.

Matériaux

Au total, 28 paires de gants de modèles différents ont été sélectionnées parmi les produits offerts par les compagnies Best et Ansell de manière à couvrir un large éventail de souplesse. Le Tableau 1.1 donne les noms des différents modèles de gants, ainsi que leur épaisseur totale (couche paume et dos incluant une éventuelle doublure) mesurée au milieu de la paume et les matériaux constituant ces gants.

Les épaisseurs totales des gants se répartissent entre 1.1 et 8.6 mm. En termes de matériaux, la majorité des modèles ont une structure composite, comprenant une doublure, le plus souvent tricotée, imprégnée ou enduite d'un polymère. Les autres types de gants sont soit faits d'élastomère pur ou d'un tricot seul.

Le gant Best 4000 P a été sélectionné pour la deuxième phase portant sur l'étude du comportement mécanique des matériaux de protection (articles 3 et 4).

Tableau 1.1 Modèles de gants testés, épaisseur et matériaux

Modèle	Modèle	Épaisseur (mm)	Matériaux
Ansell	Canners & Handlers # 392	1,1	Caoutchouc naturel
Ansell	Hyflex 11-900	2,0	Mousse de nitrile sur tricot de coton
Ansell	Hycron 27-607	2,6	Nitrile sur tricot de coton
Ansell	Golden Grab It 16-300	3,2	Caoutchouc naturel et cuir sur tricot de coton
Ansell	Scorpio 8-352	3,3	Néoprène sur tricot de coton
Ansell	Grab It Safe 28-362	3,4	Caoutchouc latex naturel sur tricot de coton/kevlar
Ansell	Seams-Rite 20-115	3,6	PVC et doublure de coton
Ansell	PowerFlex 80-100	3,6	Caoutchouc naturel sur tricot de coton
Ansell	Snorkel 4-412	3,6	PVC/ nitrile sur tricot de jersey
Ansell	Hyd Tuf 52-547	3,7	Doublure en jersey, dos en coton, enduit en nitrile
Ansell	Grab It 6-620	4,1	Caoutchouc naturel sur doublure en jersey et coton

Ansell	The Duke 70-982	4,4	Tricot Safeknit CX et renforts en cuir
Ansell	Crusader 42-325	4,5	Nitrile sur isolant feutre non-tissé
Ansell	GoldKnit Kevlar 70-225	4,5	Tricot en kevlar
Ansell	Neox 9-022	6,4	Néoprène sur tricot en coton
Ansell	Winter Monkey Grip 23-193	6,4	PVC et doublure de jersey
Best	Nitri-Solve® 747	1,2	Nitrile
Best	Nitri-Pro® 7000P	1,7	Nitrile sur tricot de coton
Best	The Original Nitri-Flex® 4000P	1,7	Nitrile sur tricot de coton
Best	Natural Rubber Latex HD® 55	2,1	Caoutchouc naturel
Best	Ultraflex Nitrile® 22-R	2,6	Nitrile sur tricot de coton
Best	Neo Hyde® 361	3,3	PVC sur tricot de coton
Best	Cannonball® 803	3,6	PVC et doublure en jersey
Best	KPG® 960	3,7	PVC sur tricot de coton
Best	Cannonball® 812M	3,8	PVC sur doublure en jersey
Best	Skinny Dip Aramid® 4811	4,3	Caoutchouc naturel sur tricot kevlar aramid
Best	Neo Grab® 6780-R	4,8	Néoprène sur doublure isolante
Best	Insulated Snowman 2950	8,6	Nitrile sur doublure molletonnée

Présentation des articles

- Le premier article, intitulé : «*Characterization of protective gloves stiffness: Development of a multidirectional deformation test method* » publié dans le journal Safety Science consiste à proposer une nouvelle méthode mécanique permettant l'évaluation de la souplesse des gants de protection, permettant de remplacer ainsi le recours à des tests biomécaniques faisant appel à des sujets humain.

- Le deuxième article, intitulé : *«Evaluation of the Flexibility of Protective Gloves »* publié dans le journal ''International Journal Of Occupational Safety And Ergonomics'' consiste à évaluer la souplesse des gants de protection par le biais de deux méthodes développées au sein de notre laboratoire.

- Le troisième article, intitulé : «Prediction of stress-strain behaviour and energy dissipation of elastomers at large deformations » a été soumis au Journal of Applied Polymer Science. L'objet de cet article consiste à prédire le comportement mécanique des matériaux élastomères et en particulier le Nitrile en terme de contrainte-déformation lors d'un cycle charge-décharge à des grande déformations et à différentes vitesses par le biais du modèle rhéologique de Zener modifié et pouvoir ainsi calculer l'énergie dissipée à des grande déformations et à différentes vitesses

- Le quatrième article, intitulé : «Prediction of stress-strain behaviour and energy dissipation of textile fabrics at large deformations » va être soumis au Journal of Applied Polymer Science. L'objet de cet article consiste à prédire, d'une façon analogue aux élastomères, le comportement mécanique des matériaux textiles en terme de contrainte-déformation lors d'un cycle charge-décharge à des grandes déformations et à différentes vitesses par le biais du modèle rhéologique de Zener et déduire par la suite l'énergie dissipée.

Enfin, une conclusion générale portera sur les principaux résultats et les différentes perspectives qui pourrait être envisagées à l'issu de ce travail.

CHAPITRE 2

ARTICLE 1 : CHARACTERISATION OF PROTECTIVE GLOVES STIFFNESS: DEVELOPMENT OF A MULTUDIRECTIONAL TEST METHOD

Article tel que publié dans la revue SAFETY SCIENCE volume **46** N°7 en 2008

Lotfi Harrabi[a], Patricia I. Dolez[a], Toan Vu-Khanh[a], Jaime Lara[b], Guy Tremblay[a], Sylvie Nadeau[a] and Christian Larivière[b]

[a] École de technologie supérieure, 1100 rue Notre-Dame Ouest, Montréal, Québec, Canada H3C 1K3

[b] Institut de recherche Robert-Sauvé en santé et en sécurité du travail, 505 boul. de Maisonneuve Ouest, Montréal, Canada H3A 3C2

Résumé

La méthode multidirectionnelle, présentée dans cet article, permet l'évaluation de la souplesse des gants de protection. Les résultats issus de cette méthode ont été comparés à ceux issus d'un test de perception impliquant des sujets humains. 28 modèles de gants, couvrant un large éventail de souplesse, ont été analysés par le biais de deux méthodes mécaniques : la méthode KAWABATA et la nouvelle méthode multidirectionnelle. Les corrélations obtenues entre la méthode multidirectionnelle et le test de perception sont plus élevées (r=0.93) qu'avec le test KAWABATA dans le deux directions longitudinale et transversale des gants (r=0.79 et 0.76). Quelques facteurs peuvent expliquer le fait que la méthode multidirectionnelle caractérise la souplesse des gants de protection de manière plus proche de ce qui est mesuré avec les sujets humains par rapport à la méthode Kawabata. D'une part, elle soumet les gants à des déformations multidirectionnelles, qui simulent de manière plus réaliste les conditions d'utilisation réelles des gants, alors que la technique Kawabata applique des flexions uniaxiales. D'autre part, elle teste les gants dans leur intégralité, c'est-à-dire que les mesures de souplesse sont faites sur les deux épaisseurs paume et dos en même temps. Ce test, en plus d'apporter essentiellement la même information que

les tests avec sujets humains, est beaucoup plus simple, requiert moins de ressources (moins coûteux) car moins sujet aux variations dans les mesures, et est plus sensible aux différences fines en terme de souplesse.

Abstract

A test method was developed to characterize the stiffness of protective gloves as perceived by users by applying multidirectional deformations to the material to simulate the behavior of gloves in use. Twenty eight protective glove models covering a broad range of stiffness were characterized with two mechanical methods: the new multidirectional test and the Kawabata Evaluation System for Fabrics (KESF) based on uniaxial deformations. Some differences were observed between the longitudinal and transversal KESF measurements even for isotropic materials. A psychophysical evaluation test was also carried out by thirty subjects in order to rank the gloves. The correlation between the psychophysical evaluation and the new multidirectional test method was higher ($r = 0.93$) than those obtained with the KESF measurements along the longitudinal and transversal directions (respectively $r = 0.79$ and 0.76). This better performance of the new test method is attributed to the difference in the type of applied deformations: uniaxial for the KESF test vs. multidirectional for the test method developed in this study. Thus, this multidirectional test method, which applies more realistic mechanical deformations, appears as a promising tool for the characterization of protective gloves stiffness as perceived by users.

2.1 Introduction

Hand injuries represent a major source of accidents, in particular at the workplace. In Quebec between 2001 and 2004, they accounted for about 20% of all occupational injuries compensated for by the Provincial Occupational Health and Safety Board (Commission de la Santé et de la Sécurité du Travail du Québec, 2003). Wearing protective gloves can reduce the occurrence of such injuries, but it often involves additional muscular constraints and reduced dexterity, two side-effects related to the glove's material stiffness (Bishu and Muralidhar, 1999; Buhmann et al., 2000; Cadoret and Smith, 1996). Furthermore, increased muscular constraints due to protective gloves have been associated to tendinitis (Chaffin et al., 1999). As a consequence, workers may choose not to wear protective gloves, exposing themselves to high risks of hand injuries.

Stiffness is one of the major properties that define how a glove interferes with the worker's ability to perform his tasks. Studies considering the biomechanical aspects of protective gloves use the effect of wearing gloves on the deployment of the maximum grip force (Kovacs et al., 2002; Mital et al., 1994; Nelson and Mital, 1995; Rock et al., 2001; Sudhakar et al., 1988). According to Mital et al. (1994), wearing protective gloves reduces the maximum gripping force by 7 to 30%. A recent study confirms this interval (5-23%) for a whole range of glove models (Rock et al., 2001). However, this type of evaluation requires for the subject to exert several maximum muscular contractions, thus limiting the number of contractions in each measurement session and asking for very fit subjects. Moreover, procedures involving the use of human subjects are prone to high levels of inter individual variability, leading to large uncertainty in the measurements.

Several mechanical test methods have been used for characterizing film and fabric flexibility. Most of them are based on uniaxial bending, which may not be representative of the type of deformations subjected to a glove in usage. For example, the Kawabata Evaluation System for Fabrics (KESF) includes a test measuring the bending moment of a strip of material as a function of its curvature, thus providing the uniaxial bending rigidity which is proportional to

the material stiffness (Kawabata, 1980). On the other side, the test method used in the ISO 5979 standard (1982) measures the uniaxial flexibility of elastomer coated textile fabrics; its principle consists in forming a loop with the material, the maximum height formed by this loop being proportional to the material stiffness. Finally, in the ASTM D 1388 standard (1996), which characterizes the flexibility properties of fabrics, the bending length is measured according to two procedures, the cantilever test and the heart loop test, which allows the flexural rigidity to be calculated.

When protective gloves are worn, they are subjected to uniaxial deformations as well as equibiaxial ones, as can be seen in Figure 2.1. Stiffness measured with a uniaxial deformation test may not describe well the glove performance in service. Characterization methods making use of multidirectional deformations are thus required.

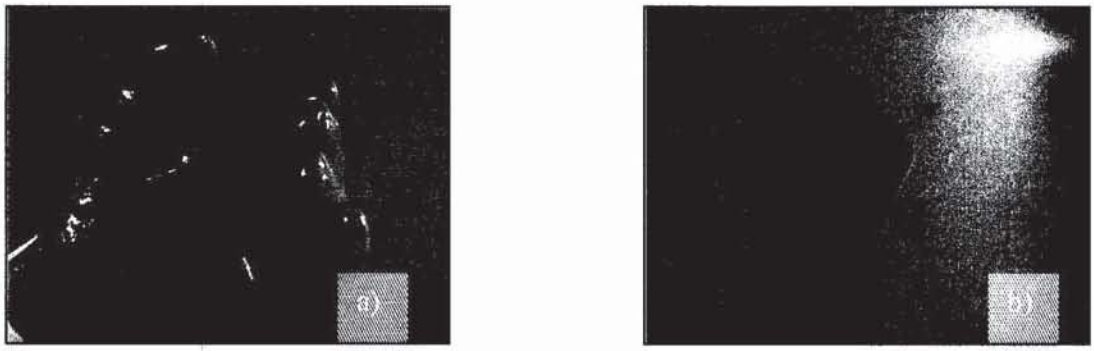

Figure 2.1 Folds (a) and biaxial deformations (b) of worn protective gloves

The test method used in the ASTM D 4032 standard (1994) makes use of a circular bend procedure for measuring the stiffness of fabrics, thus creating multidirectional deformations. A flat headed cylindrical probe forces a folded piece of the fabric sample through an orifice in a platform. The maximum force required to push the fabric through the orifice is measured and can be used as an indication of the fabric stiffness. Some authors have calculated the work corresponding to the entire passing of the piece of fabric through the orifice, which is proportional to the material stiffness (Killinc-Balci, 2004). However, the much larger thickness of gloves, in particular considering the presence of fingers, prevents

the use of this method as it is. In addition, the flat headed shape of the probe does not generate deformations typical of what is sustained by gloves in use and may create unnecessary stress concentration.

In this study, we propose a new multidirectional test method, inspired from the ASTM D 4032 standard method, which allows for the measurement of protective gloves stiffness. This new method is described below as the free-deforming multidirectional technique and has been used to measure the stiffness of twenty eight models of protective gloves. For a comparison, the stiffness of these gloves was also characterized by the KESF along both directions (longitudinal and transversal).

Since the perception of users is a major contributor to protective glove wearing, the stiffness measurements provided by both mechanical methods, the developed free-deforming multidirectional technique and the KESF, have been compared to the results of a psychophysical evaluation test in which human subjects had to rank the gloves according to their stiffness. Considering that stiffer gloves involves an increase in the forearm muscle activation (Larivière et al., 2004), the perceived exertion should change accordingly. Effectively, it is well known that muscle activation and the rating of perceived exertion are associated (Jones & Hunter, 1982). Thus, the well recognized psychophysical bases of perceived exertion (Borg, 1998) will be used to verify whether the mechanical tests of glove stiffness have some ecological (external) validity.

2.2 Materials and Methods

Table 2.1 presents the characteristics and manufacturers of the twenty eight unsupported and supported protective glove models used in this study. These gloves were subjectively selected between hundred commercially available gloves models, in order to include representatives from the most flexible to the most rigid material groups.

Table 2.1 Characteristics of the tested protective gloves

Manuf.	Model	Materials	Thickness (mm)
Ansell	Canners & Handlers # 392	Natural rubber (NR)	1.1
Best	Nitri-Solve® 747	Nitrile	1.2
Best	The Original Nitri-Flex® 4000P	Nitrile on cotton knit	1.7
Best	Nitri-Pro® 7000P	Nitrile on cotton knit	1.7
Ansell	Hyflex 11-900	Nitrile on cotton knit	2
Best	Natural Rubber Latex HD® 55	Natural rubber (NR)	2.1
Ansell	Hycron 27-607	Nitrile/cotton knit	2.6
Best	Ultraflex Nitrile® 22-R	Nitrile/cotton knit	2.6
Ansell	Golden Grab It 16-300	Leather and NR/cotton knit	3.2
Ansell	Scorpio 8-352	Neoprene on cotton knit	3.3
Best	Neo Hyde® 361	PVC on cotton knit	3.3
Ansell	Grab It Safe 28-362	NR/Kevlar/cotton knit	3.4
Ansell	Seams-Rite 20-115	Vinyl coated, jersey lined	3.6
Best	Cannonball® 803	PVC/jersey lining	3.6
Ansell	Snorkel 4-412	PVC/Nitrile/jersey knit	3.6
Ansell	PowerFlex 80-100	NR on cotton knit	3.6
Best	KPG® 960	PVC on cotton knit	3.7
Ansell	Hyd Tur 52-547	Nitrile/jersey lining	3.7
Best	Cannonball® 812M	PVC/jersey lining	3.8
Ansell	Grab It 6-620	NR/Cotton Jersey	4.1
Best	Skinny Dip Aramid® 4811	NR on Kevlar aramid knit	4.3
Ansell	the Duke 70-982	Rubber coated knit jersey	4.4
Ansell	Crusader 42-325	Nitrile on non woven felt	4.5
Ansell	GoldKnit Kevlar 70-225	Kevlar knit	4.5
Best	Neo Grab® 6780-R	Neoprene/insulating lining	4.8

Ansell	Winter Monkey Grip 23-193	PVC on jersey lining	6.4
Ansell	Neox 9-022	Neoprene on cotton	6.4
Best	Insulated snowman 2950	Nitrile coated, fleece lining	8.6

2.2.1 The KESF uniaxial bending approach

The KESF is used in the textile industry to characterize the mechanical properties and the surface condition of fabrics (Kawabata, 1980; Saville, 1999). It includes a measurement of the material stiffness, which is based on a uniaxial bending test. The whole sample is bent from -2.5 to 2.5 cm^{-1} in an arc of constant curvature (see Figure 2.2.a). The bending moment required to produce this curvature is continuously monitored. The bending rigidity is calculated as the slope of the curve of the bending moment expressed as a function of the curvature as illustrated in Figure 2.2.b. Since this measurement involves uniaxial deformations and since textiles, which are included in most of the gloves, are generally anisotropic materials, i.e. with physical properties different in each direction, gloves were tested along both main directions.

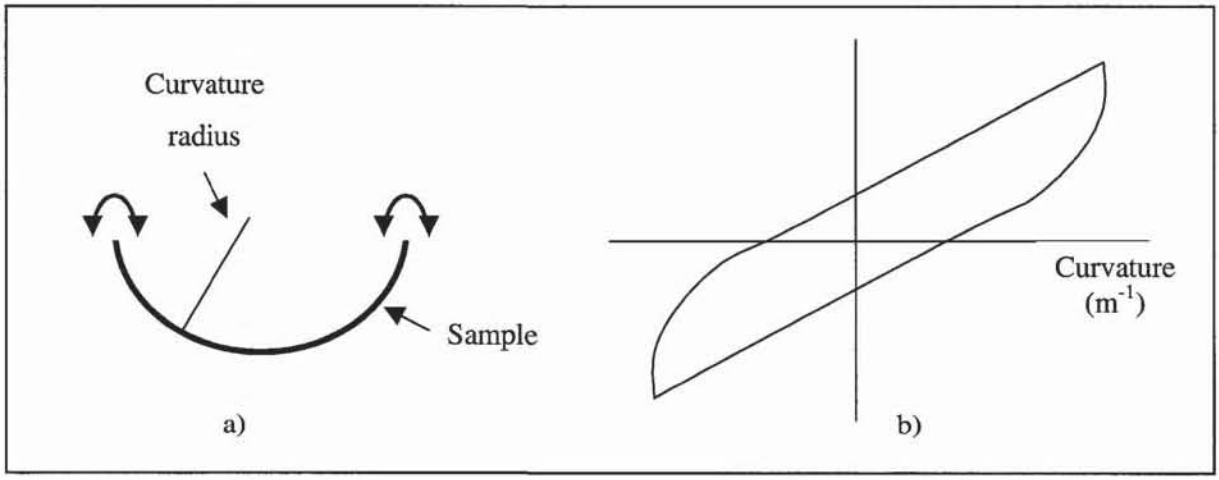

Figure 2.2 Bending rigidity with the KESF method

The bending rigidity was measured on samples taken in the glove palm along the longitudinal and transversal directions. For each glove model, three replicas were measured, allowing for the calculation of a mean and a standard deviation.

2.2. The free-deforming multidirectional test method

The principle of the free-deforming multidirectional test method is based on the use of a probe to push a sample through an orifice drilled in a platform (see Figure 2.3). The lap edge of the orifice is chamfered to limit stress concentration. Because of the larger thickness of gloves compared to fabrics, the value of the gap between the probe head and orifice diameters has been almost doubled, the probe and orifice diameters being respectively equal to 35.8 mm and 57.0 mm. In order to limit the stress concentration at the probe head and to better simulate the type of deformations applied to gloves while in use, the probe head includes a conical section with an angle of 30° and an 11.56-mm-radius spherical tip. This geometry produces double curvature deformations (Laroche and Vu-Khanh, 1993). To account for the influence of the glove fingers, the diameter of the probe is maintained at a constant value up to the top, as illustrated in Figure 2.4, which displays the experimental set-up inserted into an 1137 Instron tensile testing frame with a glove positioned palm up above the orifice.

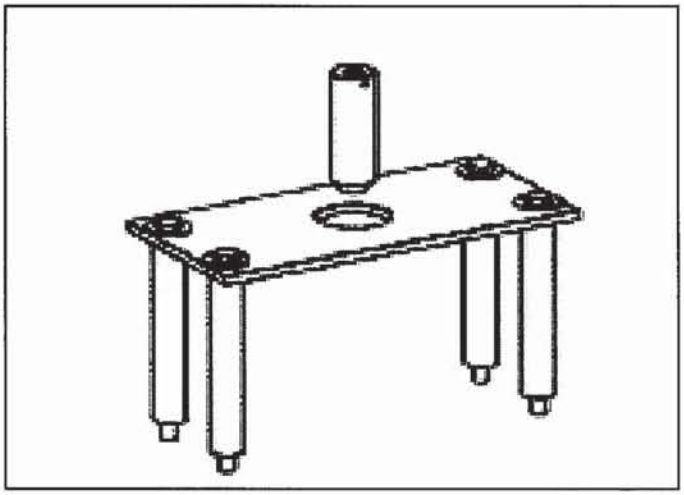

Figure 2.3 Schematic representation of the free-deforming multidirectional method set-up

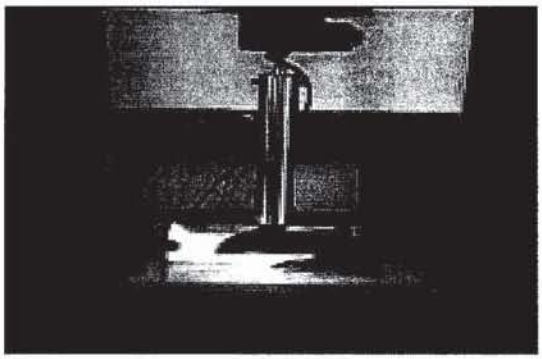

Figure 2.4 Picture of the experimental set-up of the free-deforming multidirectional test method

The force-displacement curve is recorded while the glove, positioned palm up laying on the platform with its palm centered above the orifice, is pushed through it by the probe traveling at a rate of 100 mm/min. A typical example of the obtained force vs. displacement curve is shown in Figure 2.5. During the first part of the probe displacement, the force increases regularly, then reaches a maximum and decreases rapidly. For each model, five different gloves were measured, allowing for the calculation of mean and standard deviation values.

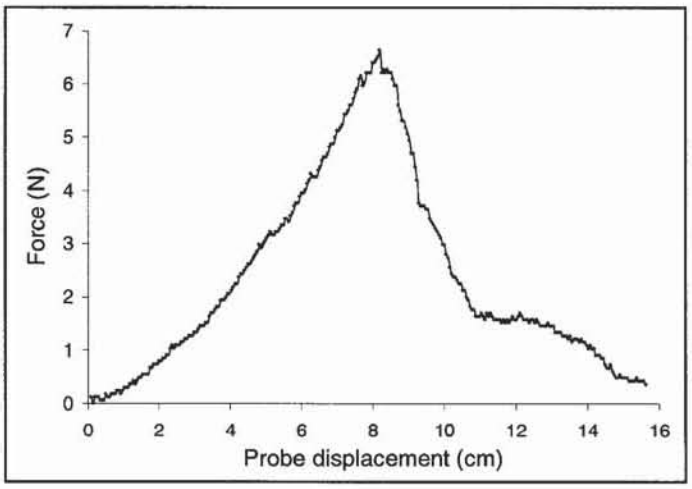

Figure 2.5 Typical force displacement curve measured as the entire glove is passed through the orifice

Three types of data analysis were performed on the force-displacement data recorded with the free-deforming multidirectional test method. First, the maximum force was measured. Second, the total work needed to push the glove through the hole was given by the surface area of the force vs. displacement curve. This work is proportional to the energy of deformation of the glove, itself proportional to the material stiffness (Killinc-Balci, 2004). Third, in order to enlarge the range of measurable stiffness values and to limit the effect of glove friction on the orifice edge surface, the calculation of the work on the first 10-mm of deformation of the glove was performed. This distance corresponds to half of the height of the conical-spherical probe head.

Figures 2.6 and 2.7 display schematic representations of the two set-up configurations between which the initial work is calculated. At configuration 0 (Figure 2.6), the two layers corresponding to both sides of the glove are not deformed and are touching each other. At configuration 1 (Figure 2.7), the probe has traveled a distance of 10 mm. The total glove thickness was measured at the center of the palm and this value was used to adjust the zero of the measurement versus the upper lap of the platform.

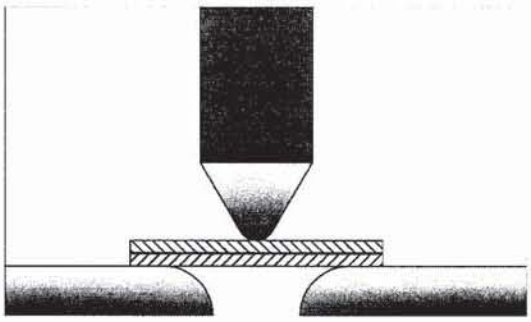

Figure 2.6 Configuration 0: Palm and back sides in contact

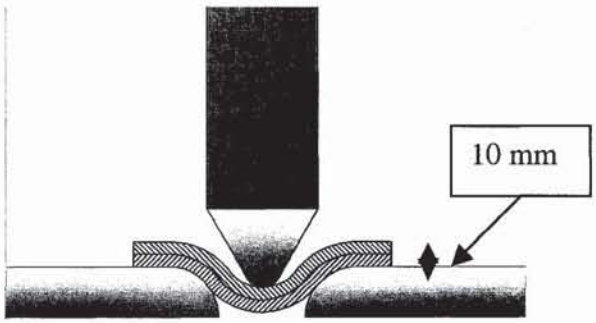

Figure 2.7 Configuration 1: 10-mm deformation of the glove

Figure 2.8 displays examples of the initial part of the force-displacement curve obtained for two different glove models. The calculation of the initial work was performed between these 10-mm-distant integration limits identified as 0 and 1 and corresponding to the configurations illustrated in Figures 2.6 and 2.7.

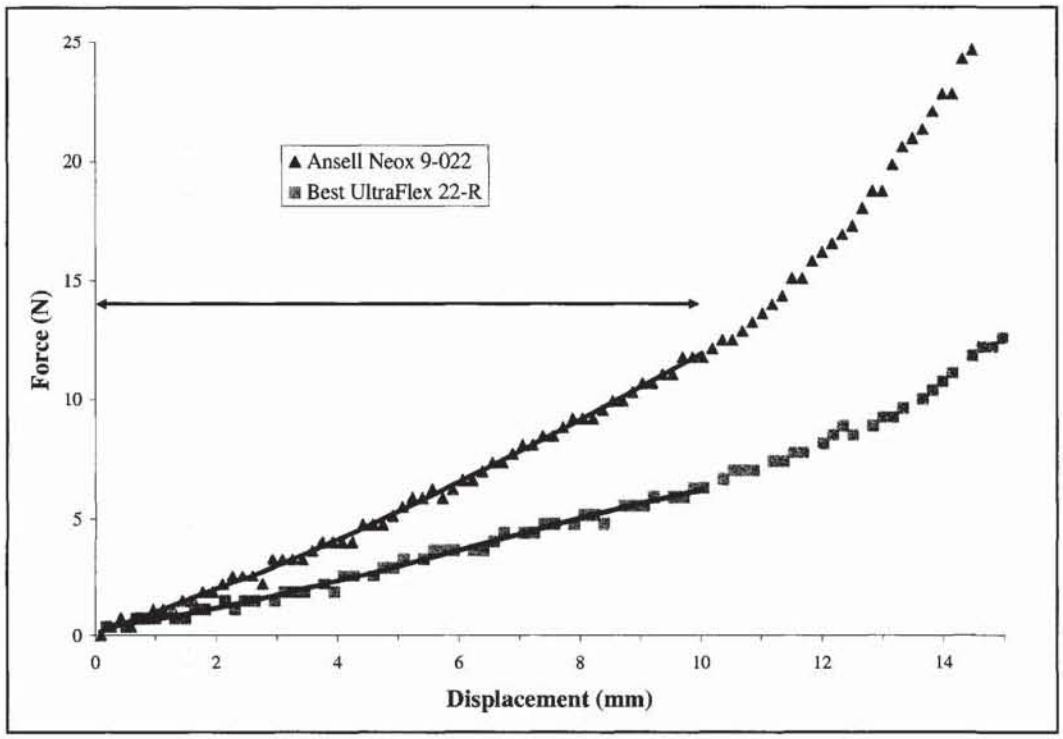

Figure 2.8 Examples of the initial part of the force displacement curve for two models of protective gloves illustrating the calculation of the initial work

2.2.2 The psychophysical evaluation test

A psychophysical evaluation of the glove stiffness was performed by thirty healthy human subjects, naive relative to this kind of evaluation, aged between 20 and 55 and selected on a voluntary basis. Each subject had to classify the gloves using a scale from 1 to 10 (1 being the most flexible and 10 the stiffest). The test was adapted from the CR-10 Borg scale (Borg, 1998), with excluding the score 0 which corresponds to the absence of constraint, i.e. the bare hand condition, and forcing the subject to select at least once the scores 1 and 10, which ensures an optimal discrimination between the gloves. In fact, the rating of perceived exertion using the CR-10 Borg scale would have likely produced values lower than 5 because numbers are anchored by verbal expression, with a 10 meaning "very, very strong" exertion (almost max) and a 5 meaning "strong" exertion.

The procedure included two steps. First, the subject had to try on all the gloves one by one in order to rank them according to their stiffness. It allowed identifying the two anchoring points of the distribution, i.e. the most flexible glove (level 1) and the stiffest glove (level 10). Clear instructions were provided that the gloves had to be evaluated according to their stiffness and not based on comfort, size or any other property. However, apart from moving the fingers, no particular task was requested or suggested for the evaluation of the glove stiffness. Then, the subject had to attribute to each of the remaining gloves a number between 1 and 10 inclusively according to its level of stiffness. In other words, no verbal expressions were used to anchor the values from 1 to 10. In order to allow for an iterative evaluation procedure, the gloves were placed by the subject in baskets numbered 1 to 10 corresponding to their level of stiffness. It was specified that the subject could put two or more gloves in one basket if evaluated of the same stiffness and that some baskets may contain no glove. The time and the number of trials for each glove were not restricted. In general, an average of 20 to 30 minutes was necessary for the subjects to sort the gloves.

One model of the list of twenty eight gloves displayed in Table 2.1 could not be included in the psychophysical evaluation test because the insufficient number of gloves available prevented providing each subject with a new specimen.

2.3 Results and Discussion

2.3.1 The KESF uniaxial bending approach

The twenty eight protective gloves have been characterized with the KESF bending technique. The results are displayed in the form of a histogram in Figure 2.9. For two glove models, it was not possible to carry out the measurements because of limitations related to the glove thickness and/or design. Except for a few exceptions, the measured bending rigidity exhibits small standard deviations, indicative of the good reproducibility of the results. The data are spread over more than a decade of μN.m, thus allowing for an easy separation of the glove performance in terms of stiffness.

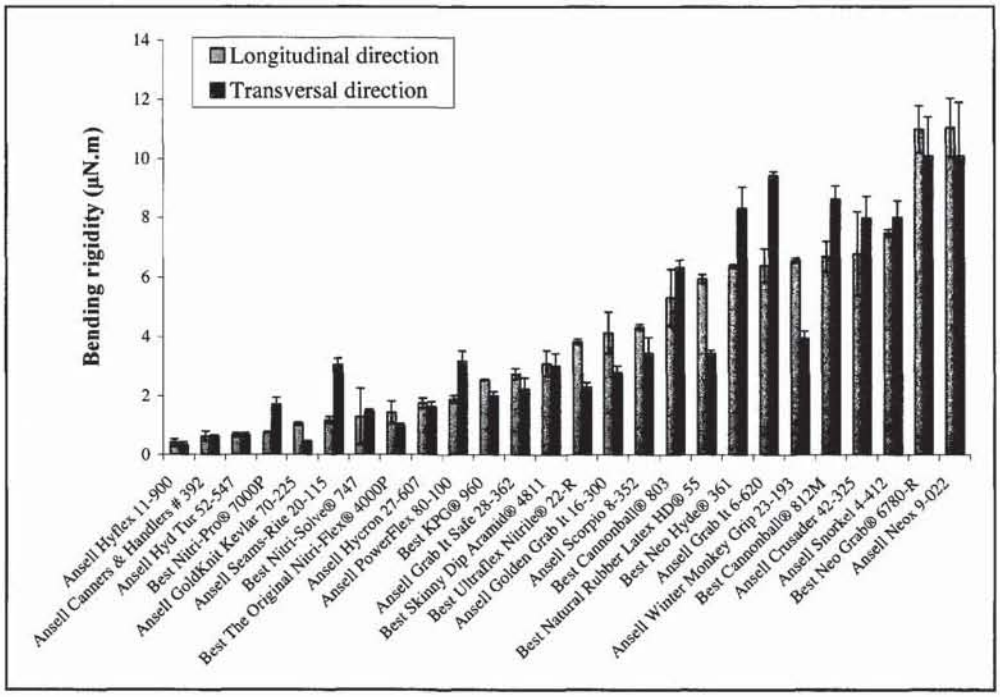

Figure 2.9 Measured bending rigidity along the longitudinal and transversal directions with the KESF technique

The comparison between the measurements performed along the longitudinal and transversal directions of the gloves shows some varied behaviours. For some of the gloves, the values of bending rigidity in the longitudinal and transversal directions are identical within the measurement uncertainty. However, for other glove models, the values measured in the longitudinal and transversal directions may differ by a factor of 2 or more. While differences between the warp and weft directions are expected for anisotropic materials like knit or woven fabrics and for composites including a textile liner, large discrepancies between the measurements performed along the glove longitudinal and transversal directions are also observed for gloves made of pure elastomer, reaching 50% for example in the case of the natural rubber Best HD 55 gloves. These sometimes large differences obtained for longitudinal and transversal bending rigidity translate into major discrepancies between the glove rankings based on their stiffness along the longitudinal and transversal directions, up to 8 places for a total of 26.

2.3.2 The free-deforming multidirectional test method

The twenty eight selected models of protective gloves were tested with this free-deforming multidirectional method. For the ten less stiff gloves, the maximum force and the total work were obtained (Harrabi et al., 2006). Both parameters lead to the same ranking of the gloves on a stiffness scale. This can be seen as an indication of the usefulness of the work as a parameter for characterizing the material stiffness as well as of the validity of the technique principles.

The results in terms of initial work are provided in Figure 2.10 in the form of a histogram for the twenty eight models of gloves. It can be seen that the data are spread over more than a decade of N.mm and display a good reproducibility as shown by the low standard deviation values. A comparison of the stiffness ranking of the ten less stiff gloves based on the maximum force and total work with that based on the initial work shows a good agreement between the different methods of data analysis (Vu-Khanh et al., 2007). The slight differences that are observed can be attributed to the large friction coefficient of some models

of gloves, which contributes in a larger extent to the maximum force and total work measurement than to the initial work.

Using the initial work, it is possible to divide the twenty eight tested gloves in six classes within which similar levels of stiffness are observed. They are illustrated in Figure 2.10. Class 1 corresponds to the most flexible gloves, with an initial work between 5 and 20 N.m, Class 2 between 20 and 50 N.m, Class 3 between 50 and 80 N.m, Class 4 between 80 and 120 N.m, Class 5 between 120 and 170 N.m and Class 6 for the stiffest measured gloves, i.e. between 200 and and 350 N.m.

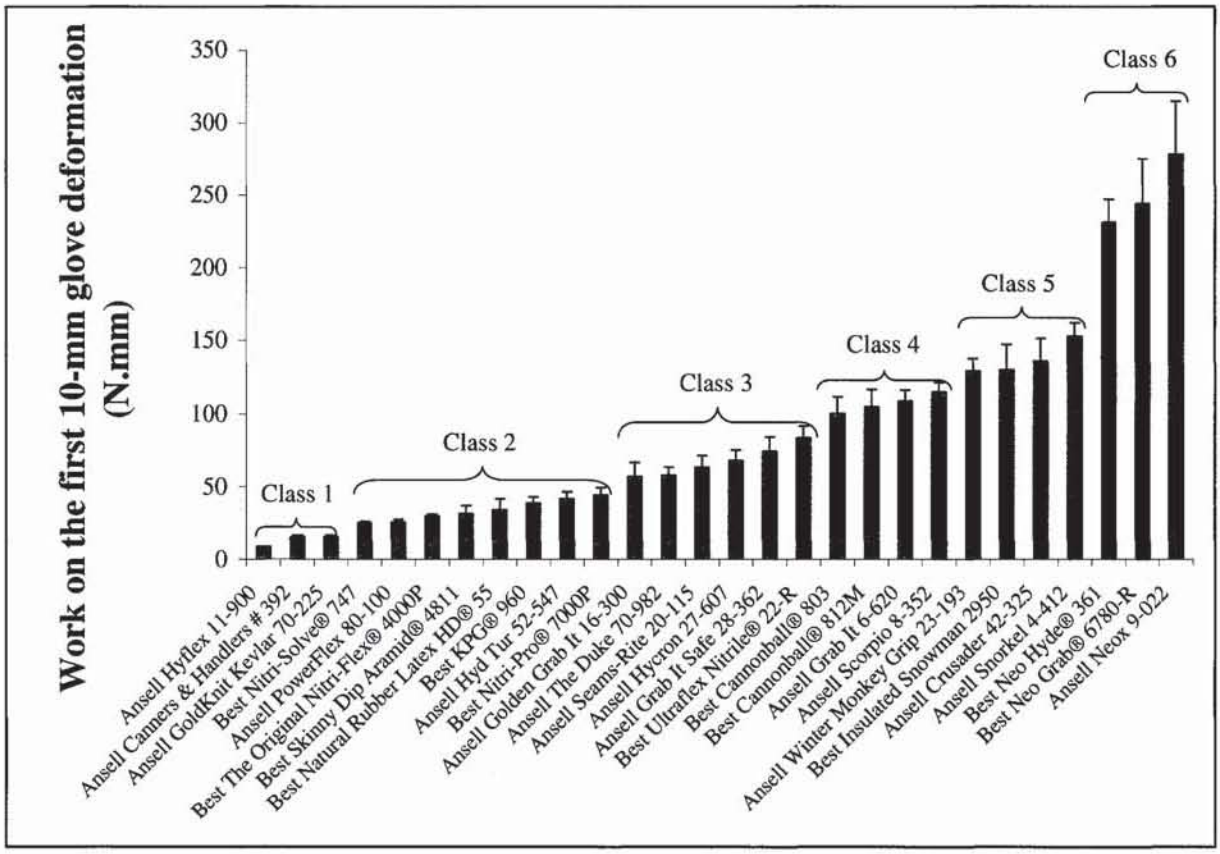

Figure 2.10 Initial work using the free-deforming multidirectional method

2.3.3 Comparison of the results of the mechanical methods with a psychophysical evaluation test

The results obtained with both mechanical test methods were compared with the rating provided by the psychophysical test for the twenty five models of gloves characterized by all three methods.

Figure 2.11 displays the relationship between the stiffness of the gloves measured with the multidirectional method using the initial work and the result of the psychophysical evaluation test. Standard deviations obtained for the glove rating using the psychophysical evaluation test, not shown for clarity purpose, are situated between 0.3 and 2.5. The data points can be described by an exponential function with a correlation of 0.92. When results from the KESF measurements along the longitudinal and transversal directions are plotted as a function of the psychophysical evaluation test rating, the association is less satisfactory, with correlation coefficients of respectively 0.79 and 0.81.

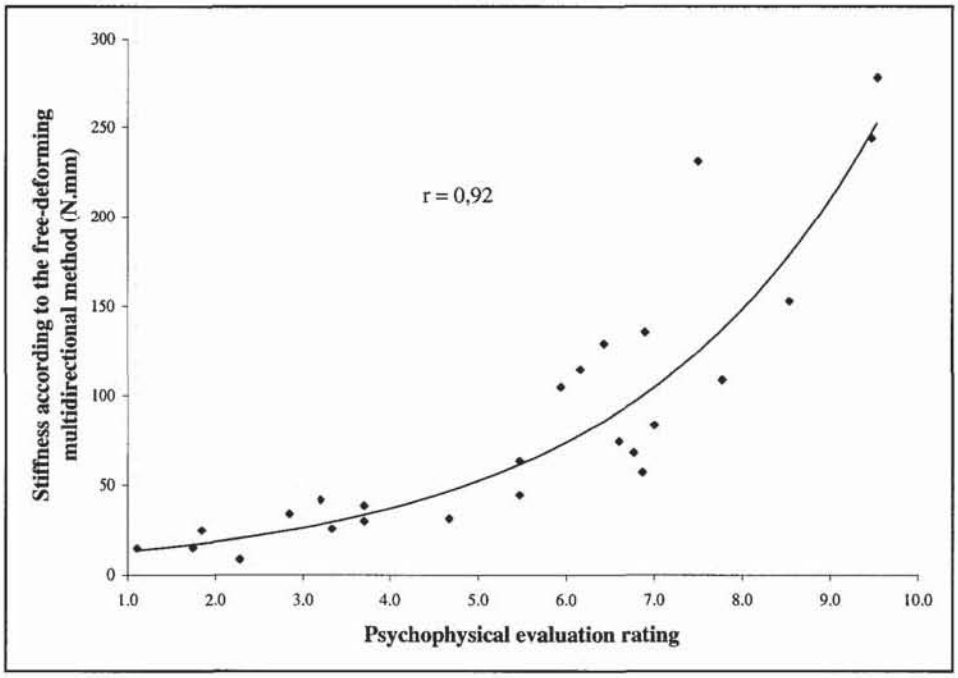

Figure 2.11 Association between the stiffness of the gloves measured with the multidirectional method using the initial work and the psychophysical evaluation test results

Correlations between the sets of measurements were also calculated. Since scores provided by the KESF and multidirectional methods are not normally distributed, Spearman's rank correlation method was used, in which data are converted to ranks before the calculation is carried out. It is illustrated in Figures 2.12, 2.13 and 2.14 for the association between the psychophysical evaluation rating and respectively the KESF measurements along the longitudinal and transversal directions and the free-deforming multidirectional method results. Significant correlations are obtained in all cases. Correlations between the mechanical methods are good (≈ 0.85). However, the results of the multidirectional method are more correlated to the psychophysical evaluation ($r = 0.93$) than the different indices produced by the KESF ($r = 0.79$ for the measurements along the longitudinal direction and $r = 0.76$ for those along the transversal direction). This shows that the free-deforming multidirectional method describes much more closely the stiffness of protective gloves as wearers perceive it.

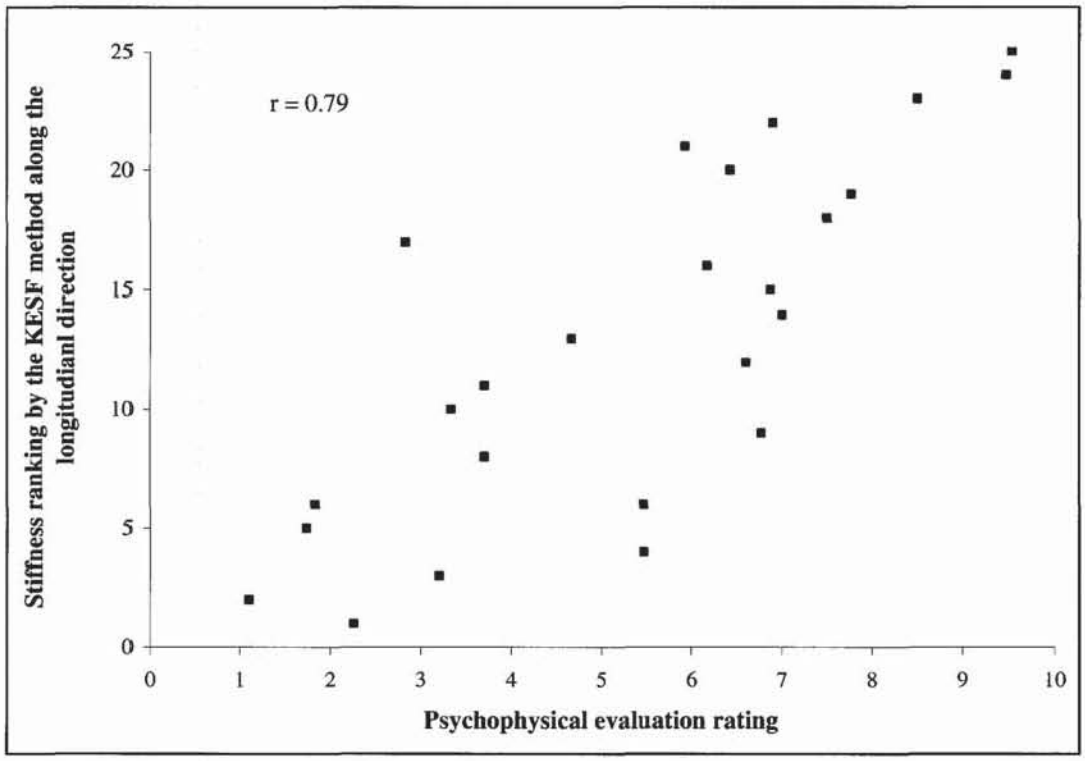

Figure 2.12 Association between the psychophysical evaluation test results and the stiffness ranking provided by the KESF measurements along the longitudinal direction

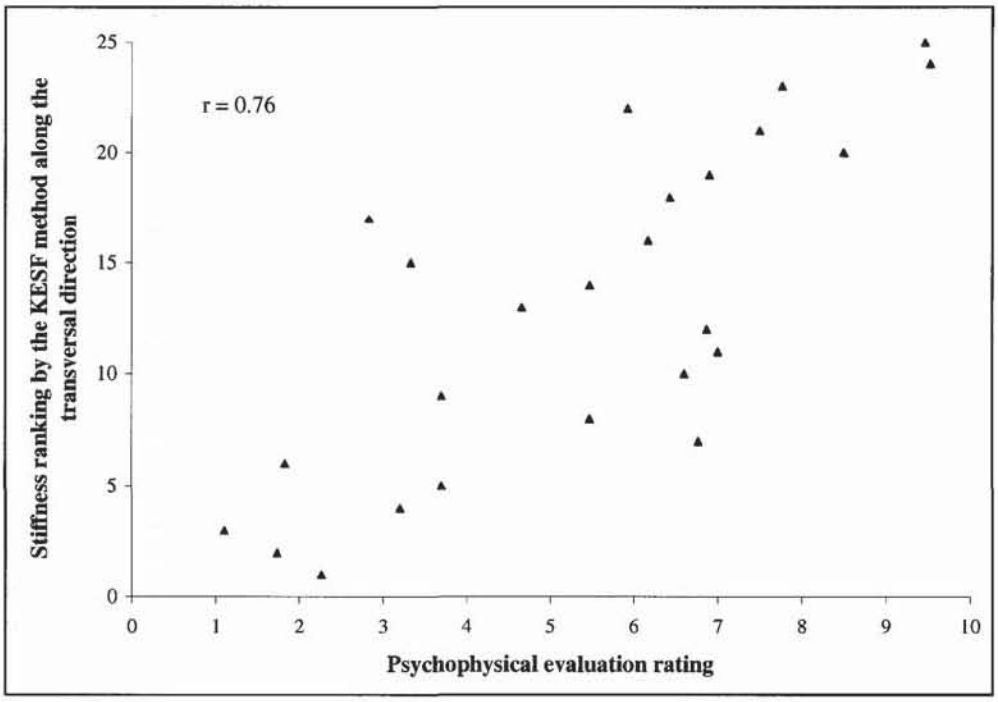

Figure 2.13 Association between the psychophysical evaluation test results and the stiffness ranking provided by the KESF measurements along the transversal direction

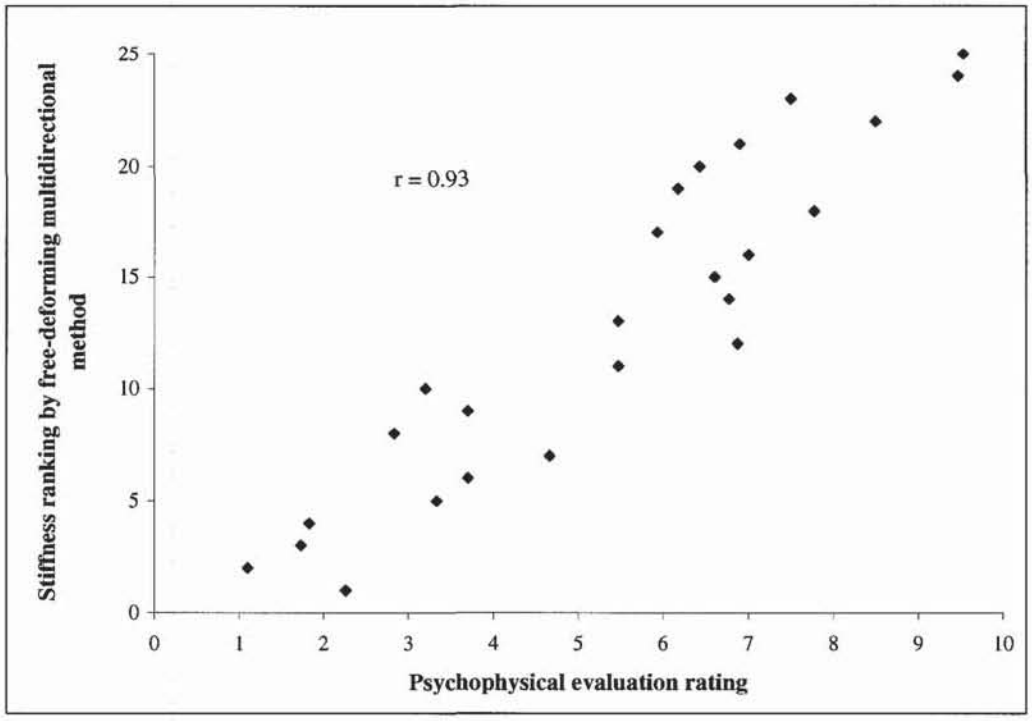

Figure 2.14 Association between the psychophysical evaluation test results and the stiffness ranking provided by the free-deforming multidirectional method

The differences observed between the results of the psychophysical evaluation test and the measurements provided by the KESF technique do not appear to be related either to the differences measured between the KESF uniaxial rigidity results along the longitudinal and transversal directions of the glove, the type of material used in the composition of the glove, or the presence of a different material for the back side of the glove than for the palm side. The better correlation between the psychophysical evaluation and the free-deforming method is thus attributed to the type of deformations subjected to the glove during the measurement, uniaxial for the KESF system test method and multidirectional for the free-deforming technique.

2.4 Conclusion

A new test method applying multidirectional deformations and using a conical spherical probe head which better simulates the type of mechanical deformations sustained by glove in use has been developed and evaluated. The stiffness of twenty eight models of protective gloves was measured by this new multidirectional test method and by the KESF method for fabrics that measures the uniaxial bending rigidity in both directions (longitudinal and transversal) of the gloves. It was also characterized using a psychophysical evaluation test performed with thirty subjects.

Large differences in the bending rigidity measured by the KESF technique were found between the measurements along the longitudinal and transversal directions for some protective gloves, causing large differences in the stiffness rankings along the longitudinal and transversal directions. These differences can not be related to the anisotropic nature of the material since they exist even for some models of elastomer gloves. In addition, two models of gloves could not be characterized due to thickness limitations.

For the free-deforming multidirectional technique, the analysis of the force-displacement curves in terms of the initial work corresponding to the first 10 mm of deformation of the glove has allowed characterizing all twenty eight models of protective gloves according to their stiffness. The analysis of the correlations between the glove stiffness measurements produced by the two mechanical test methods and the results of a psychophysical evaluation test shows a much better agreement with the free-deforming multidirectional method, which indicates that this method describes much more closely the stiffness of protective gloves as wearers perceive it. This can be attributed to the multidirectional deformations applied to the glove during the test, which better simulate the deformations subjected to gloves in service. Using the initial work values, the tested gloves have been divided into six classes corresponding to six levels of stiffness, which can be used for a selection of gloves as a function of the tasks.

Two additional practical advantages of the free-deforming multidirectional technique should be mentioned: first, it is very easy to implement, the simple set-up of probe and drilled plate being inserted in a mechanical test frame with limited requirements in terms of load capacity. Second, this method is non destructive, especially since the glove is deformed only through a 10-mm course of the probe.

This new method should prove as a valuable tool for protective glove manufacturers in their search for improving their product quality, allowing for the characterization of their existing products in terms of stiffness and for the development of new ones better fitting workers' needs. In addition, if adopted as a standard in conjunction with a system of classification levels, this method will also have more direct positive repercussions on workers, since it will permit the systematic rating of protective gloves versus a universal stiffness criterion, thus allowing for an easier selection of the protective glove best fitted to the performed tasks.

Acknowledgements

This research has been supported by the Institut de recherche Robert-Sauvé en santé et sécurité du travail (IRSST), Montréal, Canada.

References

ASTM D 1388, Standard test method for stiffness of fabrics. Annual Book of ASTM Standards. 1996.

ASTM D 4032-94, Standard test method for stiffness of fabric by circular bend procedure. Annual Book of ASTM Standards. 1994.

Bishu, R., Muralidhar, A., 1999. Gloves. In: Karwowski, W., Marras, W.S. (Eds.). The Occupational Ergonomics Handbook, CRC Press, NY, pp. 865–876.

Borg, G. (Eds.), 1998. Borg's perceived exertion and pain scales, Champaign, IL, USA : Human Kinetics.

Buhmann, D.C., Cherry, J. A., Bronkema-Orr, L., Bishu, R., 2000. Effect of gloves, orientation, pressure, load and handle on submaximal grasp force. International Journal of Industrial Ergonomics 25(3), 247-256.

Cadoret, G., Smith, A.M., 1996. Friction, not texture, dictates grips forces used during object manipulation. Journal of Neurophysiology 75 (5), 1963-1969.

Chaffin, D.B., Anderson, G., Martin, B.J., (Eds.), 1999. Occupational Biomechanics (3rd edition), Wiley, New York, Toronto.

Commission de la santé et de la sécurité du travail du Québec, Fichier sur les lésions professionnelles, updated September 2003, Montréal, QC.

Harrabi, L., Dolez, P., Vu-Khanh, T., Lara, J., 2006. Evaluation of the flexibility of protective gloves. Proceeding of the 3rd European Conference on Protective Clothing, Gdynia, Poland, 10-12 May.

ISO 5979, Rubber or plastics coated fabrics -- Determination of flexibility -- Flat loop method. 1982.

Jones, L. A., Hunter, I. W., 1982. The relation of muscle force and EMG to perceived force in human finger flexors. European Journal of Applied Physiology 50:125-131.

Kawabata, S., (Eds.), 1980. The Standardization and Analysis of Hand Evaluation, the Textile Machinery Society of Japon, Osaka.

Killinc–Balci, F. S., 2004. A study of the nature of fabric comfort [dissertation]. Auburn University (Alabama).

Kovacs, K.M., Splittstoesser, R., Maronitis, A., Marras, W.S., 2002. Grip force and muscle activity differences due to glove type. Journal of the American Industrial Hygiene Association 63 (3):269-274.

Lariviere, C., Plamondon, A., Lara, J., Tellier, C., Boutin, J., Dagenais, A., 2004. Biomechanical assessment of gloves. A study of the sensitivity and reliability of electromyographic parameters used to measure the activation and fatigue of different forearm muscles. International Journal of Industrial Ergonomics 34:101-116.

Laroche, D., Vu-Khanh, T., 1993. Modeling of the thermo-elastic properties of Woven fabric composites in complex shapes. Composite Materials: Testing and design, ASTM STP 1206, pp.386-414.

Mital, A, Kuo, T, Faard, H.F., 1994. A quantitative evaluation of gloves used with non-powered hand tools in routine maintenance tasks. Ergonomics 37(2):333-343.

Nelson, J.B., Mital, A. , 1995. An Ergonomic evaluation of dexterity and tactility with increase in examination/surgigical glove thickness. Ergonomics 38, 723-733.

Rock, K.M., Mikat, R.P., Foster, C., 2001. The effects of gloves on grip strength and three-point pinch. Journal of Hand Therapy 14(4), 286-290.

Saville, B.P., 1999. Objective evaluation of fabric handle. In: The Textile Institute CRC Press (Eds.). Physical Testing of Textiles, Woodhead Publishing Limited, pp. 77-114.

Sudhakar, L.R., Schoenmarklin, R.W., Lavender, S.A., Marras, W.S., 1988. The effects of gloves on grip strength and muscle activity. In Proceeding of the Human Factors Society, Santa Monica, CA, USA.

Vu-Khanh, T., Dolez, P., Harrabi, L., Lara, J., Larivière, C., Tremblay, G., Nadeau, S., 2007. Caractérisation de la souplesse des gants de protection par des méthodes mécaniques et une méthode biomécanique basée sur l'électromyographie de surface. Report, Étude et Recherche Series, Institut de recherche Robert-Sauvé en santé et en sécurité du travail au Québec.

CHAPITRE 3

ARTICLE 2: EVALUATION OF THE FLEXIBILITY OF PROTECTIVE GLOVES

Article tel que publié dans la revue Internationale Journal of Occupational Safety and Ergonomics (JOSE) volume **14** N°1 en 2008

Lotfi Harrabi*, Patricia I. Dolez*, Toan Vu-Khanh* and Jaime Lara[#]

* École de technologie supérieure, Montréal, Canada.

[#] Institut de recherche Robert-Sauvé en santé et sécurité du travail, Montréal, Canada.

Résumé

Deux méthodes mécaniques sont présentées dans cet article permettant la caractérisation de la souplesse des gants de protection. Le principe de la première méthode est détaillé dans l'article 1, il est inspiré de la méthode ASTM D 4032. Elle concerne surtout les gants qui ne sont pas portés serrés sur les mains. La deuxième méthode caractérise la souplesse des gants qui sont plutôt portés serrés sur les mains des utilisateurs. Sa validité a été vérifiée dans le cas des matériaux élastomères en utilisant le formalisme théorique de Mooney-Rivlin. Avec ces deux nouveaux outils qui viennent combler le manque qui existait au niveau de la caractérisation de la souplesse des gants de protection, les manufacturiers auront donc les moyens de travailler à l'amélioration de la souplesse des gants, qui constitue encore souvent soit une entrave à la bonne exécution de ses tâches par le travailleur, soit une raison à la décision de ne pas porter de gants de protection.

Abstract

Two mechanical methods have been developed for the characterization of the flexibility of protective gloves, a key factor affecting their degree of usefulness for workers. The principle of the first method is similar to the ASTM D 4032 standard relative to fabric stiffness and

simulates the deformations encountered by gloves that are not tight fitted to the hand. The second method characterizes the flexibility of gloves that are worn tight fitted. Its validity was theoretically verified for elastomer materials. Both methods should prove themselves as valuable tools for protective glove manufacturers, allowing for the characterization of their existing products in terms of flexibility and the development of new ones better fitting workers' needs.

3.1 Introduction

Hand injuries represent a major source of accidents, in particular at the workplace. In Québec, they account for 17% of all occupational lesions compensated for by the Québec Occupational Health and Safety Commission (Commission de la Santé et de la Sécurité du Travail du Québec) between 2001 and 2004 [1]. Wearing protective gloves can reduce the occurrence of such injuries, but with a price in terms of loss of dexterity and sensitivity, and additional muscular constraints among others [2]. This can lead to either the worker not being able to perform adequately his tasks, or deciding not to wear protective gloves. In both cases, the risk of injury is increased.

Flexibility, which contributes to dexterity and sensitivity, is one of the major properties that define how a glove interferes with the worker's ability to perform his tasks. Some studies have been considering the biomechanical aspects of protective glove use on the deployment of the maximum grip force. It was shown for example that wearing protective gloves reduces the maximum gripping force by 7-30% [3]. Other authors developed a method based on surface electromyography to assess the effect of glove wearing on the activation and fatigue of several forearm muscles [4]. However, procedures involving human subjects are prone to high levels of inter individual variability. On the other side, purely mechanical methods [5-7] have been developed for characterizing film and fabric stiffness or flexibility (its inverse). Most of them are based on uniaxial bending, which may not be representative of the type of deformations sustained by gloves in usage. On the other side, the ASTM D 4032 standard [7], which provides a method for measuring the stiffness of fabrics, makes use of a circular bend procedure, thus creating multi-directional deformations. According to the ASTM D 4032 method, a flat-headed cylindrical probe forces a folded piece of fabric through a circular orifice in a platform. The maximum force required to push the fabric through the orifice is measured and used as an indication of the fabric stiffness.

In order to characterize the flexibility of protective gloves without the need for human subjects, the free-deforming method has been developed based on the same principle as the

ASTM D 4032 standard, but with a larger gap between the probe head and the orifice edge, and a more relevant shape for the probe. This method measures mostly out-of-plane material deformations and can be seen as describing the behavior of gloves that are not tight fitted to the hand.

For simulating the behavior of gloves that are worn tightly fitted, a fixed technique is also proposed, which uses the same type of probe geometry as for the free-deforming method, but with securing the glove material along the circumference of the orifice. In that case, deformations are mostly in the plane of the tested material. The measurements performed on elastomer gloves were compared to a theoretical description based on the Mooney formalism [8] using uniaxial tensile tests.

3.2 Experimental

3.2.1 The free-deforming technique

As for the ASTM D 4032 standard, this technique is based on the use of a probe to push a sample through an orifice drilled in a platform. However, some distinctive features of the free-deforming technique are dictated by the requirements related to the measurement of protective gloves. First, to account for glove larger thickness compared to fabrics, the value of the gap between the probe head and the orifice edge is almost doubled. Second, in order to limit the stress concentration at the probe head and to better simulate the type of deformations applied to gloves while in use, a cylindrical probe with a spherical-conical shaped head is used, producing double curvature deformations [9]. Third, to account for the influence of glove fingers, the diameter of the probe is maintained at a constant value up to the top, as illustrated in Figure 3.1, which displays the experimental set-up inserted into an 1137 Instron tensile testing frame with a glove positioned palm up above the orifice.

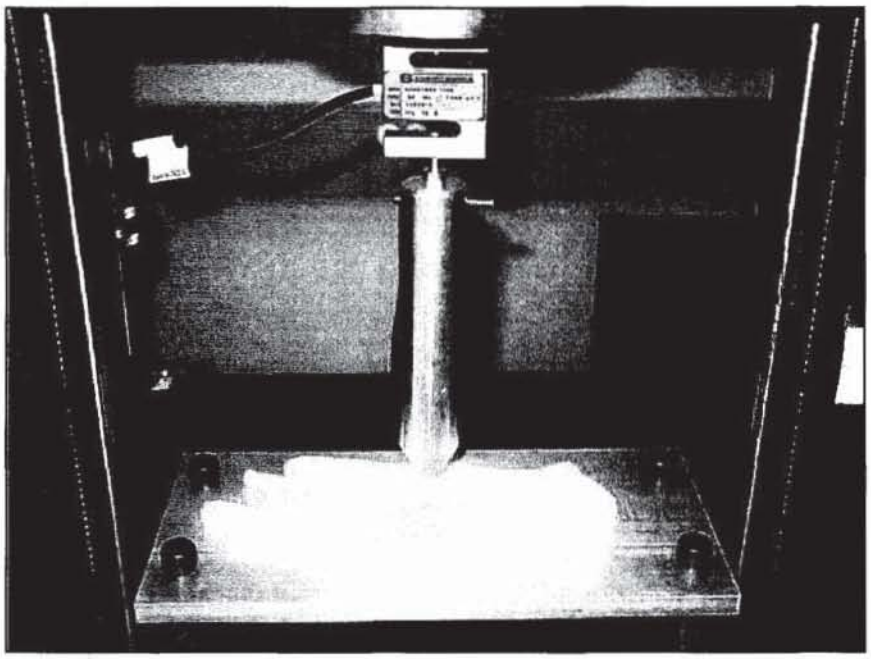

Figure 3.1 Experimental set-up of the free-deforming technique

Force-displacement data are recorded by the testing frame as the glove is pushed by the probe through the orifice, an example of the corresponding curve being shown in Figure 3.2. Principal and secondary maxima correspond to the passage of glove fingers through the orifice. In terms of data analysis, the value of the maximum force was extracted from the force-displacement data, in accordance with the ASTM D 4032 standard where it is used as a characterization of the glove flexibility. In addition, following some authors studying fabric comfort [10], the total work necessary to push the entire glove through the orifice was also calculated, this work being proportional to the deformation energy, itself inversely proportional to flexibility.

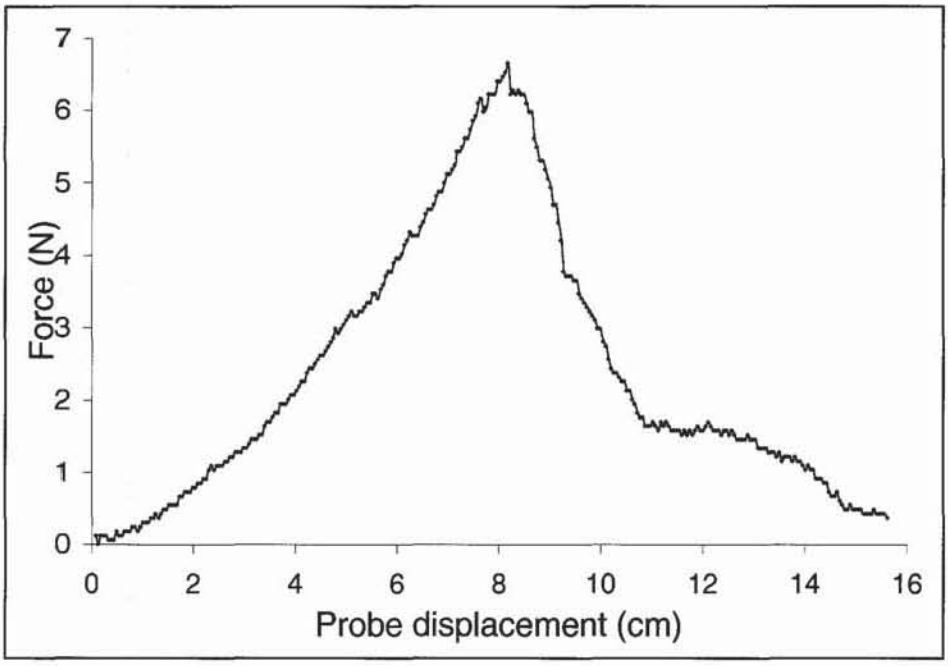

Figure 3.2 Example of the force displacement curve measured as a glove is pushed through the orifice

3.2.2 The fixed technique

In order to obtain a realistic determination of the flexibility of tight fitting gloves, the above set-up was modified so that a layer of the glove material taken in the palm area was secured along the circumference of the orifice as illustrated in Figure 3.3. The same geometry of the probe was used and the deformation of the membrane was recorded as a function of the force applied by the probe.

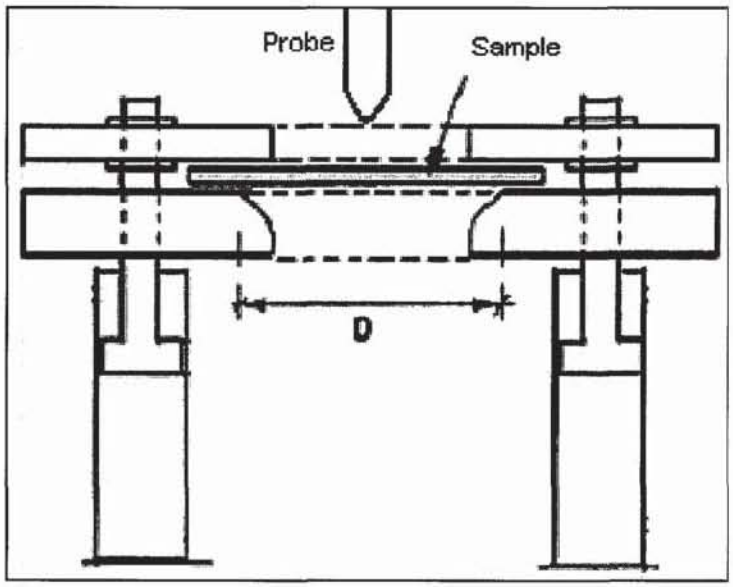

Figure 3.3 Set-up of the fixed technique

Figure 3.4 displays an example of a force displacement curve measured for a natural rubber glove. In the configuration corresponding to the fixed technique, the material stiffness is characterized as the slope of the force displacement curve, the flexibility being its inverse.

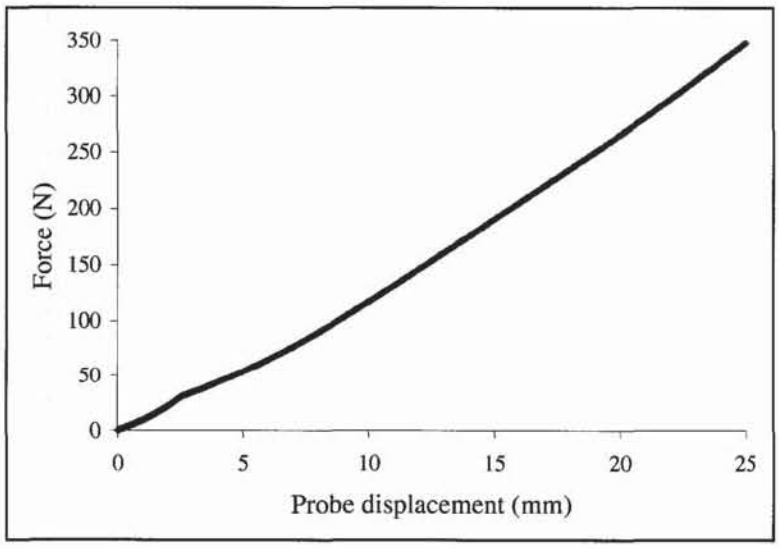

Figure 3.4 Example of a force deformation curve measured with the fixed technique

3.2.3 Materials and methodology

Ten models of protective gloves from two manufacturers (Best and Ansell) were measured using the free-deforming technique. Some are made of pure elastomer, one of a knit fabric, and some feature a knit liner dipped in a polymer. The description of the composition of each glove is provided, along with its thickness measured in the middle of the palm section, in the corresponding results table (Table 3.1, section 4). For each model, five measurements were performed on different gloves to ensure that the measurement uncertainty includes property variability between gloves of the same model.

Five models of gloves were also characterized with the fixed technique, three of them elastomers, along with two thicknesses of a neoprene membrane. The results table (Table 3.3, section 4) includes information about glove and membrane materials. As for the free-deforming test, each result is the average of five measurements.

3.3 Theoretical description of the fixed technique

In order to validate the developed fixed technique, a theoretical description is presented below corresponding to the deformation of elastomer materials.

As shown in Figure 3.5, the surface of the deformed membrane can be divided into three zones: a lower one (zone A) in contact with the spherical part of the probe head, a middle one (zone B) in contact with the conical part of the probe head and a top one (zone C) not in contact with the probe. The force applied by the probe is the sum of two contributions [11]: F_A relative to zone A and F_B relative to zone B.

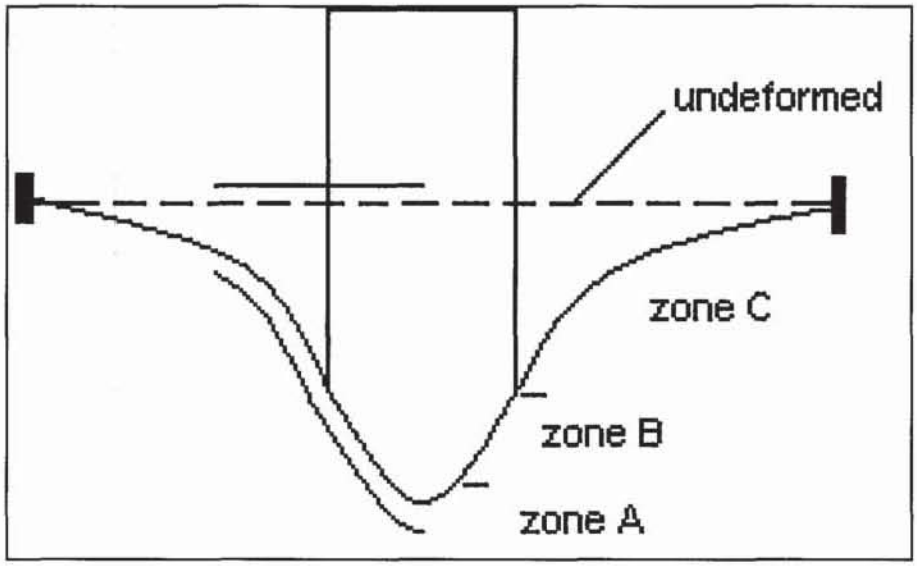

Figure 3.5 Schematic representation of the deformed membrane in the fixed technique

For the description of the elastomer mechanical properties, the Mooney formalism, valid for elastic, isotropic and incompressible materials, has been used in its two-constant version by the way of the Mooney strain energy function W [8]:

$$W(\lambda_1,\lambda_2)=C_1(\lambda_1^2+\lambda_2^2+\lambda_1^{-2}\lambda_2^{-2}-3)+C_2(\lambda_1^{-2}+\lambda_2^{-2}+\lambda_1^2\lambda_2^2-3) \tag{3.1}$$

Where λ_1 and λ_2 are respectively the radial and circumferential extension ratios in the (ρ, ξ) cylindrical coordinate system (see Figure 3.5).

The Mooney-Rivlin constants, C_1 and C_2, can be obtained by uniaxial tensile tests performed according to the ASTM D 412 standard [12]. The resulting stresses T_1 and T_2 per unit edge length respectively along the radial and the circumferential directions become:

$$T_1=2h\left(\frac{\lambda_1}{\lambda_2}-\lambda_1^{-3}\lambda_2^{-3}\right)\left(C_1+\lambda_2^2C_2\right) \qquad T_2=2h\left(\frac{\lambda_2}{\lambda_1}-\lambda_1^{-3}\lambda_2^{-3}\right)\left(C_1+\lambda_1^2C_2\right) \tag{3.2}$$

With h the thickness of the membrane.

In zone A, at the tip of the probe, the membrane is in an equibiaxial stress state, leading to $\lambda_1=\lambda_2=\lambda_0$. The force applied by the probe on the membrane inside zone A can be expressed as:

$$F_A = 12 R C_1 h \left(1-\lambda_0^{-6}\right)\left(1+\alpha\lambda_0^2\right) \tag{3.3}$$

With R the radius of curvature of the spherical part of the probe head and $\alpha = C_2/C_1$.
In zone B corresponding to the conical part of the probe head, the force can be expressed as:

$$F_B = 4\pi(R_2-R_1)\cos\theta\ C_1 h\left(\frac{\overline{\lambda_1}}{\overline{\lambda_2}}+\frac{\overline{\lambda_2}}{\overline{\lambda_1}}-\frac{2}{\overline{\lambda_1}^3\overline{\lambda_2}^3}+\alpha\left(2\overline{\lambda_1}\overline{\lambda_2}-\frac{1}{\overline{\lambda_1}^3\overline{\lambda_2}}-\frac{1}{\overline{\lambda_2}^3\overline{\lambda_1}}\right)\right) \tag{3.4}$$

Where θ, R_1 and R_2 are respectively the angle and the two radii of the conical part of the probe head and $\overline{\lambda_1}$ and $\overline{\lambda_2}$ are the average values of λ_1 and λ_2 over the zone B section of the membrane.

3.4 Results and discussion

Table 1 displays the results in terms of maximum force and total work values measured with the free-deforming method for ten models of protective gloves. Both parameters lead to the same ranking of the gloves on a decreasing flexibility scale (rank 1 corresponds to the most flexible glove). Also provided in Table 3.1 is each glove composition and its total thickness (front and back layers together) measured in the middle of the palm.

Table 3.1 Results of the free-deforming technique measurement for ten models of protective gloves (standard deviation in parenthesis)

Model	Material	Thickness (mm)	Maximum force (N)	Total work (N.cm)	Ranking
Ansell Canners & Handlers # 392	Natural rubber (NR)	1.12 (0.05)	3.8 (0.3)	0.51 (0.04)	1
Ansell Goldknit Kevlar 70-225	Kevlar knit	4.5 (0.1)	22.5 (2.6)	7.2 (0.7)	2
Ansell Hyflex 11-900	Nitrile rubber on cotton knit	2.03 (0.08)	22.6 (0.9)	7.7 (1.0)	3
Best Nitri-Solve® 747	Nitrile rubber	1.17 (0.04)	51.6 (2.0)	22.0 (1.8)	4
Best Latex HD® 55	Natural rubber	2.11 (0.08)	130 (17)	51 (11)	5
Best KPG® 960	PVC on cotton knit	3.71 (0.03)	222 (18)	93 (3)	6
Best Skinny Dip Aramid® 4811	NR on Kevlar aramid knit	4.3 (0.3)	235 (32)	98 (19)	7
Best The Original Nitri-Flex® 4000P	Nitrile rubber on cotton knit	1.65 (0.06)	250 (22)	99 (12)	8
Ansell PowerFlex 80-100	NR on poly/cotton knit	3.6 (0.3)	267 (21)	110 (7)	9
Best Nitri-Pro® 7000P	Nitrile rubber on cotton knit	1.7 (0.4)	433 (65)	138 (52)	10

The low variability of the results as well as the fact that both the maximum force and the total work lead to the same ranking of the glove flexibility show this free-deforming technique as a valuable tool for the determination of the flexibility of loosely fitting protective gloves by mechanical means. However, these flexibility measurements may include a slight parasitic

contribution of the glove surface properties due to friction developing between the glove and the orifice edge surface.

The theoretical validation of the fixed technique for the determination of tight fitting glove flexibility was performed by comparing the measured and calculated values of the force corresponding to the position where the contact zone between the membrane and the probe head reaches the top of the probe head conical part (corresponding to the schematic in Figure 3.5). Table 3.2 provides the results for a nitrile rubber and two natural rubber gloves as well as for a neoprene membrane, the thickness value corresponding to the measured layer of material.

Table 3.2 Comparison of the measured and calculated force for the validation of the fixed technique (standard deviation in parenthesis)

Material / Model	Thickness (mm)	Measured force (N)	Calculated force (N)
Natural rubber (Ansell Canners & Handlers 392)	0.58 (0.03)	162 (19)	153
Neoprene membrane	0.40 (0.01)	239 (33)	218
Natural rubber (Best Latex HD® 55)	1.09 (0.04)	324 (49)	299
Nitrile rubber (Best Nitri-Solve® 747)	0.69 (0.03)	495 (60)	449

The force values correspond within the error bars. Indeed, for elastomers, and by extension, isotropic materials, material flexibility is independent of the type of deformation. For such materials, flexibility can be characterized by a simple uniaxial tensile test. However, for gloves made of anisotropic materials, a multi-directional deformation measurement such as the fixed technique is required.

The results in terms of the calculated flexibility coefficient (the inverse of the slope of the force displacement curve) are displayed in Table 3.3 for five models of gloves as well as for two thicknesses of a neoprene membrane. Due to limitations in the load cell capacity of the testing frame used for these measurements, the total extent of the linear part of the force displacement curve was not obtained for the composite gloves, leading to a slightly higher measurement uncertainty.

Table 3.3 Values of the flexibility coefficient measured with the fixed technique (standard deviation in parenthesis)

Model	Material	Thickness (mm)	Flexibility coefficient (mm/N)
Ansell Canners & Handlers 392	Natural rubber	0.58 (0.03)	0.118 (0.010)
Membrane	Neoprene	0.40 (0.01)	0.080 (0.009)
Best Latex HD® 55	Natural rubber	1.09 (0.04)	0.062 (0.007)
Best Nitri-Solve® 747	Nitrile rubber	0.69 (0.03)	0.036 (0.003)
Membrane	Neoprene	1.57 (0.07)	0.023 (0.002)
Ansell Goldknit Kevlar 70-225	Kevlar knit	2.13 (0.04)	0.014 (0.002)
Ansell Hyflex 11-900	Nitrile rubber on cotton knit	1.07 (0.04)	0.0043 (0.0006)

For natural rubber gloves and neoprene membranes, for which two thicknesses are available, the flexibility coefficient is inversely proportional to the material thickness, which is consistent with equations 3.3 and 3.4. With this fixed method, non-elastomer based gloves do show a much smaller flexibility compared to elastomer ones, producing a different glove ranking than that obtained with the free-deforming technique. To circumvent this reduced in-plane flexibility of composite materials while taking advantage of their increased protective

properties, composite gloves often include uncoated or more flexible material on the back side of the glove and on knuckles to allow more movement freedom for the user.

3.5 Conclusion

Two methods have been developed for the mechanical characterization of the flexibility of protective gloves. The free-deforming technique simulates the behavior of gloves that are worn loosely fitted and undergo mostly out-of-plane deformations, while the fixed technique characterizes the flexibility of tight fitting gloves. The validity of the fixed method was theoretically validated for elastomer materials. Both techniques produced different rankings for the tested gloves in terms of their flexibility, illustrating the importance of a careful selection of materials during glove design and the advantage of multipart configurations with properties of each glove section being tailored to the type and amplitude of deformations undergone at that location.

In order to verify the validity of the glove flexibility rankings provided by these two methods, the same gloves will be tested by human subjects, using both a biomechanical technique based on surface electromyography and a psychophysical evaluation test. The ultimate goal is to obtain a mechanical test method, i.e. not involving human subjects, able to characterize the glove flexibility as users perceive it. Much simpler to implement, such mechanical method could be easily used by protective glove manufacturers to provide quantitative information about their product's flexibility, thus allowing for an easier process of glove selection by users. In addition, the availability of such characterization tool could provide manufacturers with the incentive as well as the capability for improving the flexibility of their products while maintaining the same level of protection, such increased flexibility translating into improved dexterity and sensitivity for users.

Acknowledgements

This research has been supported by the Institut de recherche Robert-Sauvé en santé et en sécurité du travail. The financial contribution of the CREPEC is also acknowledged.

References

[1] Commission de la santé et de la sécurité du travail du Québec (Québec Occupational Health and Safety Commission). Occupational lesion database. Updated in December 2005.

[2] Bishu R, Muralidhar A. Gloves. In: Karwowski W, Marras WS, editors. The Occupational Ergonomics Handbook. CRC Press (NY); 1999. p. 865–876.

[3] Mital A, Kuo T, Faard HF. A quantitative evaluation of gloves used with non-powered hand tools in routine maintenance tasks. Ergonomics. 1994; 37(2): 333-343.

[4] Lariviere C, Plamondon A, Lara J, Tellier C, Boutin J, Dagenais A. Biomechanical assessment of gloves – A study of the sensitivity and reliability of electromyographic parameters used to measure the activation and fatigue of different forearm muscles. International Journal of Industrial Ergonomics. 2004; 34: 101-116.

[5] ISO 5979 Standard. Rubber or plastics coated fabrics – Determination of flexibility – Flat loop method. International Organization for Standardization; 1982.

[6] Kawabata S. The Standardization and Analysis of Hand Evaluation. The Textile Machinery Society of Japon (Osaka); 1980.

[7] ASTM D 4032 Standard. Standard test method for stiffness of fabric by circular bend procedure. American Society for Testing and Metals; 1994.

[8] Mooney M. A theory of large elastic deformation. Journal of Applied Physics. 1941; 11: 582-590.

[9] Laroche D, Vu-Khanh T. Modelling of the thermo-elastic properties of woven fabric composites in complex shapes. Composite Materials: testing and design. ASTM, STP 1206; 1993. p. 386-414.

[10] Fatma Selcen Killinc –Balci. A study of the nature of fabric comfort: Design-oriented fabric comfort model [Ph.D. dissertation]. Auburn University (Alabama); 2004 (AAT 3124275).

[11] Nguyen CT, Vu-Khanh T, Lara J. Puncture characterization of rubber membrane. Theoretical and Applied Fracture Mechanics. 2004; 42(1): 25-33.

[12] ASTM D 4012 Standard. Standard test methods for vulcanized rubber and thermoplastic elastomers - Tension. American Society for Testing and Metals; 1994 (Reapproved 2002).

CHAPITRE 4

ARTICLE 3: PREDICTION OF STRESS-STRAIN BEHAVIOUR AND ENERGY DISSIPATION OF ELASTOMERS PROTECTIVE MATERIALS

Article tel que soumis à la revue Journal of Polymer Applied Science en Mars 2008

Lotfi Harrabi[1], Tarek Abboud[1], Toan Vu-Khanh[1*], Patricia Dolez[1] and Jaime Lara[2]

[1] Université du Québec, École de Technologie Supérieure (ÉTS), 1100, Notre-Dame West, Montréal (Québec) H3C 1K3

[2] Institut de recherche Robert-Sauvé en santé et en sécurité du travail, 505 boul. de Maisonneuve Ouest, Montréal, Canada H3A 3C2

Résumé

Afin d'accomplir une certaine tache, comme le déplacement d'un objet ou le maintient d'une pièce nécessitant l'utilisation des gants de protection, les utilisateurs se trouvent souvent contraints à déformer leurs gants à des grandes échelles. De plus, l'effort fourni ainsi que l'énergie dissipée et par conséquent la fatigue musculaire augmentent quand il s'agit d'une tache à accomplir rapidement, entre autre à grande vitesse. Afin de pouvoir simuler ce genre de situation et caractériser le comportement des matériaux formant les gants de protection, nous nous proposons d'utiliser un test mécanique correspondant à un cycle de charge-décharge à des grandes déformations et à plusieurs vitesses. L'énergie dissipée correspond ainsi à l'aire de la boucle d'hystérésis obtenue. Pour ce fait, on se propose de comprendre ce comportement en modélisant la boucle d'hystérésis des élastomères et en particulier celle du Nitrile, afin de simuler les déformations réelle présentes dans un gant de protection en cours d'utilisation et en utilisant un modèle rhéologique à 3 éléments, celui de Zener. Les résultats trouvés ici montrent que le comportement de la membrane est géré par la contribution de deux parties : la première représente l'état d'équilibre de l'élastomère tandis que la seconde

représente plutôt la dépendance non linéaire du temps. une bonne corrélation entre la modélisation et l'expérimentation a été trouvée. Ceci nous permettra de prédire le comportement mécanique en terme de boucle d'hystérésis à n'importe quelle vitesse à partir d'un seul test de chargement à une vitesse donnée. La vérification de la validité de cette approche ainsi que plus de détails concernant la détermination des paramètres du modèle sont présentés dans l'ANNEXE II.

Abstract

Utilization of protective glove involves usually very large deformations. Strain rates involved in these deformations are highly variable. For elastomers, energy dissipation by hysteresis is very important and constitutes a major parameter to be optimized. In order to be able to predict the stress-strain behaviour of elastomers at large deformations, a theoretical description was developed for the loading-unloading hysteretic loop at large deformations and as a function of the strain rate. Bergström and Boyce's proposition that the elastomer behaviour is controlled by two contributions, the first one corresponding to the equilibrium state and the second one to a non-linear rate-dependent deviation from that equilibrium state, and their use of Zener's rheological model, were applied to an uniaxial tension configuration. A validation of the description was performed with nitrile rubber. A good agreement of the theoretical description with experimental results was obtained. This simple description of the hysteretic behaviour of elastomers as a function of the strain rate provides a useful tool for estimating the dissipated energy at various strain rates, with potential application in the design of protective gloves.

4.1 Introduction

The use of protective gloves at the workplace allows a reduction in injury occurrence and seriousness. However, wearing protective gloves may also cause a decrease in the ability to perform tasks and an increased level of muscular fatigue, for example due to their lack of suppleness [1]. Ultimately, this can either lead to resistance to wearing the needed protective gloves, with an increase in direct injuries like skin laceration, or to the occurrence of indirect and more long-term injuries like tendonitis. The design of gloves with adequate properties requires a knowledge of the constituve material mechanical behaviour. While some studies have reported on the development of methods for the characterization of protective glove stiffness, either mechanical [2, 3] or with human subjects [3, 4], as well as on the effect of these properties on task performance [5], not much has been done on the dynamic mechanical behaviour of gloves. Yet, deformations subjected to gloves in use may involve a wide range of strain rates. This question is particularly relevant in the case of viscoelastic compounds like elastomers, which constitute a choice material for protective gloves due to their good flexibility and elasticity as well as their resistance to a number of hazards [6]. For example, nitrile rubber offers good chemical performance [7, 8]. In the work reported in this paper, the dynamic mechanical behaviour of elastomers is studied at conditions relevant to the use of protective gloves, i.e. at large deformation and variable strain rates, through the analysis of the hysteretic loop corresponding to a loading-unloading cycle.

Several authors have worked on the mechanical behaviour of elastomers [9-30]. Two approaches can be identified: the molecular approach is based on network physics [12-14, 21, 22, 27, 31] while the phenomenological approach relies on mathematical considerations [7, 9-11, 15, 24, 25, 32]. For example Mooney and Rivlin have lay the basis for large deformation theories for elastic materials. More recently, Arruda and Boyce have proposed a new description known as the eigth chain model, which is derived from non-Gaussian statistics theory [31]. It has been used succefully to predict the behaviour of elastomers up to failure. In particular, it has had applications in optics [33] and structural mechanics [20].

In the case of cyclic loading, even if they are highly elastic, elastomers display different paths for loading and unloading [12, 34]. This hysteresis loop corresponds to the energy dissipated during the loading-unloading process. After a few cycles, this loop tends to stabilise as shown by Mullins [35]. Even if time is a fundamental factor to consider when dealing with viscoelastic materials like elastomers, very few people have looked at the effect of strain rate on the mechanical behaviour of elastomers, and in particular on the hysteresis loop. Some have limited their study to the effect of strain and stress amplitude on the hysteretic loss [36]. Others have looked at the effect of the strain rate on the parameters of the model used for finite element analysis [37]. Bergström and Boyce were the first ones to consider the case with attention; they studied the effect of strain rate on the hysteresis loop of elastomers when working in compression and at large deformation [38]. They proposed a theoretical description based on the three-element Zener rheological model and the use of non-linear constants. The same principle was later applied to the case of thermoplastics for example [39].

Bergström and Boyce's idea consists in decomposing the hysteresis loop in two parts, one characterizing the equilibrium state of the deformed elastomer, and the other a time-dependant deviation from that equilibrium [38]. The resulting total stress combines an elastic contribution and a time-dependent one. As an alternative to Bergström and Boyce's 3D complex tensorial description relative to compression, this paper proposes a simplified model based on the same principles but corresponding to a unidirectional treatment of tensile deformation. It is validated by comparison with experimental tests performed with nitrile rubber samples.

4.2 Experimental

The studied material is nitrile rubber. Samples were cut from protective gloves (Best Glove manufacturing, model number 412, thickness 0.6 mm) using dye C of the ASTM D 412 standard test method for measuring the tensile properties of elastomers [40]. The tests were performed with a MTS mechanical test frame, model Alliance RF/200 using a 1000 N load

cell. For each condition, a minimum of three replicates were measured. Maximum loading and loading-unloading experiments were carried out at various loading rates. Figure 4.1 illustrates the loading-unloading sequence applied in the case of a 50 mm/min loading rate.

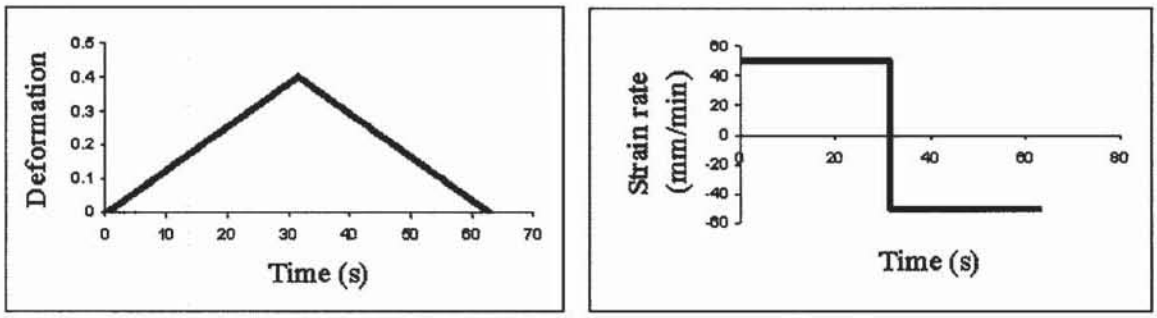

Figure 4.1 Loading-unloading test (loading rate 50 mm/min)

4.3 Theoretical description

A combination of a non linear viscoelastic model and Zener standard rheological description of solids (see Figure 4.2) has been used to predict the hysteretic behavior of nitrile rubber at large deformations and at different strain rates. More specifically, it is proposed that the hysteretic behavior of the elastomer membrane is due to the contribution of two parts: the first one (A) corresponds to the equilibrium state and can be represented by a spring R_1 while the second one (B) is due to the deviation from this equilibrium and is described by a spring R_2 in series with a damper. To take into account the non linear behavior of nitrile rubber, both springs are described using the Arruda-Boyce eight-chain model [31], while a simple linear function of the strain rate logarithm is used for the damper viscosity.

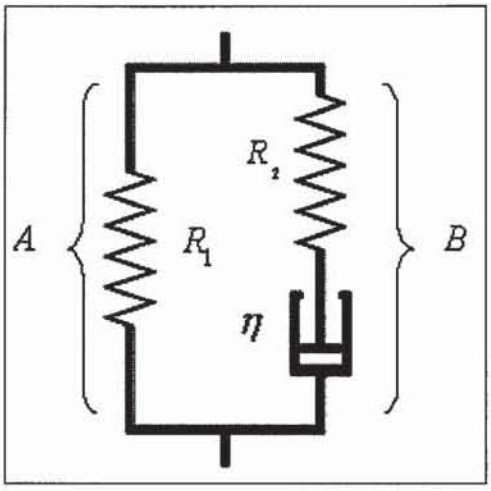

Figure 4.2 Schematic representation of the Zener viscoelastic model

The differential equation corresponding to Zener three-element model is provided by Equation (4.1) [34].

$$\dot{\sigma} + \frac{E^{(R_2)}}{\eta}\sigma = (E^{(R_1)} + E^{(R_2)})\dot{\varepsilon} + \frac{E^{(R_1)}E^{(R_2)}}{\eta}\varepsilon \tag{4.1}$$

Where $E^{(R_1)}$ is the modulus of spring R_1, $E^{(R_2)}$ is the modulus of spring R_2 and η is the viscosity of the damper, σ is the stress, $\dot{\sigma}$ is the variation of the stress with time, ε is the strain and $\dot{\varepsilon}$ is the strain rate.

Equation (4.2) represents the solution of Equation (4.1) in terms of time variation of the stress for a loading-unloading cycle.

$$\sigma(t) = \zeta\left\{\left[\eta + E^{(R_1)}t - \eta\, e^{-\frac{E^{(R_2)}}{\eta}t}\right] - 2\left[\eta + E^{(R_1)}(t-\tau_{1/2}) - \eta e^{-\frac{E^{(R_2)}}{\eta}(t-\tau_{1/2})}\right]H(t-\tau_{1/2})\right\} \tag{4.2}$$

With t is the time, ζ is the strain rate of the test, $\tau_{1/2}$ is the half cycle time and H is the Heaviside function as defined by Equation (4.3).

$$\begin{cases} H(t-\tau_{1/2})=0 \ \ pour \ t \le \tau_{1/2} \\ H(t-\tau_{1/2})=1 \ \ pour \ t \ge \tau_{1/2} \end{cases} \tag{4.3}$$

4.3.1 Representation of the equilibrium state

The strain-stress relationship corresponding to part A of the Zener model (see Figure 4.2) provides a representation of the equilibrium state. This part can be modeled by any of the hyperelasticity-based classical models. Following Bergström [38], the Arruda-Boyce eight-chain model was selected. In the case of a unidirectional test, the stress-strain relationship can be expressed by [31]:

$$\sigma_{True}^{(R_1)} = C^{(R_1)}\left(\lambda^2 - \frac{1}{\lambda}\right)\frac{\sqrt{N^{(R_1)}}}{\lambda^{(R_1)}_{\ chain}} L^{-1}\left(\frac{\lambda^{(R_1)}_{\ chain}}{\sqrt{N^{(R_1)}}}\right) \tag{4.4}$$

With

$$\lambda^{(R_1)}_{\ chain} = \sqrt{\frac{\left(\lambda^2 + 2/\lambda\right)}{3}} \tag{4.5}$$

$$C^{(R_1)} = \frac{nK_BT}{3} \tag{4.6}$$

$$N^{(R_1)} = \frac{1}{3}\left[\lambda_{\lim}^2 + \frac{2}{\lambda_{\lim}}\right] \tag{4.7}$$

Where $\sigma^{(R_1)}$ is the true stress of the membrane in the equilibrium state given, λ is the extension ratio, λ_{lim} is the limit network stretch and L is the Langevin function defined by $L(x) = \coth(x) - \frac{1}{x}$. The engineering stress is related to the true stress by Equation (4.8).

$$\sigma_{True} = \lambda \sigma_{Eng} \tag{4.8}$$

The relationship between the spring modulus, the stress and the strain is given by Equation (4.9).

$$\sigma_{Eng} = E\varepsilon \tag{4.9}$$

Combining Equations (4.4) and (4.9) provides the modulus of the spring R_1.

$$E^{(R_1)} = \frac{C^{(R_1)}\left(\lambda - \frac{1}{\lambda^2}\right)\frac{\sqrt{N^{(R_1)}}}{\lambda^{(R_1)}_{chain}} L^{-1}\left(\frac{\lambda^{(R_1)}_{chain}}{\sqrt{N^{(R_1)}}}\right)}{\varepsilon} \tag{4.10}$$

Knowing the relation between the strain and the extension,

$$\varepsilon = \lambda - 1 \tag{4.11}$$

the final expression for the modulus of the spring R_1 can be obtained:

$$E^{(R_1)} = \frac{C^{(R_1)}\left(\lambda - \frac{1}{\lambda^2}\right)\frac{\sqrt{N^{(R_1)}}}{\lambda^{(R_1)}_{chain}} L^{-1}\left(\frac{\lambda^{(R_1)}_{chain}}{\sqrt{N^{(R_1)}}}\right)}{\lambda - 1} \tag{4.12}$$

As can be seen in Equation (4.12), the modulus of the spring R_1 is defined by two parameters. The first one, $C^{(R_1)}$, which is provided by Equation (4.6), is related to the shear modulus of the network in the equilibrium state. The second parameter is $N^{(R_1)}$, defined in Equation (4.7), which can be associated with the stretch limit of the network. Both parameters are material constants.

4.3.2 Representation of the deviation from the equilibrium state

The time-dependence behavior which represents the deviation from the equilibrium state corresponds to part B of the Zener model (see Figure 4.2). The spring R_2 is characterized by a non-linear stress-strain behavior while the time dependence is provided by the damper.

The modulus of the spring R_2 can be obtained using the same method as described in section 4.3.1 for the spring R_1:

$$E^{(R_2)} = \frac{C^{(R_2)}\left(\lambda^{(R_2)} - \frac{1}{\lambda^{(R_2)2}}\right)\frac{\sqrt{N^{(R_2)}}}{\lambda^{(R_2)}_{chain}} L^{-1}\left(\frac{\lambda^{(R_2)}_{chain}}{\sqrt{N^{(R_2)}}}\right)}{\lambda^{(R_2)} - 1} \tag{4.13}$$

where $C^{(R_2)}$ and $N^{(R_2)}$ are the two parameters defining the spring R_2 and $\lambda^{(R_2)}$ is the extension ratio relative to the spring R_2.

For the damper viscosity η, we propose to use the simple relationship shown in Equation 4.14 to describe its variation with the strain rate ζ.

$$\eta = ALn(\zeta) + B \tag{4.14}$$

where A and B are constants characterizing the damper.

4.4 Determination methods for the model constants

This section describes the methods that have been used to obtain the constants $C^{(R_1)}$ and $N^{(R_1)}$ for the spring R_1, $C^{(R_2)}$ and $N^{(R_2)}$ for the spring R_2, and A and B for the damper.

4.4.1 Determination of the constants relative to the equilibrium state contribution

The membrane equilibrium state is represented by the mechanical behavior of the spring R_1. The spring modulus depends on two parameters, $C^{(R_1)}$ and $N^{(R_1)}$, according to Equation (4.12). $N^{(R_1)}$ is related to the limit network stretch λ_{lim} (Equation (4.7)). This limit stretch corresponds to the theoretical maximum extension that the elastomer molecular chains can reach in the liquid state. It can be determined from a tension test as shown in Figure 4.3. A theoretical stress-strain curve is fitted to the experimental data, and λ_{lim} is provided by its theoretical asymptotic limit at large extension.

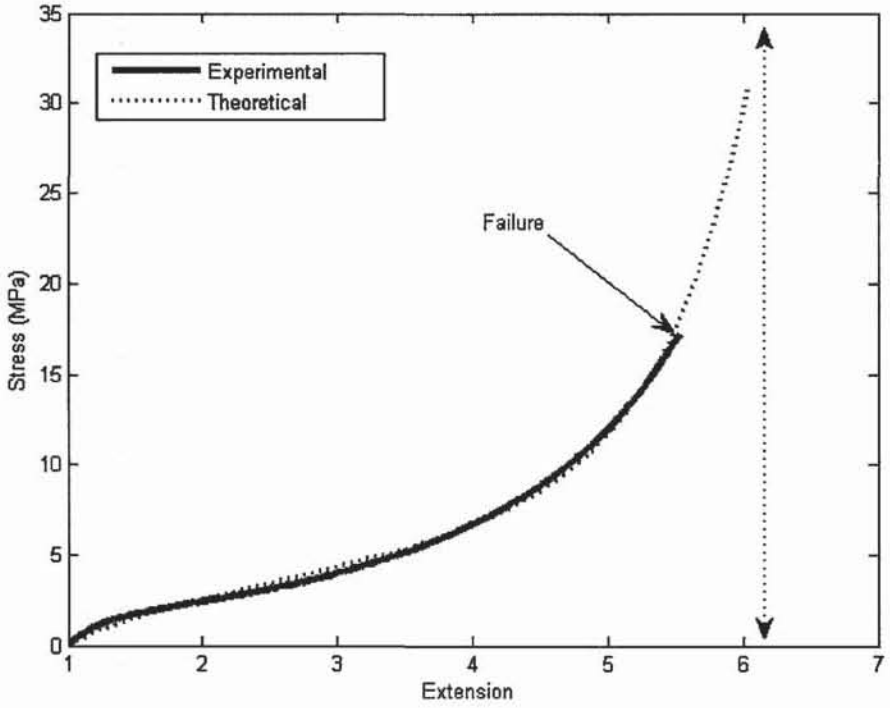

Figure 4.3 Determination of the limit network stretch

For its part, $C^{(R_1)}$ is linked to the number of entanglements and the temperature (Equation (4.6)). It can be computed using the alternative expression provided by the Arruda-Boyce model [38]:

$$C^{(R_1)} = \frac{\sigma}{\left(\lambda - \frac{1}{\lambda^2}\right)\frac{\sqrt{N^{(R_1)}}}{\lambda^{(R_1)}_{chain}} L^{-1}\left(\frac{\lambda^{(R_1)}_{chain}}{\sqrt{N^{(R_1)}}}\right)} \tag{4.15}$$

Where $\lambda^{(R_1)}_{chain}$ et $N^{(R_1)}$ are given respectively by Equations (4.5) and (4.7). $C^{(R_1)}$ can be calculated for any location within the equilibrium state defined by a theoretical path laying between the sample loading and unloading curves as shown in
Figure 4.4. In addition, since loading rates are comprised between 10 mm/min and 100 mm/min, an intermediate rate of 50 mm/min was selected for the determination of $C^{(R_1)}$.

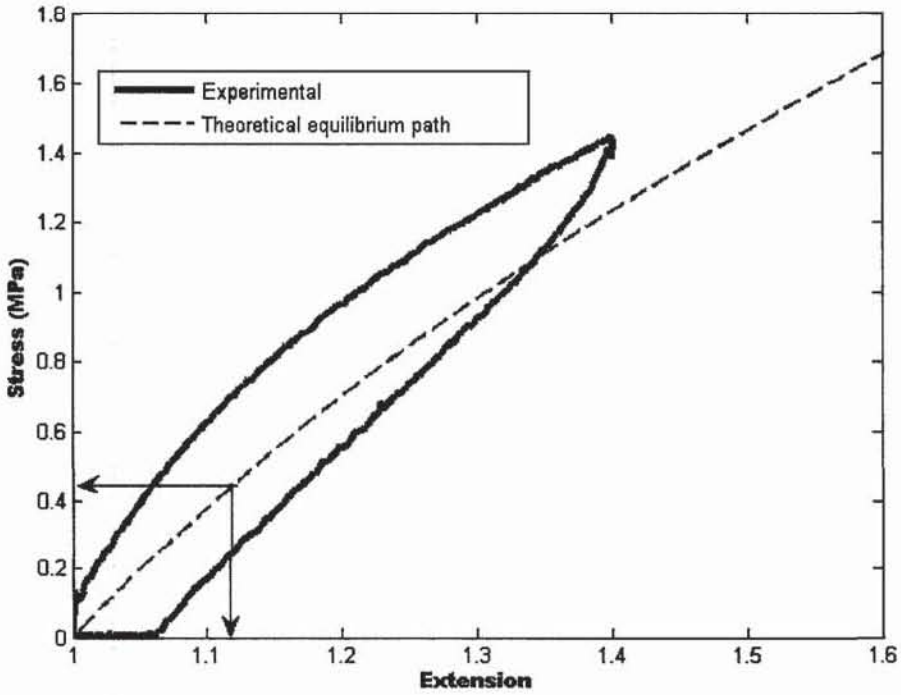

Figure 4.4 Location of the theoretical equilibrium path relatively to the loading and unloading curves

4.4.2 Determination of the constants relative to the deviation from the equilibrium state

The contribution of the deviation from the equilibrium state to the elastomer behavior is essentially due to the part B of the model, i.e. the spring R_2 and the damper. In particular, these two components provide the time dependence of the system. The damper viscosity is provided in Equation 4.14. Here, the determination of the spring R_2 constants is shown.

4.4.2.1 Determination of the spring R_2 constants

The stress-strain expression for loading is provided by Equation (4.16), which is obtained from Equation 4.2 when $t < \tau_{1/2}$.

$$\sigma = \zeta\eta + E^{(R_1)}\varepsilon - \zeta\eta\, e^{-\frac{E^{(R_2)}}{\eta}\frac{\varepsilon}{\zeta}} \tag{4.16}$$

When ε is much smaller than 1, the slope of the curve representing Equation (4.16) is given by:

$$\lim_{x\to 0}\left(\frac{\partial\sigma}{\partial\varepsilon}\right) = E^{(R_1)} + E^{(R_2)} \tag{4.17}$$

The physical meaning of this result can be interpreted as the fact that, at the beginning of the deformation, the system stress is only controlled by the two springs, with no contribution of the damper. This can be attributed to the fact that, when the deformation begins, the damper strain rate is equal to zero, leading to a zero stress. The stress at the beginning of the deformation is thus the result of the contribution of a system composed of the two springs in parallel. This leads the system modulus at the origin being provided by the sum of the two spring modulus.

Let's call E_t this slope at the origin deduced from the experimental stress-strain curve measured with the elastomer membrane.

$$E_t = E^{(R_1)} + E^{(R_2)} \tag{4.18}$$

The expressions for $E^{(R_1)}$ and $E^{(R_2)}$ are provided by Equations (4.12) and (4.13) respectively. At the beginning of the system loading, the springs R_1 and R_2 have the same extension ratio λ, consequently $\lambda^{(R_1)}{}_{chain}$ and $\lambda^{(R_2)}{}_{chain}$ are equals according to Equation (4.5). In addition, we can consider also that these two springs have the same limit stretch λ_{lim}. Thus, according to Equation (4.7), $N^{(R_1)}$ is equal to $N^{(R_2)}$ and the expression of E_t can be reduced to:

$$E_t = \frac{\left(C^{(R_1)} + C^{(R_2)}\right) \cdot \left(\lambda - \frac{1}{\lambda^2}\right) \frac{\sqrt{N}}{\lambda_{chain}} L^{-1}\left(\frac{\lambda_{chain}}{\sqrt{N}}\right)}{\lambda - 1} \tag{4.19}$$

The inverse of the Langevin function can be approximated by:

$$L^{-1}\left(\frac{\lambda_{chain}}{\sqrt{N}}\right) = 3\frac{\lambda_{chain}}{\sqrt{N}} + \frac{9}{5}\left(\frac{\lambda_{chain}}{\sqrt{N}}\right)^3 + \frac{297}{175}\left(\frac{\lambda_{chain}}{\sqrt{N}}\right)^5 + \ldots \tag{4.20}$$

For $\lambda \approx 1$, Equation (4.20) can be reduced to:

$$L^{-1}\left(\frac{\lambda_{chain}}{\sqrt{N}}\right) \approx 3\frac{\lambda_{chain}}{\sqrt{N}} \tag{4.21}$$

Equation (4.19) thus becomes:

$$E_t = 3\left(C^{(R_1)} + C^{(R_2)}\right)\frac{\left(\lambda - \frac{1}{\lambda^2}\right)}{\lambda - 1} \tag{4.22}$$

$C^{(R_2)}$ is provided by Equation (4.23), where $C^{(R_1)}$ is deduced from the experimental data using Equation (4.15) and E_t can be obtained from the slope of the loading stress-strain curve at the origin.

$$C^{(R_2)} = \frac{E_t}{3}\left[\frac{\lambda^2+\lambda+1}{\lambda^2}\right]^{-1} - C^{(R_1)} \tag{4.23}$$

4.4.2.2 Determination of the damper viscosity

The damper viscosity is described by a linear function of the strain rate logarithm (Equation (4.14)). The values of the constants A and B are obtained by regression using the mean square method as shown in Figure 4.5.

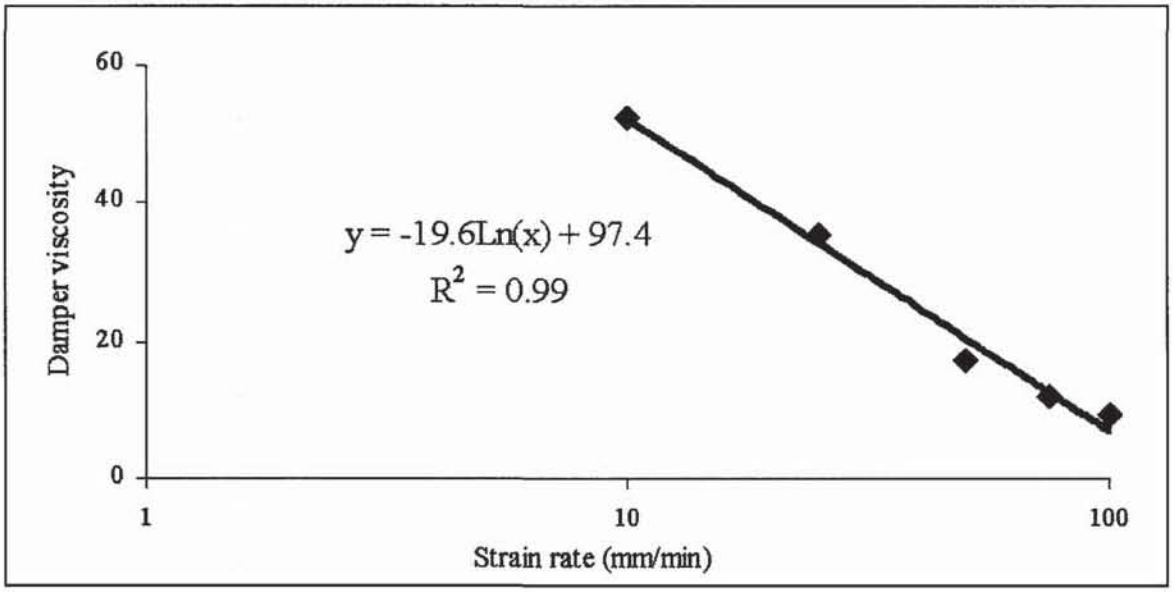

Figure 4.5 Damper viscosity constants determination

4.5 Results and discussion

The measured loading-unloading stress-strain data represented in Figure 4.6 illustrate the non linear mechanical behavior of nitrile rubber. They also show the large effect of strain rate on the hysteresis loop corresponding to a cycle of loading-unloading.

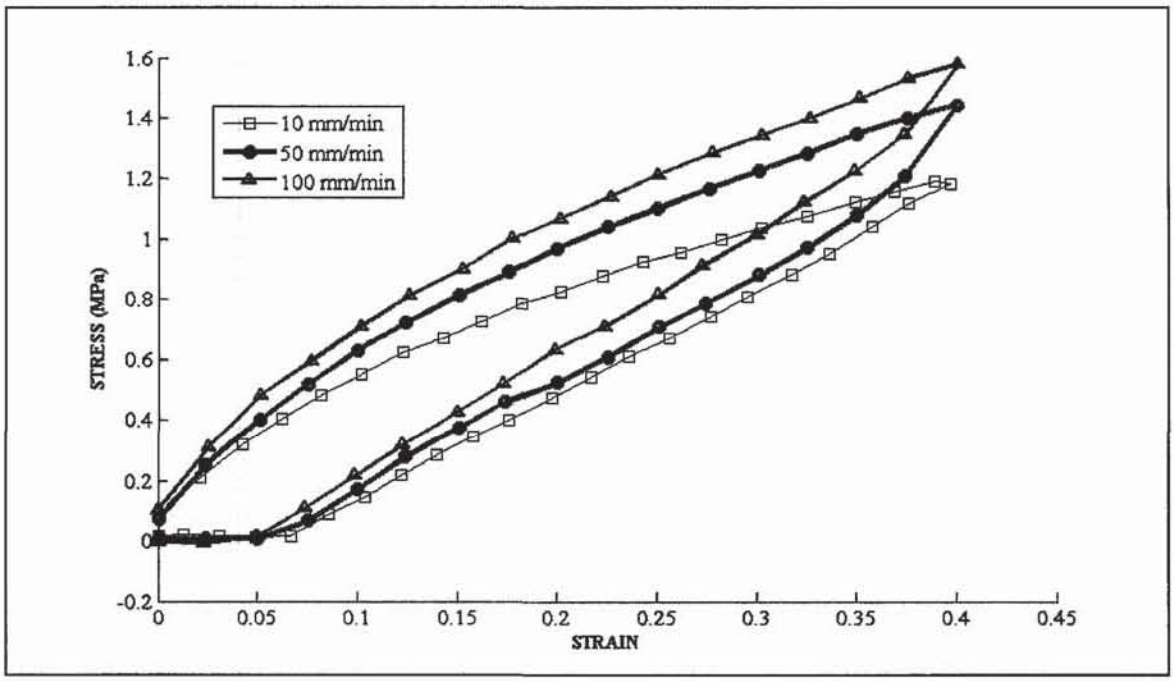

Figure 4.6 Stress-strain behavior of nitrile rubber at different strain rates

For a given strain rate, the hysteresis loop can be resolved into two curves as shown in Figure 4.7. The first one corresponds to the equilibrium state represented by the spring R_1. The second curve is associated with the deviation from this equilibrium state, described by part B of the Zener model (Figure 4.2).

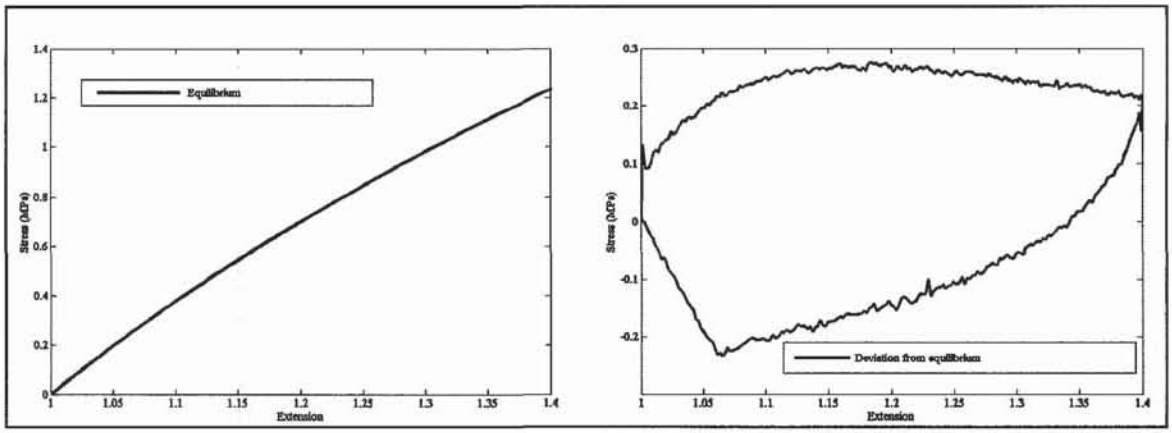

Figure 4.7 Graphic decomposition of the stress-strain behavior of the rubber

The values of the spring parameters used for the proposed description of the nitrile rubber hysteretic behavior, which should be valid at all strain rates, are determined from the test performed at 50 mm/min. They are provided in Table 4.1.

Table 4.1 Values of the spring parameters, obtained using 50 mm/min measurements

	$C^{(R_1)}$ *(MPa)*	$C^{(R_2)}$ *(MPa)*	N
Spring R_1	0.46	*	370.54
Spring R_2	*	1.17	370.54

Figure **4.8** displays the experimental results and those provided by the theoretical description using Table 4.1 parameter values for nitrile rubber hysteresis loop at 50 mm/min.

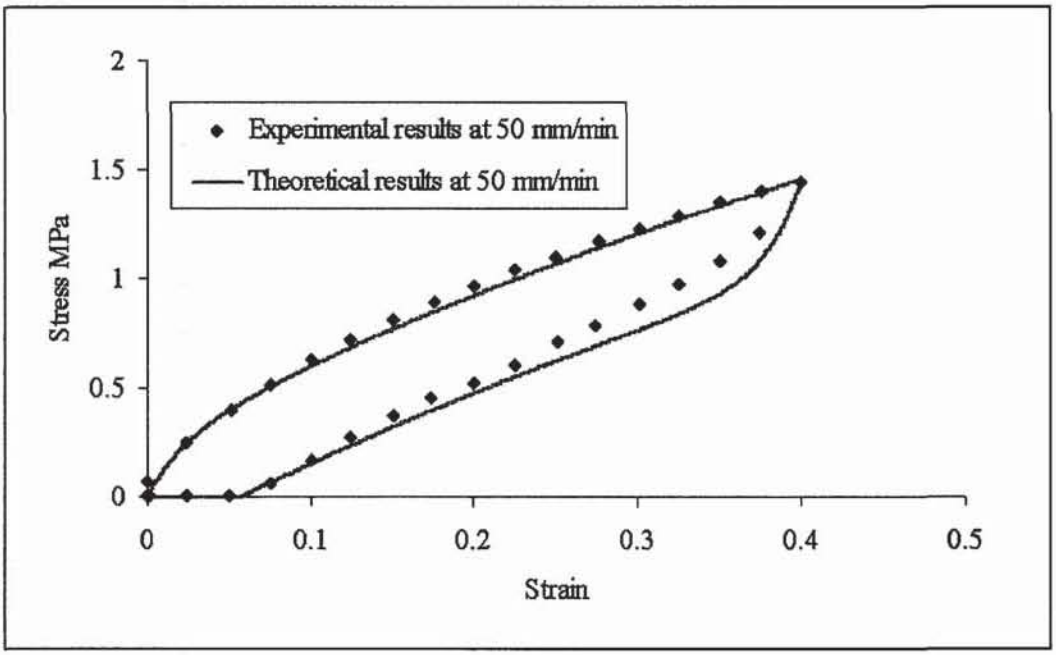

Figure 4.8 Hysteretic stress-strain loop at 50mm/min for Nitrile rubber

The values of the spring parameters obtained with the data measured at 50 mm/min were used to compute the nitrile rubber hysteretic stress-strain loop at others strain rates (10, 25, 75 and 100 mm/min). As shown in Figure 4.9, which displays the results obtained for strain rates of 10 and 100 mm/min, a relatively good correlation between experimental and theoretical results is obtained, especially for the loading part of the curve.

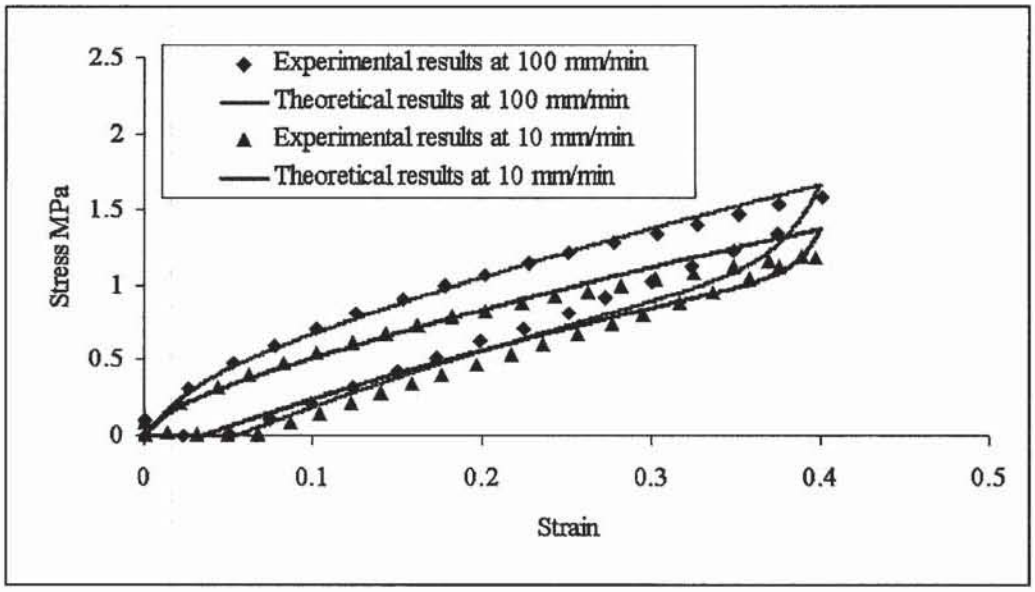

Figure 4.9 Stress-strain behavior at 10 and 100 mm/min

The dissipated energy for one charge-discharge cycle is provided by the area of the hysteresis loop. The results are displayed in Figure 4.10 as a function of the strain rate. A good agreement can be observed between experimental and theoretical results.

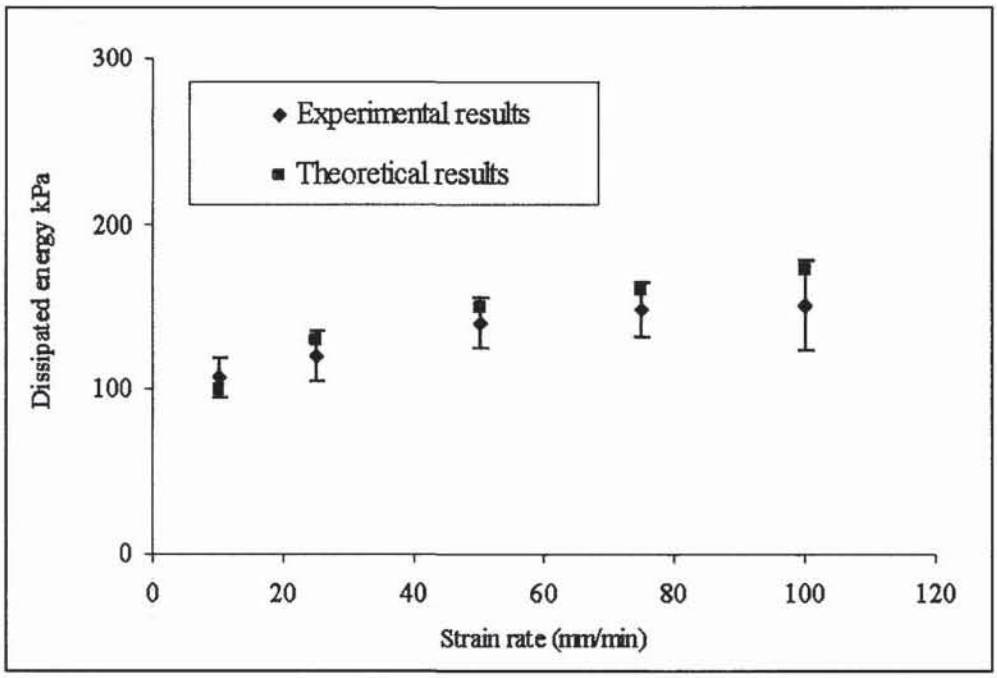

Figure 4.10 Influence of the strain rate on the dissipated energy of the membrane

These results show that the mechanical behavior of nitrile rubber during a loading-unloading cycle depends on the strain rate and therefore on the time. This time dependence is essentially brought by part B of the 3-element Zener-type model, which corresponds to a spring in series with a damper. The good agreement obtained between the experimental results and the theoretical description confirms the legitimacy of the approximations made. Finally, this study provides a simple tool to estimate the loading-unloading stress-strain behavior of nitrile as well as other elastomers at any strain rate.

4.6 Conclusion

When they are used, protective gloves are subjected on a regular basis to cyclic deformations. In order to study the behaviour at large deformations and various strain rates of elastomers, which constitute a choice material for gloves, a model was developed based on a uniaxial loading-unloading configuration. The theoretical description was provided using Zener's

rheological model in agreement with Bergström and Boyce's proposition that the elastomer behaviour is controlled by two contributions, the first one corresponding to the equilibrium state and the second one to a non-linear rate-dependent deviation from that equilibrium state. The validity of the description was verified with nitrile rubber samples. The parameters corresponding to the springs were obtained from measurements carried out at 50 mm/min. The damper viscosity is approximated by a linear function of the strain rate logarithm. A good agreement between the theoretical and experimental results was obtained. These data were used to compute the energy dissipated during the loading-unloading cycle. This simple description of the hysteretic behaviour of elastomers as a function of the strain rate provides a useful tool to estimate the dissipated energy at various strain rates. Attempts will be made to extend this approach to the case of textiles and coated textiles, which are also used as protective glove materials.

Acknowledgement

This research has been supported by the Institut de recherche Robert-Sauvé en santé et sécurité du travail (IRSST), Montréal, Canada. The authors would also like to thank Mr Michel Beaudin for his advices on mathematical modelling.

References

1. Vu-Khanh, T., Dolez, P. I., Harrabi, L., Lara, J., Larivière, C., Tremblay, G., Nadeau, S., *Caractérisation de la souplesse des gants de protection par des méthodes mécaniques et une méthode biomécanique basée sur l'électromyographie de surface.* Étude et Recherche. 2007, Montréal: Institut de recherche Robert-Sauve´ en santé et en sécurité du travail au Québec. 90 pages.

2. Harrabi, L., Dolez, Patricia I., Vu-Khanh, Toan., Lara, Jaime., *Evaluation of the flexibility of protective gloves.* International Journal of Occupational Safety and Ergonomics. , 2008. **14**(1): p. 61-68.

3. Harrabi, L., Dolez, Patricia I., Vu-Khanh, Toan., Lara, Jaime., Tremblay, Guy., Nadeau, Sylvie., Larivière, Christian., *Characterization of protective gloves stiffness: Development of a multidirectional deformation test method.* Safety Science, 2008. **46**(7): p. 1025-1036.

4. Larivière, C., et al., *Biomechanical assessment of gloves. A study of the sensitivity and reliability of electromyographic parameters used to measure the activation and fatigue of different forearm muscles.* International Journal of Industrial Ergonomics, 2004. **34**(2): p. 101-116.

5. Buhman, D.C., et al., *Effects of glove, orientation, pressure, load, and handle on submaximal grasp force.* International Journal of Industrial Ergonomics, 2000. **25**(3): p. 247-256.

6. Betteni, F., *Dispositivi di protezione individuale.* Tinctoria, 2004: p. 37-43.

7. Gent, A.N., *Engineering with rubber: How to design with rubber components.* 2001, Munich: Hanser Publishers.

8. Kumar, A. and R.K. Gupta, *Fundamentals of Polymer Engineering.* 2 nd ed. 2003, New York: Marcel Dekker.

9. Mooney, M., *A Theory of Large Elastic Deformation.* Journal of Applied Physics, 1940. **11**: p. 582-592.

10. Rivlin, R.S. *Large Elastic Deformation of Isotropic Materials. Further development of the General Theory.* in *Phil. Trans. Roy. Soc. London.* 1948.

11. Rivlin, R.S., *Large Elastic Deformation of Isotropic Materials.* Royal Society of London--Philosophical Transactions Series A, 1948. **241**(835): p. 379-397.

12. Treloar, L.R.G., *The Physics of Rubber Elasticity.* 1975: Oxford University Press.

13. Treloar, L.R.G., *Elasticity and related properties of rubbers.* Rubber Chem. Technol, 1974. **47**(3): p. 625-696.

14. Treloar, L.R.G., *A non-gaussian theory for rubber in biaxial strain- I. Mechanical properties.* Proc. R. Soc. London A, 1979. **369**: p. 261-280.

15. Ogden, R.W., *Large deformation isotropic elasticity- on the correlation of the theory and experiment for incompressible rubberlike solids.* Proceedings of the Royal Society of London, Series A (Mathematical and Physical Sciences), 1972. **326**(1567): p. 565-84.

16. Ogden, R.W., *Background on nonlinear elasticity, Chapter 2.2,* J. Lemaitre, Editor. 2001, in the handbook of materials behavior models: Boston. p. 75-83.

17. Yeoh, O.H., *Some forms of the strain energy function for rubber.* Rubber Chemistry and Technology, 1993. **66**(5): p. 754-771.

18. Yeoh, O.H., *Hyperelastic material models for finite element analysis of rubber.* J. Nature Rubber Res., 1997. **12**: p. 142-153.

19. Allen, G., et al., *Thermodynamics of rubber elasticity at constant volume.* Trans. Faraday Soc, 1971. **67**: p. 1278-1292.

20. Allport, J.M. and A.J. Day, *Statistical mechanics material model for the constitutive modelling of elastomeric compounds.* Proceedings of the Institution of Mechanical Engineers, Part C: Journal of Mechanical Engineering Science, 1996. **210**(6): p. 575-585.

21. Flory, P.J., *Network structure and the elastic properties of vulcanized rubber.* Chem. Rev., 1944. **35**: p. 51-75.

22. Flory, P.J., *Theory of elasticity of polymer networks. The effect of local constraints on junctions.* J. Chem. Phys, 1977. **14**(2): p. 80-92.

23. Ferry, J.D., *Viscoelastic Properties of Polymers.* 1980: John Wiley and Sons, Inc.

24. Gent, A.N. and thomas A.G., *Forms of the stored (strain) energy function for vulcanized rubber.* J. Polym. Sci, 1958. **28**: p. 625-637.

25. Hart-Smith, L.J., *Elasticity parameters for finite deformation of rubber-like materials.* Z. Angew. Mathe. Phys., 1966. **17**: p. 608-626.

26. Gumbrell, S.M., Mullins L., and Rivlin R.S., *Departures of the elastic behaviour of Rubbers in simple extension from the kinetic theory.* Trans Faraday Soc, 1953. **49**: p. 1495-1505.

27. James, H.M. and Guth E., *Theory of the elastic properties of rubber.* J. Chem. Phys., 1943. **11**(10): p. 455-481.

28. Mark, J.E., *The constants 2 C_1 and 2 C_2 in phenomenological elasticity theory and their dependence on experimental variables.* Rubber Chemistry and Technology, 1975. **48**(3): p. 495-512.

29. Varga, O.H., *Stress-Strain behavior of elastic materials: selected problems of large deformation.* New York: Interscience publisher, 1966: p. 190 p.

30. Gee, G., *The present status of the theory of rubber elasticity.* Polymer., 1966. **7**: p. 373-385.

31. Arruda, E.M. and M.C. Boyce, *A three-dimensional constitutive model for the large stretch behavior of rubber elastic materials.* Journal of the Mechanics and Physics of Solids, 1993. **41**(2): p. 389-412.

32. Valanis, K.C. and R.F. Landel, *Strain-energy function of hyperelastic material in terms of extension ratios.* Journal of Applied Physics, 1967. **38**(7): p. 2997-3002.

33. Von Lockette, P.R. and E.M. Arruda, *A network description of the non-Gaussian stress-optic and Raman scattering responses of elastomer networks.* Acta Mechanica, 1999. **134**(1-2): p. 81-107.

34. McCrum, N.G., C.P. Buckley, and C.B. Bucknall, *Principles of Polymer Engineering.* 2004, New York: OXFORD UNIVERSITY PRESS.

35. Mullins, L., *Softening of rubber by deformation.* Rubber Chem. Technol, 1969. **42**: p. 339-362.

36. Kucherskii, A.M., *Hysteresis losses in carbon-black-filled rubbers under small and large elongations.* Polymer Testing, 2005. **24**(6): p. 733-738.

37. Song, B., W. Chen, and M. Cheng, *Novel model for uniaxial strain-rate-dependent stress-strain behavior of ethylene-propylene-diene monomer rubber in compression or tension.* Journal of Applied Polymer Science, 2004. **92**(3): p. 1553-1558.

38. Bergstrom, J.S. and M.C. Boyce, *Constitutive modeling of the large strain time-dependent behavior of elastomers.* Journal of the Mechanics and Physics of Solids, 1998. **46**(5): p. 931-954.

39. Qi, H.J. and M.C. Boyce, *Stress-strain behavior of thermoplastic polyurethanes.* Mechanics of Materials, 2005. **37**(8): p. 817-839.

40. ASTM D 412., *Standard Test Methods for Vulcanized Rubber and Thermoplastic Elastomers - Tension.* 1998, Annual Book of ASTM Standards.

41. Doi, M. and S.F. Edwards, *The Theory of Polymer Dynamics.* 1986: Oxford University Press.

42. Bergstrom, J.S., *Large Strain Time-Dependent Behavior of Elastomeric Materials*, in *Department of Mechanical Engineering.* 1999, MASSACHUSETTS INSTITUTE OF TECHNOLOGY.

CHAPITRE 5

ARTICLE 4: PREDICTION OF STRESS-STRAIN BEHAVIOUR AND ENERGY DISSIPATION OF TEXTILE PROTECTIVE MATERIALS AT LARGE DEFORMATIONS

Article à soumettre à la revue Journal of Polymer Applied Science

Lotfi Harrabi[1], Tarek Abboud[1], Toan Vu-Khanh[1], Patricia Dolez[1] and Jaime Lara[2]

[1] École de Technologie Supérieure (ÉTS), 1100, Notre-Dame West, Montréal (Québec) H3C 1K3

[2] Institut de recherche Robert-Sauvé en santé et en sécurité du travail, 505 boul. de Maisonneuve Ouest, Montréal, Canada H3A 3C2

Résumé

Le but de cet article consiste à modéliser le comportement viscoélastique des matériaux textiles utilisés dans la fabrication des gants de protection à grande déformation et à différentes vitesses. Nous nous intéressons particulièrement `à un cycle de charge-décharge. Le modèle présenté ici est basé sur le modèle rhéologique de Zener. D'une façon analogue aux élastomères, les résultats trouvés ici montrent que le comportement du textile est géré par la contribution de deux parties : la première représente l'état d'équilibre du tricot tandis que la seconde représente plutôt la dépendance non linéaire du temps. une bonne corrélation entre la modélisation et l'expérimentation a été trouvée. Ceci nous permettra de prédire le comportement mécanique en terme de boucle d'hystérésis à n'importe quelle vitesse à partir d'un seul test de chargement à une vitesse donnée. La vérification de la validité de cette approche ainsi que plus de détails concernant la détermination des paramètres du modèle sont présentés dans l'ANNEXE III.

Abstract

The aim of this study is to develop a model for the mechanical behavior of knitted fabrics, which are used in protection gloves, at large deformation and different strain rates in terms of extension/recovery cycling. The non linear viscoelastic model is based on the standard solid model. The choice of this model is based on its simplicity due to the limited number of elements. It contains three nonlinear spring and damper elements. The idea is to consider that, by analogy with elastomers, the mechanical behavior of the fabric in terms of hysteresis loop is due to the contribution of two parts: the first one represents the equilibrium state of the fabric and the second one is due to the deviation from this equilibrium. Then, the stress-strain behavior of the fabric at different strain rates can be computed using the same parameters determined at one value of strain rate. The dissipated energy is provided by the area under the hysteresis loop. A good agreement has been obtained between the experimental and theoretical results.

5.1 Introduction

The application of textile fabrics in engineering design is a very interesting development. For example various knitted, woven and non woven fabrics have been more and more used for technical protective gloves recently. When they are used as reinforcement, the obtained composite materials present various advantages, for example in terms of increased resistance to mechanical risks such as cutting and puncture [1]. Various investigations of the tensile properties of fibrous fabrics can be found in the literature. However, the mechanical behavior of these materials in terms of hystheresis loop at large deformation and at different strain rates has rarely been studied.

In 1937, Pierce [2] developed a model in which the constituent yarns were assumed to be sufficiently flexible and the cross sections of yarns to be circular. This model was used to study the mechanical behavior of various woven fabrics [3-7]. As an alternative method, De Jong and Postle [8, 9] developed a mechanistic model based on energy analysis. The first step of this method consists of identifying and formulating all the individual terms of the energy contribution to an elastic system. The energy minimum is determined by means of the optimal control theory, providing the mechanical equilibrium of the system under general conditions of external loads. This model has been used to study several kinds of knitted fabrics [10-13] as well as plain weave structures [14, 15].

Other researchers [16-20] have proposed various models in order to predict the deformation behavior of knitted fabrics. They are generally based on micro-mechanical analyses of a knitted loop in the plain weft-knitted structure where the unit cell is often a single loop. The tensile properties of knitted fabrics are derived from the loop configuration and the yarn properties. However, these analyses are mostly limited to the case of knitted fabrics subjected to biaxial stresses. In addition, most of these models are difficult to apply in practice, due to their complexity.

Kawabata [21, 22] proposed the linearizing method to predict mechanical anisotropy and non linearity in fabrics and knits. This method is based on the assumption that logarithmic plots of stress versus logarithmic values of strain display a linear relationship up to the large strain region close to 100%. The linearizing method is essentially a modification of the linear elastic theory at very small strain. However, most fabrics do not behave linearly, and the slope of the curve in the large strain region is generally steeper than that in the small strain region, with two or three breaking points. To cope with this complicated behavior, Kawabata et al. [21, 22] tried to linearize the stress-strain relationship within two strain zones. They pointed out that double-zone linearization attempts to improve the accuracy of prediction and to expand the validity of this method over a wider range of strains. However, as pointed out by Yamada et al [23] two such clear zone have never been observed for knitted fabrics.

More recently, the Finite Element Method was used to study the stress-strain behavior of textile fabrics [24-26]. However, this technique requires long computation times. Finally, taking into account the viscoelastic nature of textiles, rheological models have been used to describe their mechanical behavior. In particular, the 4-element Burger's model, which is composed of a Maxwell and a Kevin-Voigt model in series, was applied by Webster [27] to the study of stitched seams under longitudinal loading subjected to extension/recovery cycling at a constant rate of extension. Matsuo [28] have used that same model to analyze the stress relaxation behavior of knitted fabrics under uniaxial and strip biaxial excitation. However, the implementation of the Burger's model for textile applications is rather complicate.

In this paper, we propose to apply a non linear and rate-dependant description based on Zener's rheological model to the study of the mechanical behavior of knitted fabrics in terms of hysteresis loop at large deformation and at different strain rates. This model was initially developed for elastomers deformed in compression by Bergström and Boyce [29]. It is based on the concept that their behavior is controlled by two contributions, the first one corresponding to the equilibrium state and the second one to a non-linear rate-dependant

deviation from the equilibrium state. This description was later simplified for the unidirectional treatment of elastomer tensile deformation [30].

5.2 Experimental method

A cotton knit used as support for protective gloves was investigated in this study. Samples were cut in the uncoated liner of Best 4000 P gloves manufactured by the Best Company. Specimens had the shape of 1 x 10 cm rectangular strips. The uniaxial tensile tests at various strain rates were carried out using a MTS mechanical test frame, model Alliance RF/200. Figure 5.1 displays the time variation of the deformation and strain rate during a 50 mm/min test.

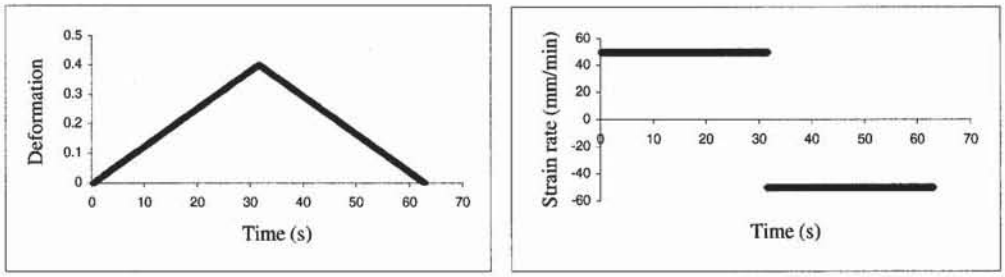

Figure 5.1 Loading-unloading test (strain rate 50 mm/min)

5.3 Theoretical model

The non-linear viscoelastic model is based on Zener's standard solid model (see Figure 5.2). Both springs are non-linear and the time dependence is provided by the damper. It is based on the concept that the hysteretic mechanical behavior of the material can be attributed to the contribution of two parts: the first one represents the equilibrium state and is provided by the spring R_1 while the second one is due to the deviation from this equilibrium and is described by the spring R_2 and the damper in series.

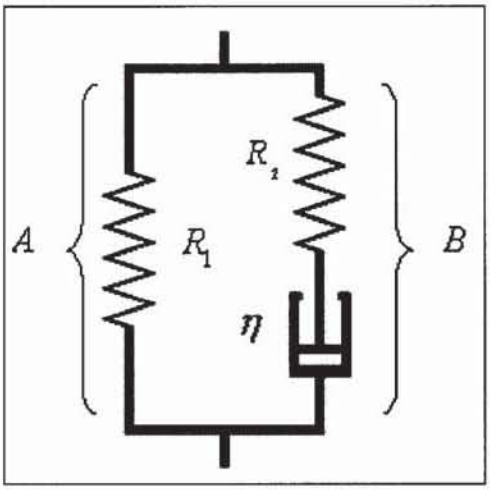

Figure 5.2 Schematic representation of the Zener viscoelastic model

The differential equation corresponding to Zener's three-element model is provided by Equation (5.1).

$$\dot{\sigma} + \frac{E^{(R_2)}}{\eta}\sigma = (E^{(R_1)} + E^{(R_2)})\dot{\varepsilon} + \frac{E^{(R_1)}E^{(R_2)}}{\eta}\varepsilon \tag{5.1}$$

Where $E^{(R_1)}$ is the modulus of spring R_1, $E^{(R_2)}$ is the modulus of spring R_2 and η is the viscosity of the damper, σ is the stress, $\dot{\sigma}$ is the variation of the stress with time, ε is the strain and $\dot{\varepsilon}$ is the strain rate.

Equation (5.2) represents the solution of Equation (5.1) in terms of time variation of the stress for a loading-unloading cycle.

$$\sigma(t) = \zeta\left\{\left[\eta + E^{(R_1)}t - \eta e^{-\frac{E^{(R_2)}}{\eta}t}\right] - 2\left[\eta + E^{(R_1)}(t-\tau_{1/2}) - \eta e^{-\frac{E^{(R_2)}}{\eta}(t-\tau_{1/2})}\right]H(t-\tau_{1/2})\right\} \tag{5.2}$$

With t is the time, ζ is the strain rate, $\tau_{1/2}$ is the half cycle time and H is the Heaviside function defined by Equation (5.3).

$$\begin{cases} H(t-\tau_{1/2})=0 \ \ pour \ t \le \tau_{1/2} \\ H(t-\tau_{1/2})=1 \ \ pour \ t \ge \tau_{1/2} \end{cases} \tag{5.3}$$

5.3.1 Representation of the equilibrium state

The equilibrium state relative to the loading-unloading cycle is provided by the theoretical path laying between the sample loading and unloading curve as shown in Figure 5.3. It is represented by the mechanical behavior of the part A of the model, i.e. of the spring R_1.

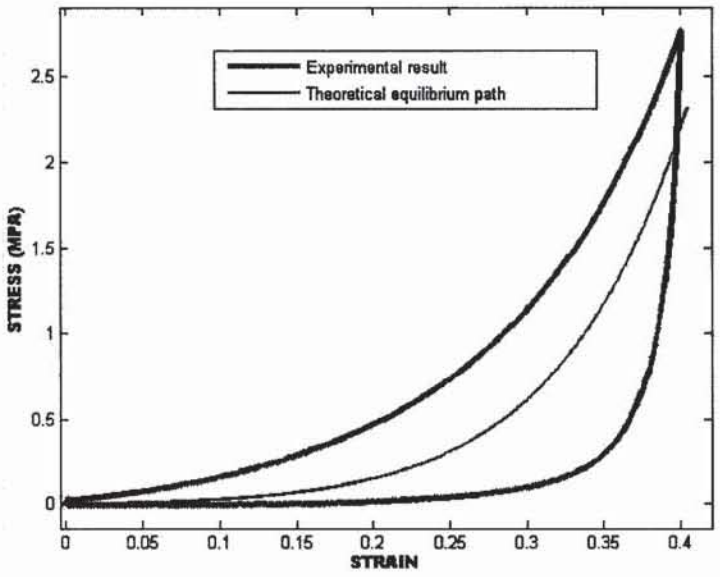

Figure 5.3 Location of the theoretical equilibrium path relatively to the loading and unloading curves

This equilibrium path can be satisfactorily fitted by the exponential function shown in equation (5.4).

$$\sigma^{(R_1)} = A_1 \varepsilon \exp(B_1 \varepsilon) \tag{5.4}$$

As a result, the modulus function of the spring R_1 used in equation (5.2) can be expressed by:

$$E^{(R_1)} = A_1 \exp(B_1 \varepsilon) \tag{5.5}$$

5.3.2 Representation of the deviation from the equilibrium state

The deviation from the equilibrium state is represented by the behavior of the part B of the model, i.e. the spring R_2 in series with the damper. In the same way as for the spring R_1, the modulus of the spring R_2 is described by an exponential function (see equation 5.6).

$$E^{(R_2)} = A_2 \exp(B_2 \varepsilon^{(R_2)}) \tag{5.6}$$

For its part, the damper viscosity can be expressed using the relationship that was established for the case of elastomers [29]. It is based on the application of the Doi and Edoirds reptation motion theory to the network chain segments [29].

$$\eta = \frac{\sigma^{\hat{m}}}{\hat{C}_1 \left[\frac{\sqrt{3}}{3} \left((\varepsilon+1)^2 + \frac{2}{\varepsilon+1} \right)^{1/2} - 1 \right]^{C_2}} \tag{5.7}$$

Where $\hat{m}$, $\hat{C}_1$ and C_2 are three parameters which can be determined by iteration.

5.4 Results and discussions

The experimental results represented in Figure 5.4 illustrate the non linear mechanical behavior displayed by the studied knit. They also demonstrate the effect of the strain rate on the hysteresis loop, especially for the loading part of the cycle.

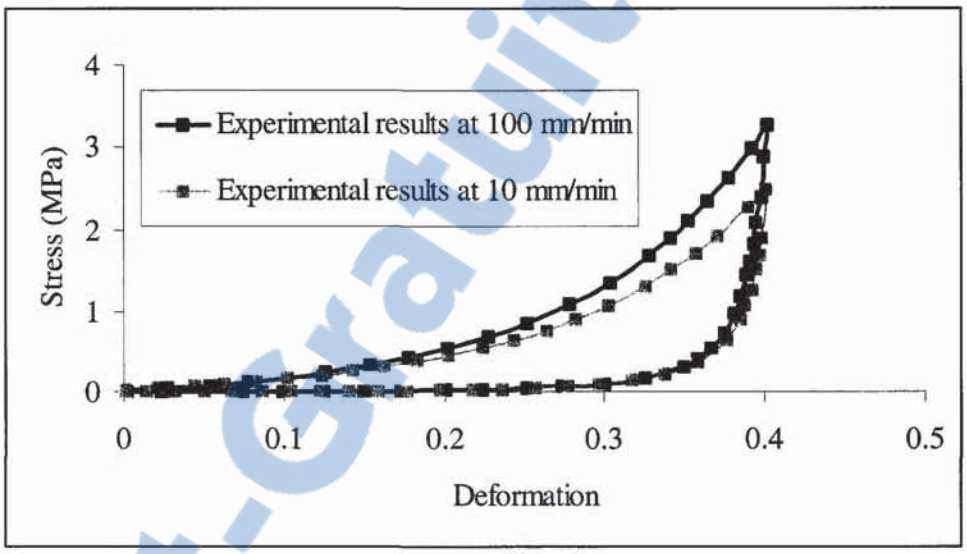

Figure 5.4 Stress-strain behavior of the knit samples at different strain rates (10 and 100 mm/min)

For a given strain rate, we can decompose the hysteresis loop into two curves as shown in the Figure 5.5. The first one (Figure 5.5.a) represents the equilibrium state of the fabric and is associated with the behavior of the spring R_1. The second curve (Figure 5.5.b) corresponds to the deviation from the equilibrium state and is described by the part B of the model (spring R_2 and damper in series).

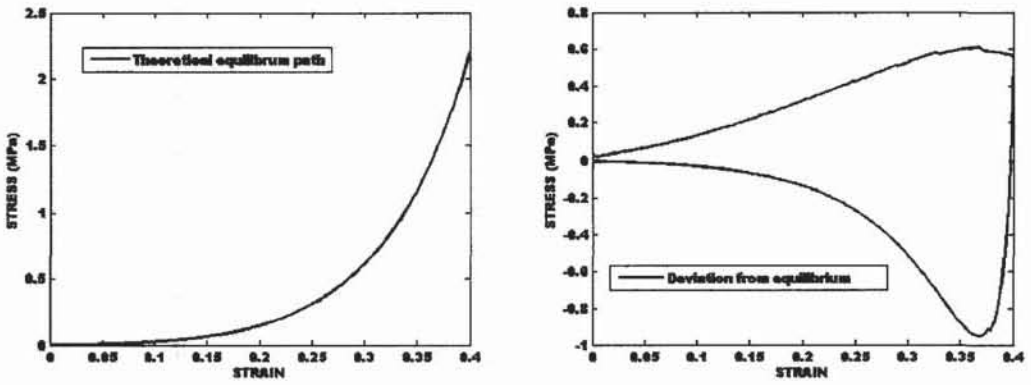

(a) (b)

Figure 5.5 Graphic decomposition of the stress-strain behavior of the knit sample; a) equilibrium state, b) deviation from equilibrium state

The model parameters corresponding to the two springs and the damper are obtained from a loading-unloading test performed at 50 mm/min. They are displayed in Table 5.1.

Table 5.1 Model constants provided by a loading-unloading test performed at 50 mm/min

	Parameters				
Elements	$A_{i\,(i=1;2)}$	$B_{i\,(i=1;2)}$	$\widehat{m}$	$\widehat{C}_1$	C_2
Spring R_1	0.1052	9.899	-	-	-
Spring R_2	100.4	0.5	-	-	-
Damper	-	-	0.034	-12.4	1.85

A good agreement between the experimental data points taken at 50 mm/min and the theoretical description provided by the non-linear viscoelastic model using the constants displayed in Table 5.1 can be observed in Figure 5.6.

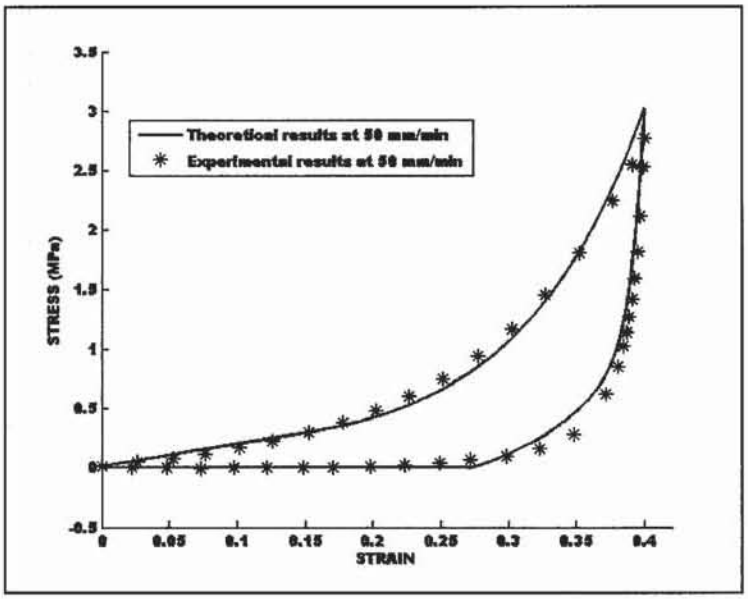

Figure 5.6 Comparison of the experimental data points and the theoretical description for the hysteresis loop at 50 mm/min

The constants displayed in Table 5.1 and obtained from measurements performed at 50 mm/min were used to compute the hysteresis loop of the sample knit at others strain rates (10, 25, 75 and 100 mm/min). As shown in Figure 5.7 for strain rates of 10 and 100 mm/min, a good agreement with the corresponding experimental data points is obtained. This model thus a mean for predicting the hysteretic behavior of knit fabrics over a range of strain rate using a single test performed at an intermediate value.

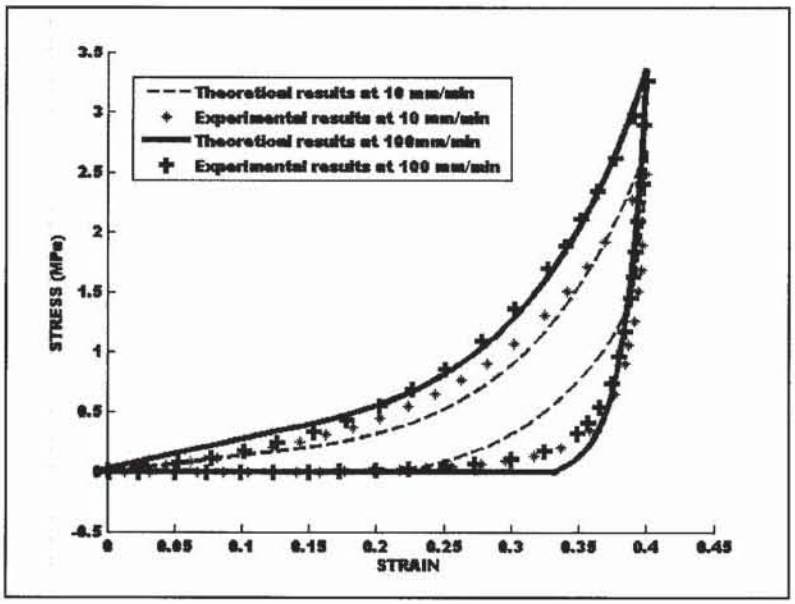

Figure 5.7 Comparison of the experimental data points and the theoretical description computed with Table 5.1 model constants for the hysteresis loop at 10 and 100 mm/min

The dissipated energy for one loading-unloading cycle is provided by the area under the hysteresis loop. The results provided by the experimental measurements and the theoretical description using Table 5.1 model constants are compared in Figure 5.8 for the various values of the strain rate. Each data point is the average of five replicates. A good agreement can be observed over the studied range of strain rates, which spans over a decade. In addition the dissipated energy corresponding to a loading-unloading cycle appears to be proportional to the strain rate.

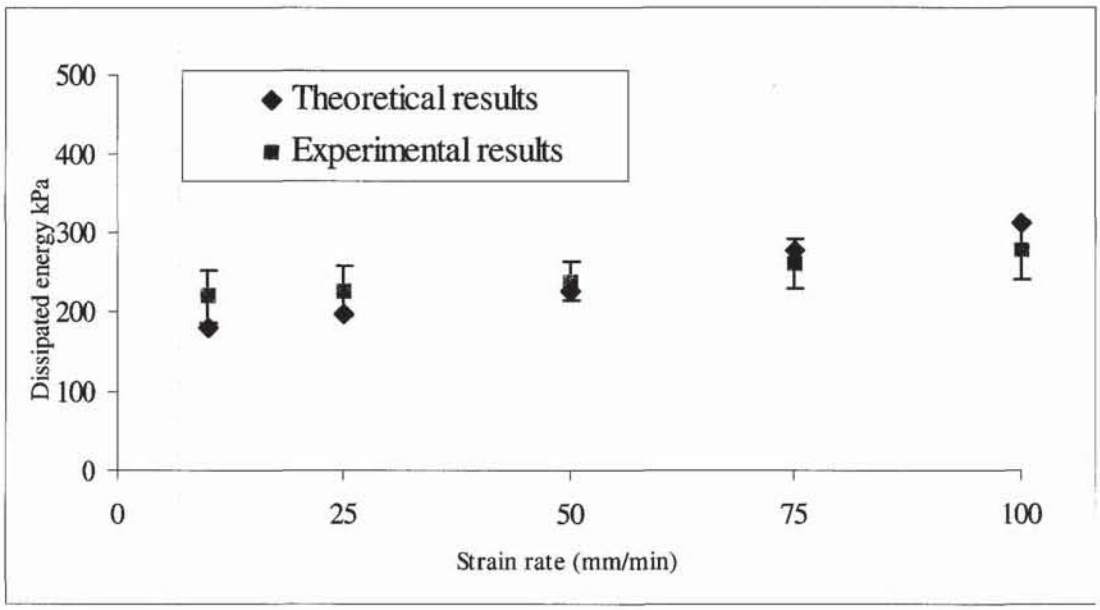

Figure 5.8 Influence of the strain rate on the dissipated energy

5.5 Conclusion

In this paper, we have proposed a non-linear viscoelastic model to predict the stress-strain behavior of knitted textile fabrics at large deformations and different strain rates using the data computed from a single test performed at an intermediate strain rate. The time dependence was satisfactorily described by a spring in series with a damper within Zener's rheological model. The non-linearity of the knit mechanical behavior is provided by using an exponential function for the two spring modulus of the model. This description corresponds to the concept initially developed for elastomers that the hystheresis behaviour is controlled by two contributions, the first one corresponding to the equilibrium state and the second one to a non-linear rate-dependent deviation from that equilibrium state. This concept was satisfactorily applied here to the case of knitted fabrics with a good agreement obtained between experimental and theoretical results at different strain rates. This model thus provides a simple tool for predicting the hysteresis loop of knitted fabrics at various strain rates from the results of one test carried out at an intermediate strain rate. This approach may

eventually also be applied to other kinds of textile fabrics such as woven as well as non woven fabrics.

Acknowledgment

This research has been supported by the Institut de recherche Robert-Sauvé en santé et sécurité du travail (IRSST). The authors would like to thank Professor Michel Beaudin for his advices.

References

1. Vu-Khanh, T., et al., *Gants de protection : étude sur la résistance des gants aux agresseurs mécaniques multiples*, in *Études et recherches / Rapport R-424*. 2005, IRSST: Montréal. p. 86 pages.

2. Pierce, F.T., *Cloth geometry.* Journal of Textile Institute, 1937. **28**: p. T45-T112.

3. Buisson, Y.L., et al., *Qualitative and Quantitative Evaluation of Cotton Fabric Damage by Tumble Drying.* Textile Research Journal, 2000. **70**(8): p. 739-743.

4. Chen, Y., D.W. Loyd, and S.C. Harlock, *Mechanical characterestics of coated fabrics.* Journal of Textile Institute, 1995. **86**: p. 690-700.

5. Boong Soo, J., C. So Yeon, and H. Cheol Jae, *Structural and Mechanical Properties of Woven Fabrics Employing Peirce's Model.* Textile Research Journal, 2003. **73**(10): p. 929-933.

6. Olofsson, B., *A general model of a fabric as a geometric mechanical structure.* Journal of Textile Institute, 1964. **55**: p. T541-T557.

7. Sinoimeri, A. and J.Y. Dréan, *Mechanical behavior of the plain weave structure using energy methods: fabric uniaxial extension.* Textile Research Journal, 1997. **67**(5): p. 370-378.

8. De Jong, S. and R. Postle, *An introduction to the study of fabric mechanics using energy methods.* Textile Inst. Ind, 1977. **15**: p. 376-379.

9. De Jong, S. and R. Postle, *A General Energy Analysis of Fabric Mechanics Using Optimal Control Theory.* Textile Research Journal, 1978. **48**(3): p. 127-135.

10. De Jong, S. and R. Postle, *An energy analysis of the mechanics of weft-knitted fabrics by means of optimal control theory, Part I: The nature of the loop-inter-locking in the plain-knitted structure.* Journal of Textile Institute, 1977. **68**: p. 307-315.

11. De Jong, S. and R. Postle, *An energy analysis of the mechanics of weft-knitted fabrics by means of optimal control theory, Part II: Relaxed-fabric Dimensions and tensile properties of the plain-knitted structure.* Journal of Textile Institute, 1977. **68**: p. 316-323.

12. De Jong, S. and R. Postle, *An energy analysis of the mechanics of weft-knitted fabrics by means of optimal control theory, Part III: The 1 X 1 rib-knitted structure.* Journal of Textile Institute, 1977. **68**: p. 324-329.

13. Hart, K., S. De Jong, and R. Postle, *Analysis of the Single Bar Warp Knitted Structure Using an Energy Minimization Technique: Part I: Theoretical Development.* Textile Research Journal, 1985. **55**(8): p. 489-498.

14. De Jong, S. and R. Postle, *An energy analysis of woven fabric mechanics by means of optimal-control theory, Part I: Tensile properties.* Journal of textile Institute, 1977. **68**: p. 350-361.

15. De Jong, S. and R. Postle, *An energy analysis of woven fabric mechanics by means of optimal-control theory, Part II: Pure bending properties.* Journal of Textile Institute, 1977. **68**: p. 362-369.

16. Wei-Liang, W., H. Hiroyuki, and M. Zen-ichiro, *Computer simulation of the deformation of weft-knitted fabrics for composite materials.* Journal of Textile Institute, 1994. **85**(2): p. 198-214.

17. Shanahan, W.J. and R. Postle, *A Theoretical Analysis of the Plain-Knitted Structure.* Textile Research Journal, 1970. **40**(7): p. 656-665.

18. Whitney, J.M. and J.L.J. Epting, *Three-Dimensional Analysis of a Plain Knitted Fabric Subjected to Biaxial Stresses1.* Textile Research Journal, 1966. **36**(2): p. 143-147.

19. MacRory, B.M. and A.B. McNamara, *Knitted Fabrics Subjected to Biaxial Stress--An Experimental Study.* Textile Research Journal, 1967. **37**(10): p. 908-a-911.

20. Popper, P., *The Theoretical Behavior of a Knitted Fabric Subjected to Biaxial Stresses.* Textile Research Journal, 1966. **36**(2): p. 148-157.

21. Kageyama, M., S. Kawabata, and M. Niwa, *The validity of a ''linearizing method''for prediction the biaxial-extension properties of fabrics.* Journal of Textile Institute, 1988. **79**(543).

22. Kawabata, S., et al. *Validity of the "Linearizing Method" for describing the biaxial stress-strain relationship of textiles.* in *Proc. UMIST Int. Conf., Textiles, Engineered for Performance,*. 1998. Manchester, U.K.

23. Yamada, T., N. Ito, and M. Matsuo, *Mechanical Properties of Knitted Fabrics Under Uniaxial and Strip Biaxial Extension as Estimated by a Linearizing Method.* Textile Research Journal, 2003. **73**(11): p. 985-997.

24. Boisse, P., et al., *Meso/macro-mechanical behaviour of textile reinforcements for thin composites.* Composites Science and Technology, 2001. **61**(3): p. 395-401.

25. Tarfaoui, M., J.Y. Drean, and S. Akesbi, *Predicting the stress-strain behavior of woven fabrics using the finite element method.* Textile Research Journal, 2001. **71**(9): p. 790-795.

26. Gasser, A., P. Boisse, and S. Hanklar, *Mechanical behaviour of dry fabric reinforcements. 3D simulations versus biaxial tests.* Computational Materials Science, 2000. **17**(1): p. 7-20.

27. Webster, J., R.M. Laing, and R.L. Enlow, *Effects of Repeated Extension and Recovery on Selected Physical Properties of ISO-301 Stitched Seams: Part II: Theoretical Model.* Textile Research Journal, 1998. **68**(12): p. 881-888.

28. Matsuo, M., T. Yamada, and N. Ito, *Stress Relaxation Behavior of Knitted Fabrics under Uniaxial and Strip Biaxial Excitation as Estimated by Corresponding Principle between Elastic and Visco-Elastic Bodies.* Textile Research Journal, 2006. **76**(6): p. 465-477.

29. Bergstrom, J.S. and M.C. Boyce, *Constitutive modeling of the large strain time-dependent behavior of elastomers.* Journal of the Mechanics and Physics of Solids, 1998. **46**(5): p. 931-954.

30. Harrabi, L et al, *Prediction of stress-strain behaviour and energy dissipation of elastomers at large deformations,* submitted to the Journal of Applied Polymer Science in march 2009.

CHAPITRE 6

CONCLUSIONS ET TRAVAUX FUTURS

Le but principal de cette étude était de caractériser dans un premier temps la souplesse des gants de protection sélectionnés de manière à couvrir un large éventail de degrés de souplesse (plus souple au plus rigide) par le biais de tests mécaniques et les valider par des tests biomécaniques. Ces résultats ont fait l'objet des articles 1 et 2. Dans un deuxième temps, deux nouveaux modèles sont proposés dans les articles 3 et 4 permettant de prédire le comportement viscoélastique des matériaux de protection et en particulier les élastomères et les textiles à des grandes déformations et à différentes vitesses.

En ce qui concerne l'étude de la souplesse des gants, deux grandes catégories de tests ont été utilisées : (1) des tests mécaniques exécutés sur bancs d'essais dont le test multidirectionnel développé dans le cadre de cette étude et le test Kawabata et (2) des tests avec sujets humains (considération de l'influence possible de l'interface main-gant) dont un test de perception et un test biomécanique, mis au point dans le cadre du projet IRSST 099-376.

Des corrélations élevées ont été obtenues entre les critères mécaniques et les deux critères obtenus chez les sujets humains, ce qui suppose que le rôle joué par l'interface main-gant n'est pas très important, du moins pour le type de tâche étudiée. Le test multidirectionnel démontre les meilleures corrélations avec les tests de perception et biomécanique, comparativement au test Kawabata. Ces corrélations sont si élevées ($r > 0,88$) qu'il est possible de conclure que le test biomécanique, bien qu'étant une mesure de nature objective et apparemment mieux adaptée au facteur humain, n'est pas nécessaire pour bien caractériser la souplesse des gants. Ces résultats sont très positifs car l'emploi du test biomécanique, qui donne des estimés relativement variables, aurait requis le recrutement de plusieurs sujets pour bien caractériser un gant donné, tout en tenant compte du genre des sujets, ce qui est complexe et coûteux comme approche. Le test multidirectionnel, en plus d'apporter

essentiellement la même information, est beaucoup plus simple, requiert moins de ressources (moins coûteux) car moins sujet aux variations dans les mesures, et est plus sensible aux différences fines en terme de souplesse. En résumé, cette étude est la première à valider des tests mécaniques de souplesse de gants de protection avec des critères obtenus chez des sujets humains. Ils démontrent qu'il est possible de prédire les effets qu'a un gant rigide sur la fonction musculaire à partir de tests mécaniques réalisés sur des échantillons de gants. La méthode fixée, présentée dans l'article 2, permet l'évaluation de la souplesse d'une catégorie bien spécifique de gants de protection en reproduisant les déformations biaxiales largement présentes dans ce type de gant de protection en cours d'utilisation. Elle concerne surtout ceux qui sont portés serrés sur les mains. Les résultats théoriques issus du formalisme de Mooney-Rivlin dans le cas des élastomères sont en très bonne corrélation avec l'expérimentation.

En ce qui concerne l'étude du comportement mécanique des matériaux de protection, nous nous sommes intéressés particulièrement au comportement viscoélastique de ces matériaux à des grandes déformations lors d'un cycle charge-décharge. Les modèles développés ici sont basés sur l'utilisation du modèle rhéologique de Zener pour pouvoir prédire ce comportement à différentes vitesses dans le cas des matériaux élastomères et textiles. Les résultats qui ont été trouvés ici montrent une bonne corrélation entre la modélisation et l'expérimentation. L'utilisation des modèles proposés dans cette étude permet de prédire l'effort nécessaire ainsi que l'énergie à dissiper pour accomplir une certaine tache à une vitesse donnée.

En perspectives, les efforts doivent continuer pour étudier le comportement d'autres types de matériaux de protection tels que les élastomères renforcés par des fibres textiles ou d'autres formes de renfort textile ou d'autres types d'élastomère.

L'étude d'autres propriétés tels que l'adhérence, la dextérité et la respirabilité d'une façon rigoureuse serait d'une grande importance également. Ce ci permettrait d'avoir plus d'information sur l'ensemble des paramètres qui contrôlent le confort des équipements de protection et pouvoir ainsi designer d'autres qui sont plus performants et plus confortables.

ANNEXE I

ELASTICITY OF RUBBERS

Rubber has been well known as a peculiar material which possesses an extremely high extensibility generated by low mechanical stress as well as an ability to completely recover after deformation. In addition, thermo-elastic properties of rubbers are different from those of other materials. One of the earliest contributions to the subject of the physics of rubbers was that of Gough who showed in 1805 that stretched rubber contracted on heating and extended on cooling. He also demonstrated that heat was generated on stretching and absorbed on retraction. These thermodynamic effects were confirmed later by Joule and Kelvin using the more perfectly reversible vulcanized rubbers. The peculiar mechanical and thermo-elastic properties of rubbers, however, could not be interpreted for long time because of the difficulty in explaining their very high extensibility in terms of classical concepts of the structure of materials.

It was Meyer and coworkers [51] who first clearly interpreted the long-standing problem of rubber elasticity in terms of the chainlike structure of the polymer molecule. With regarding a rubber molecule as a flexible chain of more or less freely rotating links, he found that after deformation, the rubber molecule will quickly revert to its normal crumpled form as a result of the random thermal rotations and vibrations of individual atoms. By thermodynamic considerations, Meyer also showed that the spontaneous retraction of the extended chain is due to a reduction of configurational entropy. Through the research of James and Guth [47], Treloar [52] and Wall [53], the quantitative relations between chain extension and entropy reduction were clarified. In contrast to most other materials such as metals, ceramics, etc., the retractive stress of rubber arises through the reduction of entropy rather than through changes in internal energy. The elasticity of rubber is thus not static, as is that of an ordinary crystalline solid, but kinetic.

In the following section, the essential physical background of rubber elasticity, starting from the kinetic or statistical theory is presented. It is then followed by the development of recent

methods which represent the elastic properties of rubbers in the most general mathematical form.

A/ Kinetic or statistical theory of rubbers elasticity

A.1 Thermodynamics of rubbers elasticity

In the elementary thermodynamic consideration, the work done on an elastic solid dW in an infinitesimal displacement dl can be evaluated using the first law of thermodynamics:

$$dW = f.dl = dU - dQ \tag{A-1}$$

where f is the external force applied on the solid, dU is the change in internal energy and dQ is the change in the heat supplied. For an isothermal change of state at constant volume, $dQ = TdS$, T and S being respectively the absolute temperature and entropy, thus:

$$dW = dU - dQ = (dU - TdS) = d\,(U - TS)_{T,V} = dA \tag{A-2}$$

in which $A = U - TS$ represents the Helmholtz free energy. From Equations (A-1) and (A-2), the force f required to maintain a constant length l in a sample of rubber at an absolute temperature is represented as the sum of an internal energy and an entropy component as follows:

$$f = \left(\frac{\partial A}{\partial l}\right)_T = \left(\frac{\partial U}{\partial l}\right)_T - T\left(\frac{\partial S}{\partial l}\right)_T \tag{A-3}$$

The term $\left(\frac{\partial S}{\partial l}\right)_T$ may be evaluated by studying the variation of force with temperature at constant stretched length and applying the easily derived thermodynamic relations:

$$\left(\frac{\partial f}{\partial T}\right)_l = \frac{\partial}{\partial T}\left(\frac{\partial A}{\partial l}\right)_T = \frac{\partial}{\partial l}\left(\frac{\partial A}{\partial T}\right)_l = -\left(\frac{\partial S}{\partial l}\right)_T \tag{A-4}$$

Substituting $\left(\frac{\partial f}{\partial T}\right)_l = -\left(\frac{\partial S}{\partial l}\right)_T$ into Equation (A-3) gives:

$$\left(\frac{\partial U}{\partial l}\right)_T = f - T\left(\frac{\partial f}{\partial T}\right)_l \tag{A-5}$$

Early experimental studies of Meyer and Ferri [50] on the stress-temperature behavior of rubber showed a linear relationship between the tensile force at constant length and the absolute temperature. The right-hand side of Equation (A-5) is therefore close to zero, indicating that the internal energy U is almost unchanged during deformation of rubbers. Equations (2) and (3) can be then expressed by the following approximations:

$$dW = -dQ = -TdS \tag{A-6}$$

$$f = -T\left(\frac{\partial S}{\partial l}\right)_T \tag{A-7}$$

Thus, it can be seen that an increase in the external force f in extension is associated with a negative value of $\left(\frac{\partial S}{\partial l}\right)_T$, i.e. a decrease in entropy S. The high extensibility and recovery properties of rubbers are due to deformation induced changes in entropy rather than due to changes in internal energy. The quantitative evaluation of the stress-strain characteristics of rubber then involves the calculation of the configurational entropy of the network of chains as a function of strain.

A.2 Entropy of a single chain

A quantitative expression for the entropy of a single chain starts from the application of the statistical theory. Kuhn [48] considered a single long, flexible molecule corresponding to a randomly jointed chain of n equal links, each of length l. The probability of a given distance r between the ends of such a chain, regardless of the direction, is given by a Gaussian probability function:

$$P(r) = A\exp\left(-b^2r^2\right) \tag{A-8}$$

where A is a constant and $b^2 = \frac{3}{2nl^2}$. The mean square distance between the ends, denoted $\overline{r^2}$, is then given by nl^2 or $3/2b^2$.

The entropy of the freely jointed chain is derived from the application of the Boltzmann relationship between the entropy s and the probability P, that is:

$$s = k \ln P = c - kb^2 r^2 = c - kb^2 \left(x^2 + y^2 + z^2\right) \tag{A-9}$$

where c is a constant and k is Boltzmann's constant. The interpretation of Equation (A-9) is that the difference of entropy between any two states is proportional only to the corresponding difference of r^2. It is also noteworthy that there is a reduction in entropy (like the probability) as the distance between two ends of the chain increases in extension.

A.3 Calculation of network entropy

We consider an ideal network in which each segment of a molecule between successive points of cross-linkage is considered to be a freely jointed Gaussian chain. Following the idea originally introduced by Kuhn [49], we assume that the x, y, and z components of the chain vector length r change on deformation in the same ratio as the corresponding dimensions of the bulk rubber (affine deformation assumption). Taking the principal axes of strain to be parallel to the x, y, and z axes, the components of length for the individual chain change on deformation from (x,y,z) to $(\lambda_1 x, \lambda_2 y, \lambda_3 z)$, in which λ_1, λ_2, and λ_3 are the principal extension ratios parallel to the three rectangular coordinate axes x,y, and z. From Equation (A-9), the change of entropy due to the deformation for the individual chain is therefore:

$$\Delta s = -kb^2 \left[\left(\lambda_1^{\,2} - 1\right)x^2 + \left(\lambda_2^{\,2} - 1\right)y^2 + \left(\lambda_3^{\,2} - 1\right)z^2\right] \tag{A-10}$$

For the assembly of N chains contained in a unit volume of the network, in taking into account that the molecules are randomly oriented in the unstrained state, we have:

$$\overline{x^2} = \overline{y^2} = \overline{z^2} = \frac{1}{3}\overline{r^2} \tag{A-11}$$

where $\overline{r^2}$ is the mean square chain vector length in the unstrained state. Since $\overline{r^2}$ in the undeformed state is likely to be similar to that for a corresponding set of chains in the free or uncrosslinked state (i.e. $3/2b^2$), we obtain on summation of Equation (A-10) the entropy of deformation ΔS for the network in the form:

$$\Delta S = -\frac{1}{2}Nk\left(\lambda_1^{\,2} + \lambda_2^{\,2} + \lambda_3^{\,2} - 3\right) \tag{A-12}$$

As mentioned above, all states of deformation have almost the same internal energy ($\Delta U = 0$), so the work of deformation per unit volume is:

$$W = -T\Delta S = \frac{1}{2}NkT\left(\lambda_1^{\,2} + \lambda_2^{\,2} + \lambda_3^{\,2} - 3\right) \tag{A-13}$$

In the case of simple extension: $\lambda_1 = \lambda$, $\lambda_2 = \lambda_3 = 1/\lambda^{1/2}$ (Figure B.2), the engineering stress-extension ratio is given as follows:

$$\sigma = \frac{dW}{d\lambda} = NkT\left(\lambda - \frac{1}{\lambda^2}\right) \tag{A-14}$$

The statistical theory based on a specific molecular model has been applied to many phenomena, such as swelling in solvents, thermoelastic effects, photoelasticity, etc., as well as in all of fields which require a profound physical insight into the molecular mechanisms. However, certain deviations between the observed forms of stress-strain relations for rubbers and the corresponding forms predicted by the statistical theory (particularly in the case of simple extension) lead a necessity of providing a more realistic representation of the actual properties. The following section will consider the "phenomenological" theory based on the particular type of general mathematical formulation in terms of strain invariants developed by Rivlin [21] and its application to some problems of the engineering types.

B/ Phenomenological theory - General theory of large elastic deformations

In general, the stress-strain relations for rubber-like materials can be determined if one knows the form of the function W defining the work of deformation or elastically stored energy per

unit volume. According to Rivlin [21], the form of W for an isotropic material in the unstrained state must be a symmetrical and even-powered function of the three principal extension ratios λ_1, λ_2, and λ_3. The three simplest even-powered functions are the so-called strain invariants, defined as follows:

$$\left.\begin{aligned} I_1 &= \lambda_1^2 + \lambda_2^2 + \lambda_3^2 \\ I_2 &= \lambda_1^2\lambda_2^2 + \lambda_2^2\lambda_3^2 + \lambda_3^2\lambda_1^2 \\ I_3 &= \lambda_1^2\lambda_2^2\lambda_3^2 \end{aligned}\right\} \tag{B-1}$$

In addition, for an incompressible material: $I_3 = 1$; hence the two remaining equations may then be written:

$$\left.\begin{aligned} I_1 &= \lambda_1^2 + \lambda_2^2 + \lambda_3^2 \\ I_2 &= 1/\lambda_1^2 + 1/\lambda_2^2 + 1/\lambda_3^2 \end{aligned}\right\} \tag{B-2}$$

It follows that the strain energy density W (i.e. the amount of energy stored elastically in unit volume of material) is a function of I_1, and I_2 only:

$$W = W(I_1 - 3, I_2 - 3) \tag{B-3}$$

(Since I_1 and I_2 take the value of 3 when $\lambda_1 = \lambda_2 = \lambda_3 = 1$, subtracting this amount gives strain measures that go to zero in the unstrained state). The most general form can thus be represented by the series:

$$W = \sum_{m=0,n=0}^{\infty} C_{mn}(I_1 - 3)^m (I_2 - 3)^n \tag{B-4}$$

where C_{mn} are constants ($C_{oo} = 0$). From Equation (B-4), the two simplest expressions are:

$$W = C_1(I_1 - 3) \tag{B-5}$$

$$W = C_2(I_2 - 3) \tag{B-6}$$

It can be seen that Equation (B-5) with $C_1 = \frac{1}{2}NkT$ corresponds to the relation obtained from the Gaussian network theory, as shown in Equation (A-14).

The most general first-order expression in I_1 and I_2 obtained by combination of Equations (B-5) and (B-6) is:

$$W = C_1(I_1 - 3) + C_2(I_2 - 3) \tag{B-7}$$

This particular form of strain energy function was originally proposed by Mooney [22] and is often called the Mooney-Rivlin equation. In general the Mooney-Rivlin equation gives a closer approximation to the actual behavior of rubbers than the simpler equation involving only I_1 derived from the Gaussian network theory.

B.1 General stress-strain relations

Assuming that a satisfactory strain energy function has been defined, it is now necessary to consider how the stress-strain relations are obtained.

Because any homogeneous strain can be produced by a homogeneous pure strain followed by a suitable rotation, it is only necessary to derive the relations between the principal stresses σ_1, σ_2, and σ_3 and the principal extension ratios λ_1, λ_2, and λ_3 in a homogeneous pure strain problem (Figure B-1).

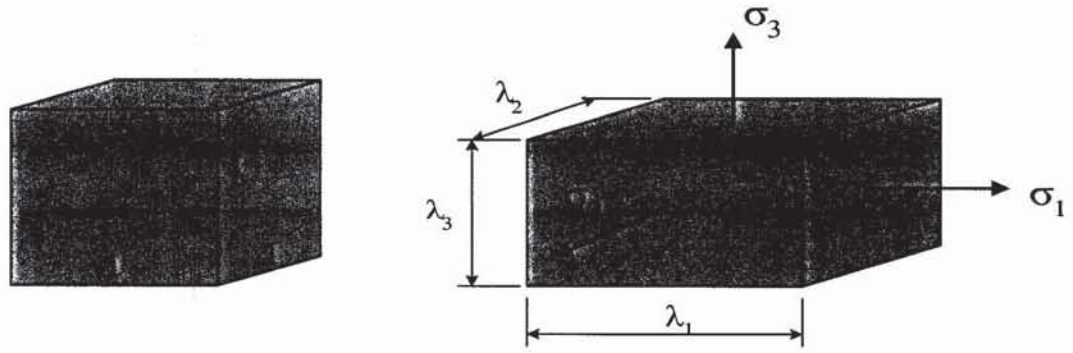

Figure B-1: Pure homogeneous strain: (a) unstrained state; (b) strained state

The work done (per unit of initial undeformed volume) by the forces f_1, f_2 and f_3 acting on the faces in an infinitesimal displacement from the deformed state where λ_1, λ_2, λ_3 change to $\lambda_1+d\lambda_1$, $\lambda_2+d\lambda_2$, $\lambda_3+d\lambda_3$ is:

$$\begin{aligned} dW &= f_1 d\lambda_1 + f_2 d\lambda_2 + f_3 d\lambda_3 \\ &= (\sigma_1 \lambda_2 \lambda_3) d\lambda_1 + (\sigma_2 \lambda_3 \lambda_1) d\lambda_2 + (\sigma_3 \lambda_1 \lambda_2) d\lambda_3 \\ &= \frac{\sigma_1}{\lambda_1} d\lambda_1 + \frac{\sigma_2}{\lambda_2} d\lambda_2 + \frac{\sigma_3}{\lambda_3} d\lambda_3 \end{aligned} \tag{B-8}$$

On the other hand, the phenomenological theory gives:

$$W = W(I_1, I_2, I_3)$$

Therefore:

$$\begin{aligned} dW = & \frac{\partial W}{\partial I_1}\frac{\partial I_1}{\partial \lambda_1} d\lambda_1 + \frac{\partial W}{\partial I_1}\frac{\partial I_1}{\partial \lambda_2} d\lambda_2 + \frac{\partial W}{\partial I_1}\frac{\partial I_1}{\partial \lambda_3} d\lambda_3 \\ + & \frac{\partial W}{\partial I_2}\frac{\partial I_2}{\partial \lambda_1} d\lambda_1 + \frac{\partial W}{\partial I_2}\frac{\partial I_2}{\partial \lambda_2} d\lambda_2 + \frac{\partial W}{\partial I_2}\frac{\partial I_2}{\partial \lambda_3} d\lambda_3 \\ + & \frac{\partial W}{\partial I_3}\frac{\partial I_3}{\partial \lambda_1} d\lambda_1 + \frac{\partial W}{\partial I_3}\frac{\partial I_3}{\partial \lambda_2} d\lambda_2 + \frac{\partial W}{\partial I_3}\frac{\partial I_3}{\partial \lambda_3} d\lambda_3 \end{aligned} \tag{B-9}$$

By equating the coefficients of $d\lambda_1$, $d\lambda_2$, and $d\lambda_3$ in Equations (B-8) and (B-9) and using the strain invariants given in Equation (B-1) to derive $\frac{\partial I_i}{\partial \lambda_j}$ *(i = 1:3; j = 1:3)* we obtain:

$$\sigma_1 = 2\left(\lambda_1^2 \frac{\partial W}{\partial I_1} - \frac{1}{\lambda_1^2}\frac{\partial W}{\partial I_2} + I_3 \frac{\partial W}{\partial I_3} \right) \tag{B-10}$$

with similar expressions for σ_2 and σ_3 . If the solid is incompressible $I_3 = 1$ and $W=W(I_1,I_2)$ only. In this case the stress is insensitive to pressure because for an incompressible material an arbitrary hydrostatic pressure p does not produce any changes in the deformation variables λ_1, λ_2, and λ_3. Thus, the principal stresses are given in index notation as:

$$\left.\begin{aligned}\sigma_{ii} &= 2\left(\lambda_i^2\frac{\partial W}{\partial I_1}-\frac{1}{\lambda_i^2}\frac{\partial W}{\partial I_2}\right)+p\\ \sigma_{ij} &= 0\end{aligned}\right\} \qquad \text{(B-11)}$$

The stress σ_{ii} denotes the force acting on a unit of area measured in the deformed state. In practice, it is more convenient to use the force f_{ii} (engineering stress) acting on a unit of undeformed cross-sectional area. For an incompressible material, there is a simple relationship between the two kinds of stress:

$$f_{ii}=\frac{\sigma_{ii}}{\lambda_i} \qquad \text{(B-12)}$$

B.2 Particular stress-strain relations

B.2.1 Simple extension (or uniaxial compression)

A simple extension is defined by strain ratios: $\lambda_1 = \lambda$, $\lambda_2 = \lambda_3 = 1/\lambda^{1/2}$ (Figure B-2).

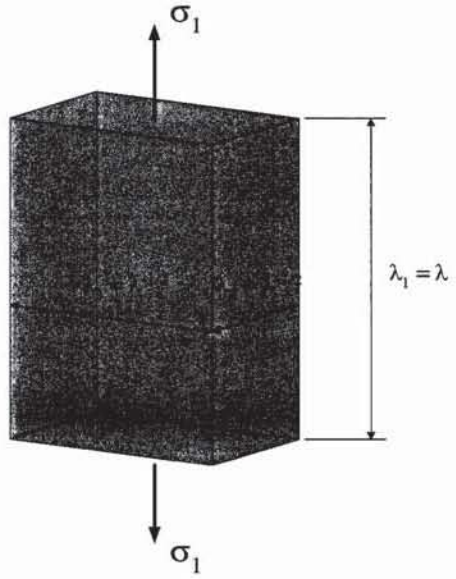

Figure B-2: Principal extension ratios in simple extension

If we choose as a reference state of stress that the sides of the block are stress-free, then $\sigma_2 = \sigma_3 = 0$, and Equation (B-11) for σ_2 and σ_3 becomes an equation for the unknown pressure p:

$$p = -2\left(\frac{1}{\lambda}\frac{\partial W}{\partial I_1} - \lambda\frac{\partial W}{\partial I_2}\right) \tag{B-13}$$

Substituting p obtained from Equation (B-13) into Equation (B-11) gives:

$$\sigma_1 = 2\left(\lambda^2 - \frac{1}{\lambda}\right)\left(\frac{\partial W}{\partial I_1} + \frac{1}{\lambda}\frac{\partial W}{\partial I_2}\right) \tag{B-14}$$

For the Mooney form of W this becomes:

$$\sigma_1 = 2\left(\lambda^2 - \frac{1}{\lambda}\right)\left(C_1 + \frac{C_2}{\lambda}\right) \tag{B-15}$$

In terms of the applied tensile force per unit of undeformed cross-sectional area, Equation (B-14) becomes:

$$f_1 = \frac{\sigma_1}{\lambda} = 2\left(\lambda - \frac{1}{\lambda^2}\right)\left(\frac{\partial W}{\partial I_1} + \frac{1}{\lambda}\frac{\partial W}{\partial I_2}\right) \tag{B-16}$$

If we consider only rather small strains, where rubber must obey the Mooney-Rivlin relation, Equation (B-7), then both $\frac{\partial W}{\partial I_1}$ and $\frac{\partial W}{\partial I_2}$ are constants and the relation between "engineering" stress and strain in simple extension becomes:

$$f = 2\left(\lambda - \frac{1}{\lambda^2}\right)\left(C_1 + \frac{C_2}{\lambda}\right) \tag{B-17}$$

By expanding in terms of the strain ε $(=\lambda - 1)$ and taking ε to be small, the ratio f/ε at infinitesimally small strain (i.e. the value of the tensile modulus E) is found to be $6(C_1+C_2)$.

B.2.2 Pure shear

A deformation state described as "pure shear" is illustrated in Figure B-3. It is defined as a tension applied in the 1-direction with the condition that the width in the 2-direction is prevented from altering (i.e., $\lambda_2 = 1$). Since a shear deformation is defined if a line parallel to one of the principal axes undergoes no change in length, the term "shear" is used for this deformation state. The term "pure" means that the principal axes do not rotate during the deformation.

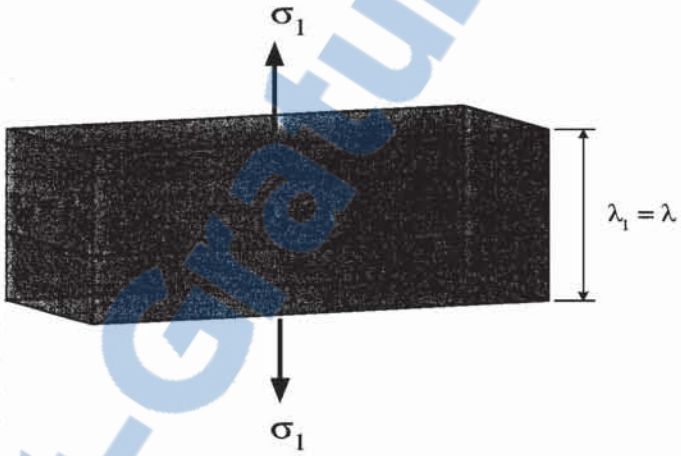

Figure B-3: Principal extension ratios in pure shear

Thus, for this strain state we have: $\lambda_1 = \lambda$, $\lambda_2 = 1$, and $\lambda_3 = 1/\lambda$. Using the condition $\sigma_3 = 0$, the pressure p is obtained from Equation (B-11) as:

$$p = -2\left(\frac{1}{\lambda^2}\frac{\partial W}{\partial I_1} - \lambda^2\frac{\partial W}{\partial I_2}\right) \tag{B-18}$$

Hence, the tension σ_1 in the stretching direction is:

$$\sigma_1 = 2\left(\frac{\partial W}{\partial I_1} + \frac{\partial W}{\partial I_2}\right)\left(\lambda^2 - \frac{1}{\lambda^2}\right) \tag{B-19}$$

and the lateral stress σ_2 supplied by the rigid clamps is:

$$\sigma_2 = 2\left(\frac{\partial W}{\partial I_1} + \lambda^2 \frac{\partial W}{\partial I_2}\right)\left(1 - \frac{1}{\lambda^2}\right) \tag{B-20}$$

In terms of the applied tensile force per unit of unstrained cross-sectional area, Equation (B-19) becomes:

$$f_1 = \frac{\sigma_1}{\lambda} = 2\left(\frac{\partial W}{\partial I_1} + \frac{\partial W}{\partial I_2}\right)\left(\lambda - \frac{1}{\lambda^3}\right) \tag{B-21}$$

ANNEXE II

COMPLÉMENT À L'ARTICLE 3

C- Calcul des paramètres du modèle

L'état d'équilibre est géré principalement par le ressort R_1 dont la rigidité dépend de deux constantes $C^{(R_1)}$ et $N^{(R_1)}$ selon l'équation (4.4). La constante $C^{(R_1)}$ est fonction de la densité des chaines moléculaire n, de la température absolue T et de la constante de Boltzmann K_B selon l'équation 4.6. La constante $N^{(R_1)}$ est reliée à la limite d'extensibilité de la chaîne par le biais de l'équation 4.7. Cette limite, représentée par λ_{lim}, est l'extension théorique maximale de la molécule formant l'élastomère. Elle est déterminée à partir d'un test d'extension allant jusqu'à la rupture [54].

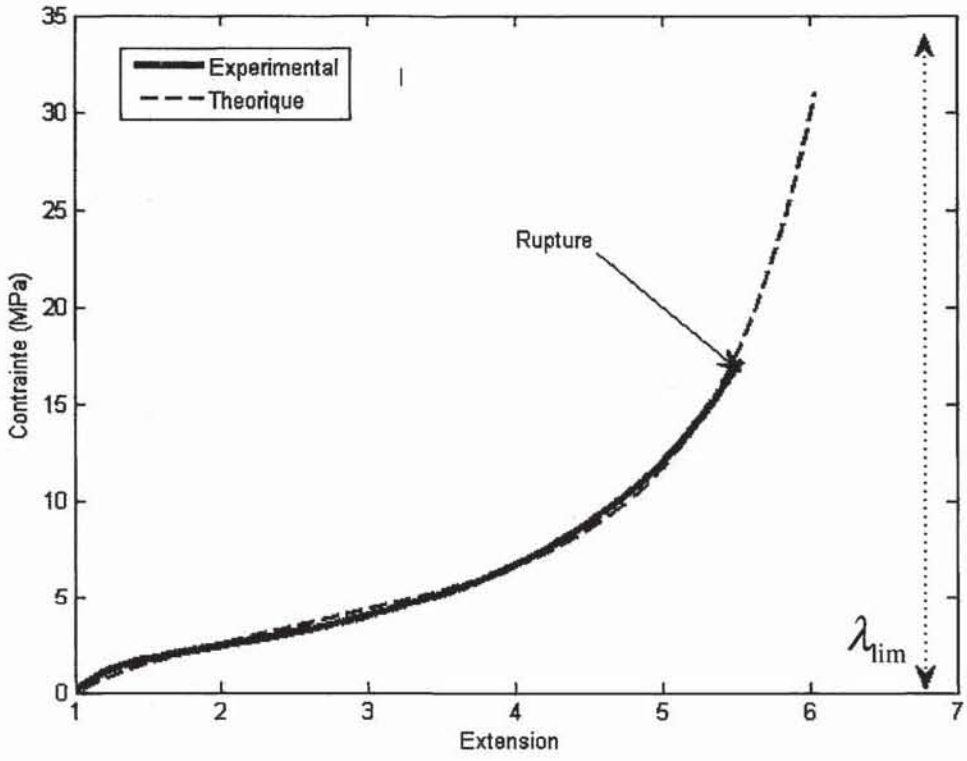

Figure C-1: Détermination de la limite d'extensibilité

La détermination de λ_{lim} revient à déterminer N qui est calculé d'une façon numérique (trial and error) sur matlab en utilisant le modèle à 8 chaînes (équation C-1) [54].

$$\sigma_{True} = C^R \left(\lambda^2 - \frac{1}{\lambda} \right) \frac{\sqrt{N}}{\lambda_{chain}} L^{-1} \left(\frac{\lambda_{chain}}{\sqrt{N}} \right) \tag{C-1}$$

Avec C^R est relié au module initial E de l'élastomère par le biais de l'équation C-2 :

$$C^R = \frac{E}{3} \tag{C-2}$$

Ainsi, λ_{lim} peut être calculée en utilisant l'équation C-3.

$$N = \frac{1}{3} \left[\lambda_{\text{lim}}^2 + \frac{2}{\lambda_{\text{lim}}} \right] \tag{C-3}$$

En ce qui concerne la valeur de $C^{(R_1)}$, elle est déterminée à partir d'un point au milieu de la boucle d'hystérésis en début de déformation. Sa valeur est donnée par l'équation C-4.

$$C^{(R_1)} = \frac{\sigma}{\left(\lambda - \frac{1}{\lambda^2} \right) \frac{\sqrt{N^{(R_1)}}}{\lambda^{(R_1)}_{chain}} L^{-1} \left(\frac{\lambda^{(R_1)}_{chain}}{\sqrt{N^{(R_1)}}} \right)} \tag{C-4}$$

Le chemin d'équilibre peut ensuite être estimé en utilisant le model d'Arruda-Boyce selon l'équation C-5 (Figure C-2).

$$\sigma^{(R_1)}_{True} = C^{R_1} \left(\lambda^2 - \frac{1}{\lambda} \right) \frac{\sqrt{N^{(R_1)}}}{\lambda^{(R_1)}_{chain}} L^{-1} \left(\frac{\lambda^{(R_1)}_{chain}}{\sqrt{N^{(R_1)}}} \right) \tag{C-5}$$

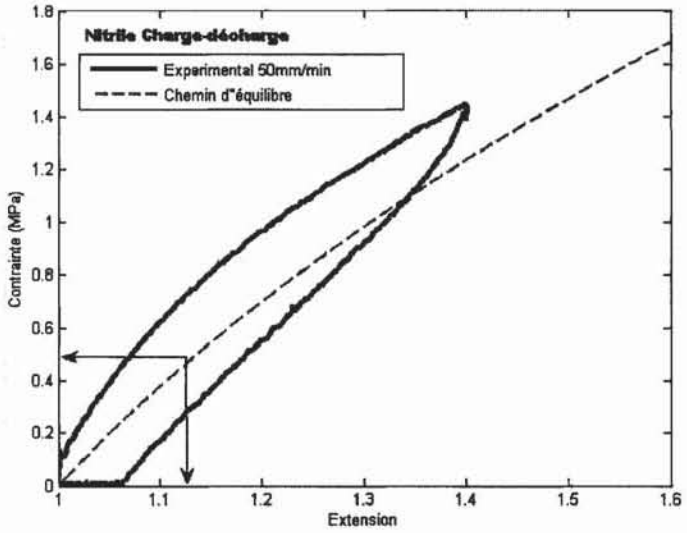

Figure C-2 : Chemin d'équilibre estimé

La viscosité a été déterminée par itération sur Matlab pour chaque vitesse. Les valeurs trouvées de η sont représentées dans la Figure C-3, leur évolution suit une loi logarithmique.

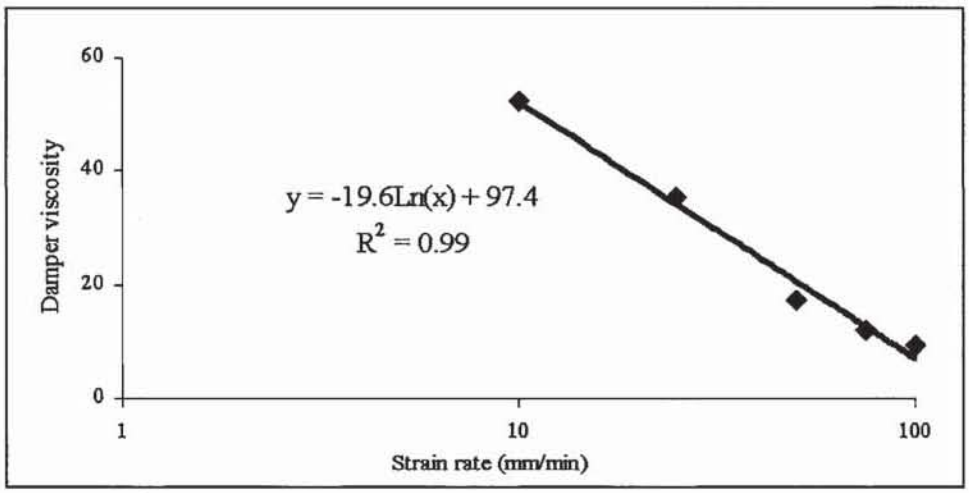

Figure C-3 : Évolution de la viscosité en fonction de la vitesse

Connaissant les paramètres du modèle, la courbe théorique à chaque vitesse peut être calculée en utilisant l'équation 4.2.

D- Vérification numérique

La validité de l'équation 4.2 a été vérifiée en confrontant l'équation différentielle 4.1. L'idée consiste à comparer les deux membres de gauche et de droite de l'équation différentielle 4.1 à chaque état de déformation. L'erreur induite par notre approche est de l'ordre de 2-5 %. Les résultats de vérification sont représentés dans les Figures D-1—D-3.

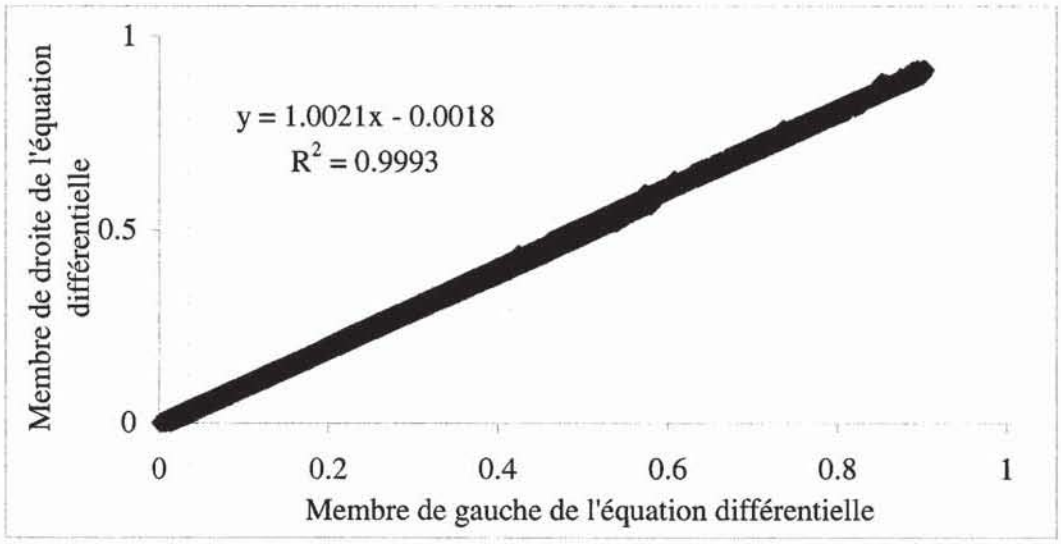

Figure D-1 : Vérification dans le cas du nitrile à la vitesse 10 mm/min

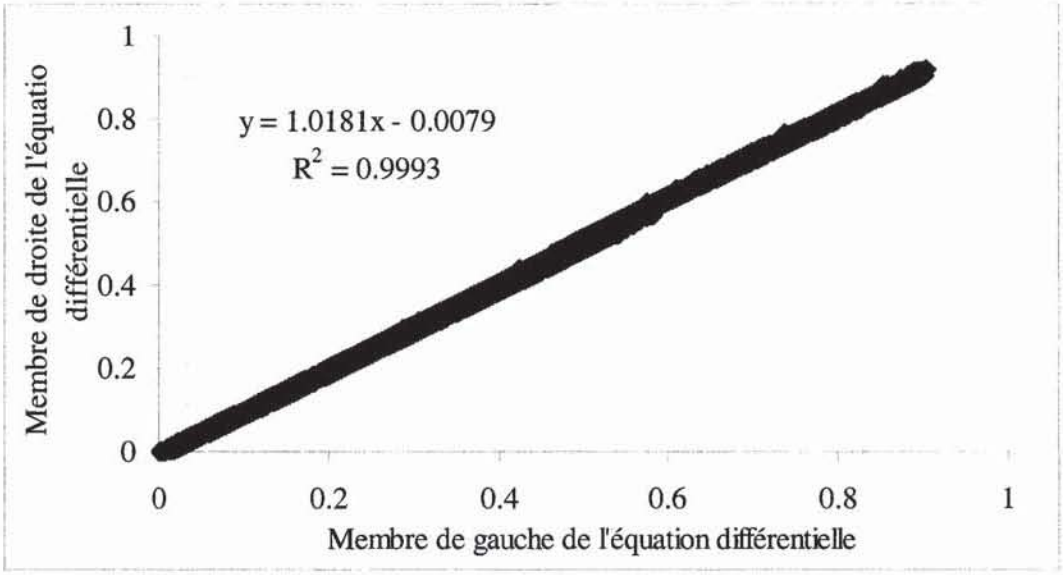

Figure D-2 : Vérification dans le cas du nitrile à la vitesse 50 mm/min

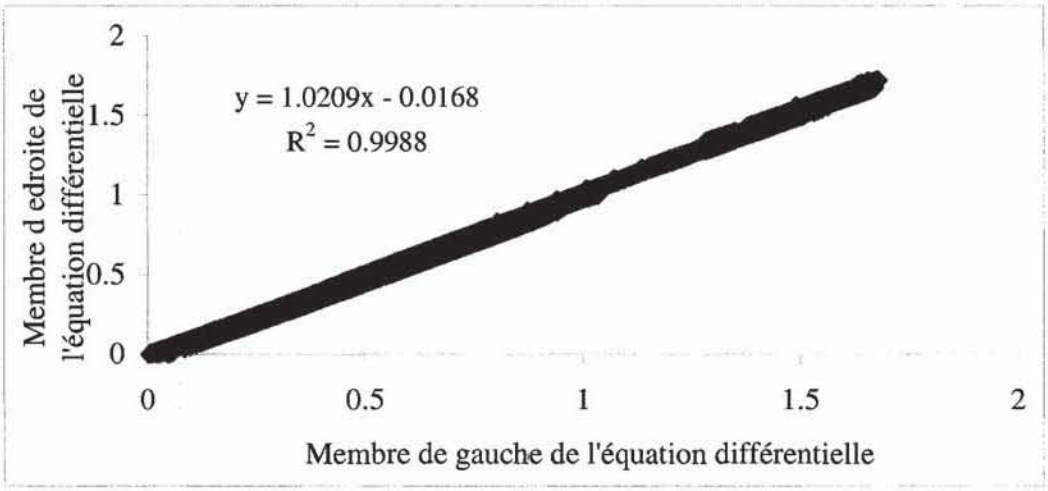

Figure D-3 : Vérification dans le cas du nitrile à la vitesse 100 mm/min

ANNEXE III

COMPLÉMENT À L'ARTICLE 4

E- Calcul des paramètres du modèle

L'état d'équilibre est géré principalement par le ressort R_1 dont la rigidité dépend de deux constantes A_1 et B_1 selon une loi exponentielle qu'on propose dans ce travail et qui est représentée par l'équation (5.4). Le chemin traduisant cet état est estimé par une courbe qui passe au milieu de la boucle d'hystérésis (Figure E-1).

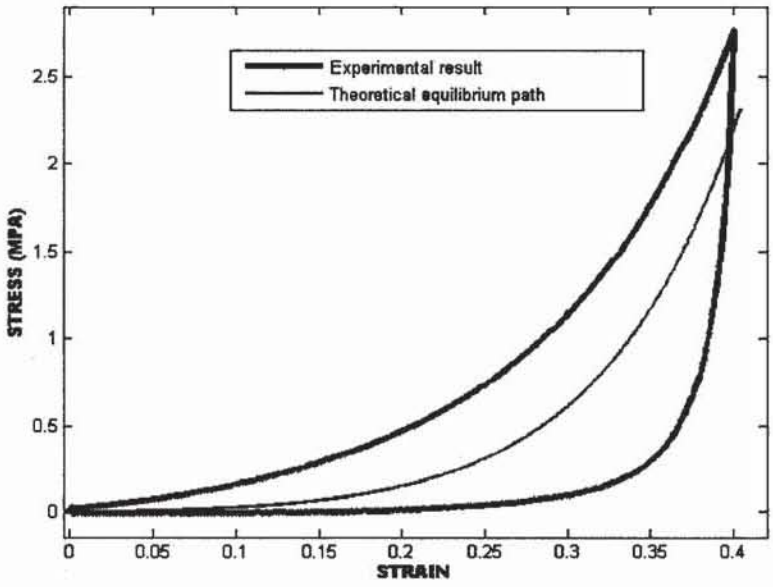

Figure E-1: Estimation du chemin d'équilibre

La relation entre la contrainte et la déformation dans le cas d'un chargement peut être obtenue en remplaçant le temps par la déformation, ainsi l'équation (5.2) devient :

$$\sigma = \zeta\eta + E^{(R_1)}\varepsilon - \zeta\eta\, e^{-\frac{E^{(R_2)}}{\eta}\frac{\varepsilon}{\zeta}} \qquad \text{(E-1)}$$

La pente de la courbe donnée par l'équation (E-1) lorsque ε << 1 est égale à :

$$\lim_{x\to 0}\left(\frac{\partial\sigma}{\partial\varepsilon}\right)= E^{(R_1)} + E^{(R_2)} \tag{E-2}$$

L'interprétation physique de ce résultat est que lorsque la déformation commence, l'amortisseur du modèle de Zener a une vitesse nulle, par conséquent la contrainte résultante de ce dernier est nulle aussi, car la contrainte de l'amortisseur est donné par l'équation (E-3):

$$\sigma = \eta\frac{\partial\varepsilon}{\partial t} \tag{E-3}$$

Donc au début de la déformation, la contrainte résultante du modèle est due seulement aux deux ressorts en parallèles. Ce qui explique que la pente de la courbe au début de la déformation est égale à la somme des deux modules des ressorts.

À partir de la courbe expérimentale, on peut déterminer la pente de la courbe de charge au début de la déformation. Soit E_t cette pente, on aura donc:

$$E_t = E^{(R_1)} + E^{(R_2)} \tag{E-4}$$

Or $E^{(R_1)}$ et $E^{(R_2)}$ sont donnés par les équations (5.5) et (5.6) respectivement. De plus, au début du chargement, ils sont égaux à A1 et A2 respectivement. Donc,

$$E_t = A_1 + A_2 \tag{E-5}$$

Ainsi, la valeur d'A_2 peut être déduite en utilisant l'équation (E-5).

En ce qui concerne les valeurs de B_2 du ressort R_2 ainsi que les paramètres de l'amortisseur, elles sont déterminées par itération sur matlab.

F- Vérification numérique

La validité de l'équation 5.2 a été vérifiée en confrontant l'équation différentielle 5.1. L'idée consiste à comparer les deux membres de gauche et de droite de l'équation différentielle 4.1 à chaque état de déformation. L'erreur induite par notre approche est de l'ordre de 2-5 %. Les résultats de vérification sont représentés dans les Figures F-1—F-3.

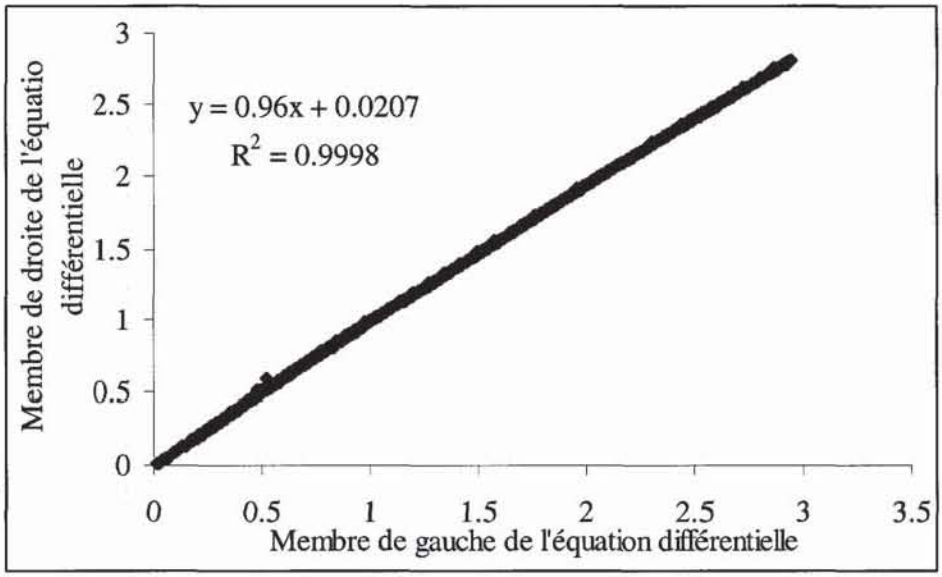

Figure F-1 : Vérification dans le cas du textile à la vitesse 10 mm/min

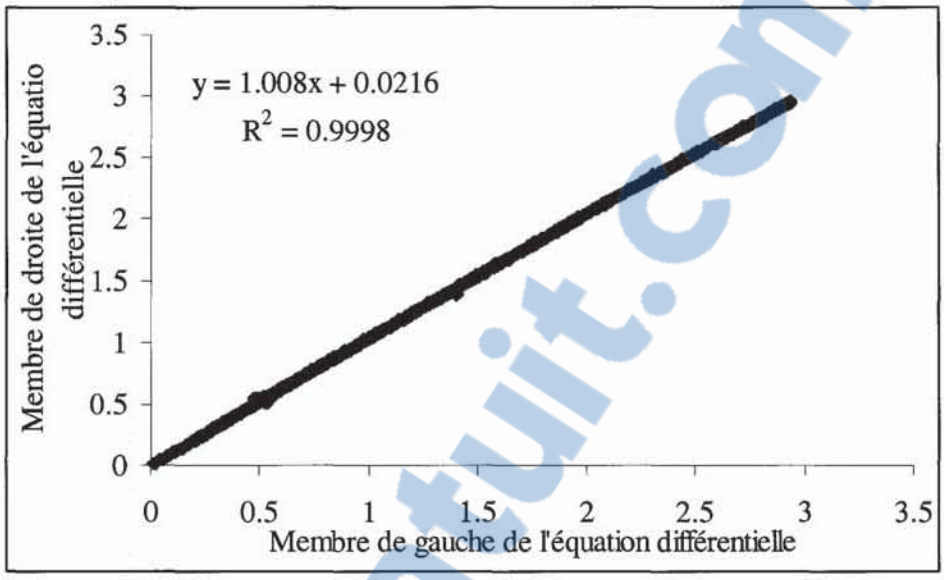

Figure F-2 : Vérification dans le cas du textile à la vitesse 50 mm/min

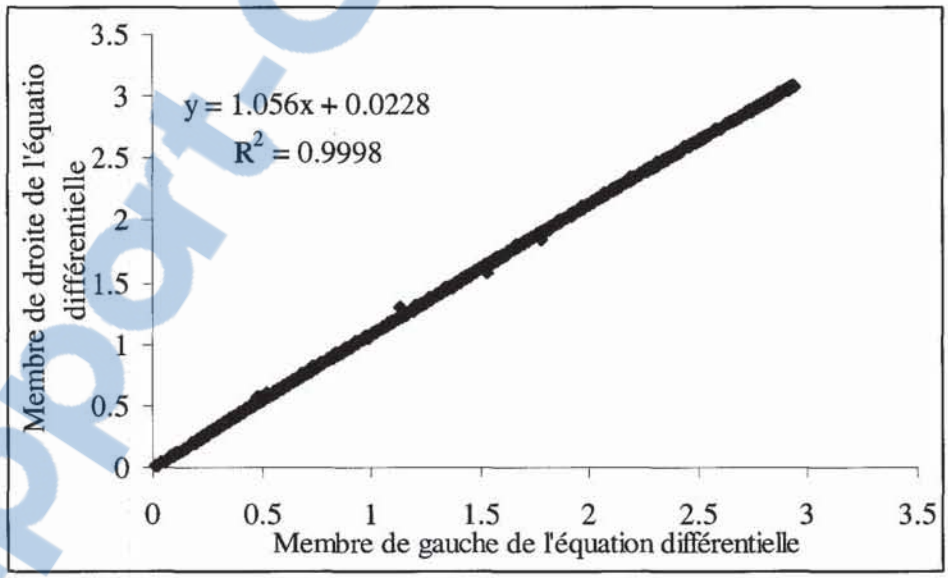

Figure F-3 : Vérification dans le cas du textile à la vitesse 100 mm/min

LISTE DE RÉFÉRENCES BIBLIOGRAPHIQUES

1. *Commission de la santé et de la sécurité du travail du Québec, Fichier sur les lésions professionnelles, mis à jours en septembre 2003, Montréal, QC.*

2. *ISO 17235 Cuir essai physique et mécanique – Détermination de la souplesse, 2002.*

3. *ISO 5979 Supports textiles revêtus de caoutchouc ou de plastique - Détermination de la souplesse -- Méthode de la boucle plate, 1982.*

4. *KAWABATA, S., The Standardization and Analysis of Hand Evaluation, The Textile Machinery Society of Japon, Osaka, 1980.*

5. *Norme ASTM D 4032-94, Standard test method for stiffness of fabric by circular bend procedure.*

6. *NELSON. J.B. MITAL, A. An Ergonomic Evaluation of Dexterity and Tactility with Increase in Examination/Surgigical Glove Thickness. Ergonomics 38. 723-733, 1995.*

7. *MITAL A, KUO T, FAARD HF. A Quantitative Evaluation of Gloves Used with Non-powered Hand Tools in Routine Maintenance Tasks. Ergonomics, 37(2):333-343, 1994.*

8. *ROCK KM, MIKAT RP, FOSTER C. The effects of Gloves on Grip Strength and Three-point Pinch. Journal of Hand Therapy, 14(4):286-290, 2001.*

9. Vu-Khanh, T., Dolez, P. I., Harrabi, L., Lara, J., Larivière, C., Tremblay, G., Nadeau, S., *Caractérisation de la souplesse des gants de protection par des méthodes mécaniques et une méthode biomécanique basée sur l'électromyographie de surface.* Étude et Recherche. 2007, Montréal: Institut de recherche Robert-Sauve´ en santé et en sécurité du travail au Québec. 90 pages.

10. GENT, A.N., *Engineering with rubber: How to design with rubber components.* 2001, Munich: Hanser Publishers.

11. McCrum, N.G., C.P. Buckley, and C.B. Bucknall, *Principles of Polymer Engineering.* 2004, New York: OXFORD UNIVERSITY PRESS.

12. WARD, I.M. and D.W. HADLEY, *An introduction to the mechanical properties of solid polymers.* 1993, New York: J. Wiley &Sons. 334.

13. KUMAR, A. and R.K. GUPTA, *Fundamentals of Polymer Engineering*, ed. ^{n} edition. 2003, New York: Marcel Dekker. 693.

14. SPERLING, L.H., *Introduction to Physical Polymer Science*. J Wiley & Son ed, ed. r. edition. 1992. 671.

15. MCCRUM, N.G., C.P. BUCKLEY, and C.B. BUCKNALL, *Principals of Polymer Engineering*. 1988, Oxford University Press: Oxford, New York. p. 19-170.

16. POWELL, P.C. and A.J.I. HOUSZ, *Engineering with Polymers*. S. Thornes ed, ed. n. edition. 1998, Cheltenham, England. 479.

17. P.K.FREAKLY and Q.R. PAYNE. *Theory and practice of engineering with rubber*. 1978. London: Applied Science Publishers.

18. GENT, A.N., *Engineering with rubber: how to design with rubber components*. 1992, Hanser Publishers: Munich. p. 211-238.

19. INSTITUTE, I.R., *Rubber engineering*. 2000, New York; London: McGraw-Hill. 52-59, 521-552.

20. Seymour, R.B. *Polymers for engineering applications*. in *ASM International*. 1987. Metals Park, Ohio.

21. RIVLIN, R.S. *Large Elastic Deformation of Isotropic Materials. Further development of the General Theory*. in *Phil. Trans. Roy. Soc. London*. 1948.

22. MOONEY, M., *A Theory of Large Elastic Deformation*. Journal of Applied Physics, 1940. **11**: p. 582-592.

23. YEOH, O.H., *Some forms of the strain energy function for rubber*. Rubber Chemistry and Technology, 1993. **66**(5): p. 754-771.

24. YEOH, O.H., *Hyperelastic material models for finite element analysis of rubber*. J. Nature Rubber Res., 1997. **12**: p. 142-153.

25. Arruda, E.M. and M.C. Boyce, *A three-dimensional constitutive model for the large stretch behavior of rubber elastic materials*. Journal of the Mechanics and Physics of Solids, 1993. **41**(2): p. 389-412.

26. OGDEN, R.W., *Large deformation isotropic elasticity- on the correlation of the theory and experiment for incompressible rubberlike solids*. Proceedings of the Royal Society of London, Series A (Mathematical and Physical Sciences), 1972. **326**(1567): p. 565-84.

27. OGDEN, R.W., *Background on nonlinear elasticity, Chapter 2.2*, J. Lemaitre, Editor. 2001, in the handbook of materials behavior models: Boston. p. 75-83.

28. VALANIS, K.C. and R.F. LANDEL, *Strain-energy function of hyperelastic material in terms of extension ratios.* Journal of Applied Physics, 1967. **38**(7): p. 2997-3002.

29. Gommers, B., I. Verpoest, and P. Van Houtte, *Analysis of knitted fabric reinforced composites: Part I. Fibre orientation distribution.* Composites - Part A: Applied Science and Manufacturing, 1998. **29**(12): p. 1579-1588.

30. Leong, K.H., et al., *Potential of knitting for engineering composites - a review.* Composites - Part A: Applied Science and Manufacturing, 2000. **31**(3): p. 197-220.

31. Ramakrishna, S., *Characterization and modeling of the tensile properties of plain weft-knit fabric-reinforced composites.* Composites Science and Technology, 1997. **57**(1): p. 1-22.

32. HEARLE, W.S., P.GROSBERG, and S. BACKER, *Structure Mechanics of Fibers.* Yarns and Fabrics, 1969. **1**: p. 450.

33. Warner, S.B., *Fiber science, Englewood Cliffs* 1995: Prentice-Hall, Inc.

34. YVES, T. and S. PAUL, *High modulus polymers - Approach to Design and Development*, ed. R.S.P. edited by Anagnostis E. Zachariades. 1988, New York: Marcel Dekker, Inc.

35. Durville, D., *Modélisation par éléments finis de propriétés mécaniques de structures textiles: de la fibre au tissu*, in *Colloque sur le calcul de structures*. 2001: Giens.

36. Wang, Y. and X. Sun, *Digital-element simulations of textile processes.* Composite Science and Technology, 2001. **61**: p. 311-319.

37. Hanklar, S., *Modélisation mécanique et numérique du comportement des tissus de fibres: simulations du comportement mésoscopique de la maille élémentaire*. 1998, Université de Paris 6: Paris.

38. Peng, X., *A dual homogenization and finite elements approach for material characterization of textile composites.* Composites Part B, 2002. **33**: p. 45-56.

39. Boisse, P., et al., *Meso/macro-mechanical behaviour of textile reinforcements for thin composites.* Composites Science and Technology, 2001. **61**(3): p. 395-401.

40. Boisse, P., J.C. Gelin, and H. Sabhi. *Experimental study and finite element simulation of glass fiber fabric shaping process*. 1993. New Orleans, LA, USA: Publ by ASME.

41. Kawabata, S., *Nonlinear Mechanics of Woven and knitted materials,* , in *Textile Structural Composites*. 1989, Elsevier.

42. Postle, R., G.A. Camaby, and S. de Jong *The Mechanics of Wool Structures*. 1988, New York: Halsted Press (division of John Wiley & Sons).

43. Matsuo, M., T. Yamada, and N. Ito, *Stress Relaxation Behavior of Knitted Fabrics under Uniaxial and Strip Biaxial Excitation as Estimated by Corresponding Principle between Elastic and Visco-Elastic Bodies.* Textile Research Journal, 2006. **76**(6): p. 465-477.

44. Buet-Gautier, K. and P. Boisse, *Experimental analysis and modeling of biaxial mechanical behavior of woven composite reinforcements.* Experimental Mechanics, 2001. **41**(3): p. 260-9.

45. Gibson, R.F., *Principles of Composite Material Mechanics*. 1994, New York: McGraw-Hill.

46. Vu-Khanh, T., et al., *Gants de protection : étude sur la résistance des gants aux agresseurs mécaniques multiples*, in *Études et recherches / Rapport R-424*. 2005, IRSST: Montréal. p. 86 pages.

47. JAMES, H. M., GUTH, E. (1949) *Simple presentation of network theory of rubber with a discussion of other theories,* Journal of Polymer Science, vol. 4, p. 153-182.

48. KUHN, W. (1934) *Shape of fibre-forming molecules in solutions,* Kolloid Zeitschrift, vol. 68, p. 2-15.

49. KUHN, W. (1936) *Elastic properties of highly polymerised substances,* Kolloid Zeitschrift, vol. 76, p. 258-271.

50. MEYER, K. H., FERRI, C. (1935) Helv. Chim. Acta, vol. 18, p. p. 570.

51. MEYER, K. H., V. SUSICH, G., VALK, OGRAVE, E. (1932) *Elastic properties of rubber-like substances,* Kolloid Zeitschrift, vol. 59, p. 208-216.

52. TRELOAR, L. R. G. (1943) *The elasticity of a network of long-chain molecules. I,* Transactions of the Faraday Society, vol. 39, p. 36-41.

53. WALL, F. T. (1943) *Statistical thermodynamics of rubber. III,* Journal of Chemical Physics, vol. 11, p. 527-530.

54. Arruda, E.M. and M.C. Boyce, *A three-dimensional constitutive model for the large stretch behavior of rubber elastic materials.* Journal of the Mechanics and Physics of Solids, 1993. **41**(2): p. 389-412.